RADIATIVE TRANSFER AND OPACITY CALCULATIONS

Thesis by

Mitchell Thomas Th

In Partial Fulfillment of the Requirements

For the Degree of

Doctor of Philosophy

California Institute of Technology

Pasadena, California

1964

ACKNOWLEDGMENTS

The author wishes to express his gratitude to Professor S. S. Penner for suggesting the research presented here and for his helpful direction. The help of Dr.-Ing. G. Adomeit in the studies presented in Secs. VI and VII is gratefully acknowledged.

This research was supported by the Air Force Office of Scientific Research through Contract AF 49(638)-984 and Grant AFOSR-7163 and by the Office of Naval Research under Contract Nonr-220(45), NR 015 401.

The author is indebted to the staff of the Booth Computing Center for their patient help through many consultations. The assistance of Mrs. Ruth Toy, Mrs. Madeline Fagergren and Mrs. Alrae Tingley in the preparation of this manuscript is gratefully acknowledged.

ABSTRACT

The similarity groups for multicomponent, reacting gas mixtures with radiative energy transport are derived. The resulting relations are used to consider the feasibility of scaling for flow processes with radiative energy transport under highly simplified conditions. Next the scaling parameters are derived for radiant energy emission from isobaric and isothermal gases for arbitrary opacities and various spectral line and molecular band models.

The radiative scaling properties for representative temperature profiles for both collision-broadened and Doppler-broadened line profiles have been found for a spectral line belonging to a molecular vibration-rotational spectral band on the basis of exact numerical calculations. Representative calculations are also given for radiant energy transfer through non-isothermal, high-temperature air.

Scaling parameters for radiant energy emission from isobaric but non-isothermal systems are discussed for arbitrary opacities and various spectral line and molecular band models under the restrictions imposed on the allowed temperature profiles for dispersion and Doppler lines by the Eddington-Barbier approximation. An examination is made of the failure of the Eddington-Barbier approximation in radiative heat transfer for line radiation.

The relative importance of thermal conduction and radiation in heated air is specified through the use of the pertinent similarity group. Finally, a procedure is given that may be used to obtain approximate continuum opacity estimates in polyelectronic plasmas.

TABLE OF CONTENTS

Part		Page
I	INTRODUCTION	1
II	DETERMINATION OF SIMILARITY PARAMETERS	5
	A. Continuity Equation	11
	B. Momentum Equation	11
	C. Energy Equation	12
III	SIMILARITY PARAMETERS FOR GAS MIXTURES INCLUDING RADIATION TRANSPORT	18
	A. Arbitrary Opacities	20
	B. Diffusion Approximation	24
	C. Transparent Gases	26
IV	EXAMPLES OF SCALING PROBLEMS	30
	A. Scaling of Flow in Transparent Gas for a Gas Burner	30
	B. Scaling of Flow in Transparent Gas for Uncoupled Radiative and Convective Energy Transport	32
V	SCALING PARAMETERS FOR RADIANT ENERGY EMISSION FROM ISOBARIC AND ISOTHERMAL SYSTEMS FOR ARBITRARY OPACITIES AND VARIOUS SPECTRAL LINE AND MOLECULAR BAND MODELS	34
VI	RADIATIVE SCALING PROPERTIES FOR REPRESENTATIVE TEMPERATURE PROFILES	39
	A. Dispersion-Broadened Line	45
	B. Doppler-Broadened Line	46
	C. Solution of the Radiant Transfer Equation for Large Optical Depths	46
	D. Determination of the Lower Bound for the $\sqrt{\rho^2 L}$ Dependence of the Steradiancy of a Pressure-Broadened Line	50

Part		Page
	E. Radiant Energy Emission from High-Temperature, Non-isothermal Air	53
	1. Calculations for a Parabolic Temperature Profile	54
	2. Calculations for a Reentry Vehicle	60
VII	SCALING PARAMETERS FOR RADIANT ENERGY EMISSION FROM ISOBARIC BUT NON-ISOTHERMAL SYSTEMS IN THE EDDINGTON-BARBIER APPROXIMATION	65
	A. Isolated Spectral Lines Belonging to Diatomic Emitters with Collision Broadening	70
	1. The Limiting Case $h\nu_o/kT \ll 1$, $u_o T_o/T \ll 1$, $(h\nu_o - E_\ell)/kT \ll 1$	70
	2. The Limiting Case $h\nu_o/kT \gg 1$, $u_o T_o/T \gg 1$	71
	3. Determination of Steradiancy $B(0, \theta)$ for $h\nu_o/kT_o \gg 1$, $u_o T_o/T \gg 1$	79
	B. Isolated Spectral Lines Belonging to Diatomic Emitters with Doppler Broadening	81
	1. The Limiting Case $h\nu_o/kT \ll 1$, $u_o T_o/T \ll 1$, $(h\nu_o - E_\ell)/kT \ll 1$	82
	2. The Limiting Case $h\nu_o/kT \gg 1$, $u_o T_o/T \gg 1$	82
	3. Determination of Steradiancy $B(0, \theta)$ for $h\nu_o/kT \gg 1$, $u_o T_o/T \gg 1$, $(h\nu_o - E_\ell)/kT \gg 1$	83
	C. Gray Body	85
	1. The Special Case $h\nu/kT < h\nu/kT_o \ll 1$	86
	2. The Special Case $h\nu/kT_o \gg 1$, $h\nu/kT \ll 1$	86
	3. The Special Case $h\nu/kT_o \gg 1$, $h\nu/kT \gg 1$	86
VIII	APPLICATION OF THE EDDINGTON-BARBIER APPROXIMATION TO DISPERSION- AND DOPPLER-BROADENED SPECTRAL LINES FOR AN ARBITRARY TEMPERATURE PROFILE	87

Part		Page
	A. Evaluation of the Spectral Steradiancy Using the Eddington-Barbier Approximation	87
	B. The Limit of Optically Thick or Optically Thin Systems	88
IX	RELATIVE IMPORTANCE OF THERMAL CONDUCTION AND RADIATION FOR ENERGY TRANSPORT IN STATIONARY HEATED AIR	98
	A. Heat Transfer Parameters	98
	B. Representative Applications of the Heat Transfer Parameters to Problems of Engineering Interest	104
X	AN APPROXIMATE SEMI-ANALYTICAL EXPRESSION FOR THE SPECTRAL ABSORPTION COEFFICIENT IN AN IONIZED, POLYELECTRONIC PLASMA	109
	A. Theoretical Consideration	111
	1. Degree of Ionization and Planck and Rosseland Mean Free Paths	111
	2. Theoretical Calculation of Spectral Absorption Coefficients	112
	B. Comparison Between the Approximate and Numerical Results	121
Appendix A.	The Diffusion Approximation	126
Appendix B.	Solution to the Radiant Energy Transfer Equation Using the Lunblad Series Expansion	128
REFERENCES		132

I. INTRODUCTION

In Secs. I - IV, we consider the problem of similarity analysis for reacting and radiating gases. We are interested in investigating the possibility of reducing the physical scale of a given system (H). This reduction will ordinarily require a corresponding variation in other physical parameters besides the spatial dimensions if we wish to obtain a result from a small-scale system or model (M) that can be related to the system H in a physically useful manner.

Similarity analysis of the Navier-Stokes differential equations allows the determination of the dimensionless form of the equations, as well as identification of the dimensionless groups that enter into solution of particular problems. From the dimensionless equations and the characteristic groups of parameters, scaling criteria, i.e., the conditions for similar operation of the two systems H and M may be determined (1, 2). From the practical point of view, this analysis determines the possibility of constructing scale models of large devices such as rocket engines, atmospheric reentry vehicles, etc., and shows under what conditions the experimental results on M may be used to find the characteristics of H.

The procedure we use is a form of dimensional analysis which is applicable whenever the basic differential equations are known explicitly although their solutions are unknown. It is not enough merely to say that the solution ought to depend upon certain physical parameters as such an analysis will overlook the existence of dimensional constants. However, the pure dimensional analysis only makes use of the existence of the

various parameters whereas in a similarity analysis the manner is considered in which the dimensional quantities enter into the differential equations.† For the initial analysis we will consider the following as dimensional dependent quantities: the length L, velocity v, binary diffusion coefficient $\mathscr{D}_{ij}$, thermal diffusion coefficient D_T, density ρ, pressure p, viscosity coefficient μ, external force f, time t, specific heat at constant volume c_v, specific heat at constant pressure c_p, temperature T, thermal conductivity λ. We will consider these quantities to be functions of the independent variables L, M, t and T (length, mass, time and temperature). From the Π theorem of dimensional analysis, it should be possible to construct 13 - 4 = 9 independent dimensionless groups (for fixed i and j) corresponding to the above basic quantities and the four degrees of freedom. We will see in the next section that, in fact, non-dimensionalizing of the Navier-Stokes equations results in exactly 9 independent dimensionless groups. There may be more groups, of course, in the sense that there may be, for example, more than one characteristic length L; but we expect that we will be unable to find any basically new quantities without introducing a new concept into the Navier-Stokes equations (e.g., relativity). When radiation terms are added to the conservation equations, the list of dependent variables will be increased and new similarity groups will result. This result will become clear from the analysis of Sec. III.

Even after all of the pertinent groups are known, it will ordinarily turn out that scaling is impossible, or perhaps possible only

†In this work, the term "similarity analysis" means the discovery of dimensionless groups by non-dimensionalizing the pertinent equations.

under a very restrictive set of conditions. There are some notable exceptions, however, where a certain amount of physical intuition may be combined with the similarity analysis, yielding a result of practical importance. Examples of these cases are given in Secs. IV and IX.

Sections V and VI deal, for isothermal and non-isothermal gases respectively, with scaling parameters for radiant energy emission for various spectral line and molecular band models. It appears that simple scaling rules generally constitute a fair approximation for dispersion lines in non-isothermal systems but that corresponding relations apply to lines with a Doppler contour only in the transparent gas regine. A solution to the radiant transfer equation for large optical depths is found which is useful in obtaining an analytic definition of an optically thick gas. The last part of Sec. VI includes studies of radiant energy transfer through high-temperature, non-isothermal air, a subject of current interest.

The applicability of the Eddington-Barbier approximation to the determination of scaling parameters is studied in Sec. VII for a gas with spectral line structure. Simple scaling rules may be obtained in certain important cases. Sec. VIII investigates the failure of the Eddington-Barbier approximation when a general non-isothermal gas is investigated.

In Sec. IX one of the radiation similarity groups of Sec. III is used to specify the relative importance of thermal conduction and radiation in high temperature air. The diffusion or transparent gas approximations are used where possible and typical problems of engineering interest are given to demonstrate the use of the results of this study.

Finally, Sec. X gives the derivation of an approximate, semi-analytical expression for the spectral absorption coefficient in an ionized, polyelectronic plasma. Only the bound-free and free-free transitions are included. The result is applicable at high temperatures, until line radiation becomes important. The data obtained from the approximate expression is in good agreement with data obtained by much more sophisticated means over much of the spectrum.

II. DETERMINATION OF SIMILARITY PARAMETERS

In this section we will non-dimensionalize the Navier-Stokes equations and determine a set of suitable similarity groups. After the nine quantities have been found, we will write them in standard form; the groups pertaining to radiation problems are discussed in the next section.

By far the most complicated situation to be considered is diffusion in a multicomponent mixture. In particular, it will be necessary to express the diffusion velocity of species i, $\vec{V}_i$, in terms of the binary diffusion coefficients which are to be characteristic quantities. Before continuing with a discussion based on the Navier-Stokes conservation equations, we shall find a convenient formulation of the diffusion velocity.

We will define the following quantities:

$\vec{M}_i = \rho_i \vec{V}_i$	mass flux of species i,
$\rho_i = Y_i \rho$	partial density of species i in the mixture,
Y_i	mass fraction of species i,
X_i	mole fraction of species i,
W_i	molecular weight of species i,
$\mathscr{D}_{ij}$	binary diffusion coefficient of species i and j.

The general diffusion equations in the near-equilibrium Chapman-Enskog solution are, to the first approximation, given by (3)

$$\vec{M}_i = \frac{C_T^2}{\rho} \sum_{j=1}^{\nu} W_i W_j D_{ij} \vec{d}_j - D_i^T \nabla \ln T, \quad i = 1, 2, 3, \ldots \nu \qquad (1)$$

where D_{ij} and D_i^T are the multicomponent and thermal diffusion coefficients respectively and C_T = total concentration. The quantity $\vec{d}_i$ is given by the expression

$$\vec{d}_i = \nabla X_i + (X_i - Y_i)\nabla \ln p - Y_i\left[\frac{\rho \vec{f}_i}{p} - \sum_{k=1}^{\nu} \frac{\rho_k \vec{f}_k}{p}\right] \tag{2}$$

where $\vec{f}_i$ is an external force/mass acting on species i.

The ν equations indicated (for a ν-component mixture) are not independent as the diffusion velocity is defined with respect to the mass-averaged velocity of the mixture. By definition, the mass fluxes of each species are related through

$$\sum_{i=1}^{\nu} \vec{M}_i = 0 \tag{3}$$

Furthermore, the multicomponent diffusion coefficients are not only functions of both ρ and T, but also of the composition of the mixture. Therefore, they cannot be tabulated for a general case because the very process of diffusion changes their values. We then must exhibit the dependence of the $\vec{V}_i$ upon the quantities $\mathcal{D}_{ij}$ which are directly proportional to $1/\rho$ and are a complicated function of T alone. Consider the quantity $\vec{M}_i'$ where

$$\vec{M}_i' = \vec{M}_i + D_i^T \nabla \ln T \,. \tag{4}$$

It can be shown that (3)

$$\sum_{j\neq i}^{\nu} X_i X_j \frac{\overline{W}}{\rho \mathcal{D}_{ij}} \left(\frac{\vec{M}_j'}{W_j X_j} - \frac{\vec{M}_i'}{W_i X_i} \right) = \vec{d}_i, \quad i = 1, 2, \ldots, \nu \tag{5}$$

where $\overline{W}$ is the mean molecular weight of the mixture. Then, rearranging the above, we find the following set of ν independent equations for the $\vec{M}'_i$:

$$\sum_{j\neq i}^{\nu} \frac{\overline{W}}{\rho \mathcal{D}_{ij}} \left(X_i \frac{\vec{M}'_j}{W_j} - X_j \frac{\vec{M}'_i}{W_i} \right) = \vec{d}_i, \quad i = 1, 2, \ldots, \nu-1, \tag{6}$$

$$\sum_{i=1}^{\nu} \vec{M}'_i = 0 \, . \tag{7}$$

Equation 7 may be used to eliminate $\vec{M}'_\nu$ in the set eq. 6. Then $\vec{M}'_1$ is given by

$$\vec{M}'_1 = \frac{\begin{vmatrix} \vec{d}_1/X_1 & A_{12} & \cdots & A_{1,\nu-1} \\ \vec{d}_2/X_2 & A_{22} & \cdots & A_{2,\nu-1} \\ \vdots & \vdots & & \vdots \\ \vec{d}_{\nu-1}/X_{\nu-1} & A_{\nu-1,2} & \cdots & A_{\nu-1,\nu-1} \end{vmatrix}}{\begin{vmatrix} A_{11} & A_{12} & \cdots & A_{1,\nu-1} \\ A_{21} & A_{22} & \cdots & A_{2,\nu-1} \\ \vdots & \vdots & & \vdots \\ A_{\nu-1,1} & A_{\nu-1,2} & \cdots & A_{\nu-1,\nu-1} \end{vmatrix}} \frac{\rho}{\overline{W}} \tag{8}$$

where

$$A_{ii} = -\sum_{j\neq i}^{\nu} \frac{X_j}{X_i W_i \mathcal{D}_{ij}} - \frac{1}{W_\nu \mathcal{D}_{i\nu}} \, , \quad i = 1, 2, \ldots, \nu-1, \tag{9}$$

and

$$A_{ij} = \frac{1}{W_j \mathcal{D}_{ij}} - \frac{1}{W_\nu \mathcal{D}_{i\nu}} \, , \quad i, j = 1, 2, \ldots, \nu-1, \quad i \neq j \, . \tag{10}$$

The solution for the other mass fluxes will be of the same form with the column of $\vec{d}_i/X_i$ substituted for the appropriate column of A_{ij}. In the subsequent discussion, the superscript * will ordinarily indicate a reduced variable and a subscript o will indicate a standard characteristic value. We define the reduced variables

$$W_i^* = W_i/W_o, \quad \nabla^* = \nabla L_o, \quad X_i^* = X_i, \quad Y_i^* = Y_i,$$

$$\mathscr{D}_{ij*} = \mathscr{D}_{ij}/\mathscr{D}_o, \quad D_i^{T^*} = D_i^T/\rho_o\mathscr{D}_o, \quad p^* = p/p_o .$$

The conditions $X^* = X$ and $Y^* = Y$ are equivalent to a restriction on our scaling to cases where we have initially similar concentrations of the fluid components. The more general case is less useful and is certainly much more complicated.

The quantity $\vec{d}_i L_o$ is (from eq. 2)

$$\vec{d}_i L_o = \nabla^* X_i^* + (X_i^* - Y_i^*)\nabla \ln p^* - Y_i^* \left[\frac{\rho L_o \vec{f}_i}{p} - \sum_{k=1}^{\nu} \frac{\rho_k L_o \vec{f}_k}{p} \right]. \qquad (11)$$

Let $f^* = f/f_o$; the term in brackets in eq. 11 then becomes

$$\left[\frac{f_o \rho_o L_o}{p_o} \left(\frac{\rho^* \vec{f}^*}{p^*} - \sum_{k=1} \frac{\rho_k^* \vec{f}_k^*}{p^*} \right) \right] .$$

Hence, in order for a similar solution to exist to the Navier-Stokes equations when the mass flux is introduced, it is necessary to have the dimensionless group $(f_o \rho_o L_o/p_o)$ constant. This is the first of the nine similarity groups. Often we are only concerned with gravity as an external force and the characteristic force per unit mass can be taken as the gravitational acceleration g. The above group may then

be expressed in terms of more common dimensionless groups as

$$g\rho_o L_o/P_o = \gamma_o M_o^2/Fr_o$$

where γ is the ratio of the specific heats at constant pressure and volume, M is the Mach number, and Fr is the Froude number. We have now succeeded in expressing the quantity $\vec{d}_i L_o$ in dimensionless form. Let us define

$$A^*_{ii} = -\sum_{j\neq i}^{\nu} \frac{X_{j*}}{X_i^* W_i^* \mathcal{D}_{ij}^*} - \frac{1}{W_\nu^* \mathcal{D}_{i\nu}^*}, \quad i = 1, 2, \ldots, \nu-1,$$

$$A^*_{ij} = \frac{1}{W_j^* \mathcal{D}_{ij}^*} - \frac{1}{W_\nu^* \mathcal{D}_{i\nu}^*}, \quad i, j = 1, 2, \ldots, \nu-1, \quad i \neq j.$$

Then, from eq. 8, we have the following expression for $\vec{V}_1'$:

$$\vec{V}_1' = \frac{\begin{vmatrix} \vec{d}_1 L_o/X_1^* & A^*_{12} & \cdots & A^*_{1,\nu-1} \\ \vec{d}_2 L_o/X_2^* & A^*_{22} & \cdots & A^*_{2,\nu-1} \\ \vdots & \vdots & & \vdots \\ \vec{d}_{\nu-1} L_o/X^*_{\nu-1} & A^*_{\nu-1,2} & \cdots & A^*_{\nu-1,\nu-1} \end{vmatrix}}{\begin{vmatrix} A^*_{11} & A^*_{12} & \cdots & A^*_{1,\nu-1} \\ A^*_{21} & A^*_{22} & \cdots & A^*_{2,\nu-1} \\ \vdots & \vdots & & \vdots \\ A^*_{\nu-1,1} & A^*_{\nu-1,2} & \cdots & A^*_{\nu-1,\nu-1} \end{vmatrix}} \frac{W_o}{\overline{W}} \frac{\rho^*}{\rho_i^*} \frac{\mathcal{D}_o}{L_o}. \qquad (12)$$

We will have a similar expression for $\vec{V}_i'$. Hence $\vec{V}_i'$ may be

written as $\vec{V}_i = (\mathcal{D}_o/L_o)\vec{G}_1^{**}$, where the $\vec{G}_1^{**}$, for instance, would be defined by eq. 12 and is a dimensionless function entirely in terms of reduced variables and the similarity group $g\rho_o L_o/p_o$.

From eq. 1 the thermal diffusion contribution to the total diffusion velocity $\vec{V}_i$ is given by $\vec{V}_i^T$ where

$$\rho_i \vec{V}_i^T = - D_i^T \nabla \ln T$$

or, if we let $T^* = T/T_o$,

$$\vec{V}_i^{T*} = - \frac{\rho_o}{\rho_i} \mathcal{D}_o D_i^{T*} \frac{1}{L_o} \nabla^* \ln T^* = \left(\frac{\mathcal{D}_o}{L_o} \right) \vec{H}_i^* .$$

Therefore, for the most general case,

$$\vec{V}_i = \left(\frac{\mathcal{D}_o}{L_o} \right) \vec{G}_i^* \tag{13}$$

where $\vec{G}_i^* = \vec{G}_i^{**} + \vec{H}_i^*$. Equation 13 is the desired result for $\vec{V}_i$. For a simple binary mixture,

$$\vec{V}_i = - D_i \nabla \ln Y_i = \left(\frac{\mathcal{D}_o}{L_o} \right) (- D_i^* \nabla^* \ln Y_i^*) ,$$

which is of the same form as eq. 13 if we let $- D_i^* \nabla^* \ln Y_i^* = \vec{G}_i^*$. Therefore, we conclude that the diffusion velocity is expressible as a function of a characteristic binary diffusion coefficient and length for the general multicomponent case as well as the binary mixture case and, furthermore, that (for the purpose of the similarity analysis) the functional form is the same in both cases. Now the Navier-Stokes equations may be non-dimensionalized.

A. Continuity Equation

The continuity equation for species i may be written as (2)

$$\frac{\partial Y_i}{\partial t} = \frac{w_i}{\rho} - v_\ell \frac{\partial Y_i}{\partial x_\ell} - \frac{1}{\rho} \frac{\partial}{\partial x_\ell} (Y_i V_{i,\ell}) \tag{14}$$

where w_i is the mass rate production of species i per unit volume $(d\rho_i/dt)$ and tensor notation is used. Let us define $t^* = tU_{io}$ where U_{io} is a characteristic frequency associated with the i^{th} chemical reaction (i.e., with the formation of species i), $w_i/\rho_o = w_i/\rho Y_i = U_{io} U_i^*$. Then, using previous relationships,

$$\frac{\partial Y_i^*}{\partial t^*} = U_i^* Y_i^* - \left(\frac{v_o}{L_o U_{io}} \right) v_\ell^* \frac{\partial Y_i^*}{\partial x_\ell^*} + \frac{\mathcal{D}_o}{U_{io} L_o^2} \frac{1}{\rho^*} \frac{\partial [G^* Y_i^* \rho^*]}{\partial x_\ell^*}. \tag{15}$$

Similar solutions are possible if the groups D_I and D_{II} are kept invariant, where these are Damkohler's groups I and II, defined by (4) $D_{Io} = U_{io} L_o / v_o$, $D_{IIo} = U_{io} L_o^2 / \mathcal{D}_o$. We actually have two different types of D_{IIo} as we have two different types of diffusion characterized by $\mathcal{D}_{ij_o}$ and D_{io}^T.

B. Momentum Equation

The general form of the equations for conservation of momentum is (5)

$$\frac{\partial v_j}{\partial t} + v_i \frac{\partial v_j}{\partial x_i} = - \frac{1}{\rho} \frac{\partial p}{\partial x_j} - \frac{1}{\rho} \frac{\partial \left[\frac{2}{3} \mu \frac{\partial v_i}{\partial x_i} \right]}{\partial x_j} + \frac{1}{\rho} \frac{\partial}{\partial x_\ell} \left[\mu \left(\frac{\partial v_\ell}{\partial x_j} + \frac{\partial v_j}{\partial x_\ell} \right) \right],$$

$$j = 1, 2, 3 \tag{16}$$

Defining $\mu^* = \mu/\mu_o$, we obtain

$$\left(\frac{L_o U_{io}}{v_o}\right)\frac{\partial v_j^*}{\partial t^*} + v_\ell^*\frac{\partial v_j^*}{\partial x_\ell^*} = -\left(\frac{p_o}{\rho_o v_o^2}\right)\frac{1}{\rho^*} + \left(\frac{\mu_o}{\rho_o L_o v_o}\right)\left\{\frac{2}{3\rho^*}\frac{\partial\left(\mu^*\frac{\partial v_i^*}{\partial x_i^*}\right)}{\partial x_j^*}\right.$$

$$\left. + \frac{1}{\rho^*}\frac{\partial}{\partial x_\ell^*}\left[\mu^*\left(\frac{\partial v_\ell^*}{\partial x_j^*} - \frac{\partial v_j^*}{\partial x_\ell^*}\right)\right]\right\}, \quad j = 1, 2, 3. \tag{17}$$

We have the new groups M and Re (the Mach and Reynolds numbers) where

$$\gamma_o M_o^2 = \frac{\rho_o v_o^2}{p_o} \quad \text{and} \quad Re_o = \frac{\rho_o v_o L_o}{\mu_o}.$$

C. Energy Equation

Assume that the heat flux vector $\vec{q}$ appearing in the general equation for the conservation of energy can be expressed in terms of a thermal conductivity λ and a term caused purely by the diffusion of enthalpy. This is perhaps not the most general case but we will see how it can easily be generalized to any situation. The energy equation is (5)

$$\frac{\partial(\rho e)}{dt} + v_i\frac{\partial(\rho e)}{\partial x_i} + \rho e\frac{\partial v_\ell}{\partial x_\ell} + \frac{\partial(\frac{1}{2}\rho v_\ell v_\ell)}{\partial t} + v_i\frac{\partial(\frac{1}{2}\rho v_\ell v_\ell)}{\partial x_i} + \frac{1}{2}\rho v_\ell v_\ell\frac{\partial v_k}{\partial x_k}$$

$$= \rho f_\ell v_\ell + \sum_{k=1}^{\nu}\rho_k f_{k,\ell} V_{k,\ell} - \frac{\partial p}{\partial x_\ell}v_\ell - \frac{\partial\left[\frac{2}{3}\mu\frac{\partial v_i}{\partial x_i}\right]}{\partial x_\ell}v_\ell$$

$$+ \frac{\partial}{\partial x_\ell}\left[\mu v_j\left(\frac{\partial v_\ell}{\partial x_j} + \frac{\partial v_j}{\partial x_\ell}\right)\right] + \frac{\partial}{\partial x_\ell}\left(\lambda\frac{\partial T}{\partial x_\ell}\right) - \frac{\partial}{\partial x_\ell}\left(\rho\sum_{k=1}^{\nu} Y_k h_k V_{k,\ell}\right), \tag{18}$$

where e and h_k are the total energy and the enthalpy for species k respectively, and we are again using tensor notation. We now define $h^* = h/c_{po}T_o$, $e^* = e/c_{po}T_o$, $\lambda^* = \lambda/\lambda_o$, $f^* = f/g$ (again we assume only gravitational external forces). We have chosen to use a characteristic specific heat rather than energy; this of course is no restriction on the results. The energy equation becomes

$$(\rho_o c_{po} T_o U_{io}) \frac{\partial(\rho^* e^*)}{\partial t^*} + \left(\frac{v_o \rho_o c_{po} T_o}{L_o}\right) \left[v_\ell^* \frac{\partial(\rho^* e^*)}{\partial x_\ell^*} + \rho^* e^* \frac{\partial(v_\ell^*)}{\partial x_\ell^*} \right]$$

$$+ (\rho_o v_o^2 U_{io}) \frac{\partial(\frac{1}{2}\rho^* v_\ell^* v_\ell^*)}{\partial t^*} + \left(\frac{\rho_o v_o^3}{L_o}\right) \left[v_i^* \frac{\partial(\frac{1}{2}\rho^* v_\ell^* v_\ell^*)}{\partial x_i^*} + (\tfrac{1}{2}\rho^* v_\ell^* v_\ell^*) \frac{\partial v_k^*}{\partial x_k^*} \right]$$

$$= (\rho_o g v_o) \rho^* f_\ell^* v_\ell^* + \left(\frac{\rho_o \mathcal{D}_o g}{L_o}\right) \sum_{k=1}^{\nu} \rho_k^* f_{k,\ell}^* G_{k,\ell}^* - \left(\frac{\rho_o v_o}{L_o}\right) \frac{\partial p^*}{\partial x_\ell^*} v_\ell^*$$

$$- \frac{\mu_o v_o^2}{L_o^2} \left\{ \frac{\partial\left[\frac{2}{3}\mu^* \frac{\partial v_i^*}{\partial x_i^*}\right]}{\partial x_\ell^*} v_\ell^* - \frac{\partial}{\partial x_\ell^*}\left[\mu^* v_j^* \left(\frac{\partial v_\ell^*}{\partial x_j^*} + \frac{\partial v_j^*}{\partial x_\ell^*}\right)\right] \right\}$$

$$+ \left(\frac{\lambda_o T_o}{L_o^2}\right) \frac{\partial}{\partial x_\ell^*} \left[\lambda^* \frac{\partial T^*}{\partial x_\ell^*}\right] - \frac{c_{po} T_o \mathcal{D}_o \rho_o}{L_o^2} \frac{\partial}{\partial x_\ell^*} \left[\rho^* \sum_{k=1}^{\nu} Y_k^* h_k^* G_{k,\ell}^*\right]. \quad (19)$$

Multiplying eq. 19 through by $L_o/p_o v_o$ gives the following dimensionless groups:

(a) $\dfrac{\rho_o c_{po} T_o U_{io} L_o}{p_o v_o}$ (d) $\gamma_o M_o^2$ (g) $\dfrac{\mu_o v_o}{p_o L_o}$

(b) $\dfrac{\rho_o c_{po} T_o}{p_o}$ (e) $\dfrac{\rho_o g L_o}{p_o}$ (h) $\dfrac{\lambda_o T_o}{p_o v_o L_o}$

(c) $\dfrac{\rho_o v_o U_{io} L_o}{p_o}$ (f) $\dfrac{\rho_o \mathcal{D}_o g}{p_o v_o}$ (i) $\dfrac{c_{po} T_o \mathcal{D}_o \rho_o}{p_o v_o L_o}$

Both (d) and (e) were derived before. We also see that

$$(g) = \left(\frac{\mu_o}{\rho_o v_o L_o}\right)\left(\frac{\rho_o v_o^2}{p_o}\right) = (\gamma)(M^2)/(\mathrm{Re}), \quad (c) = \left(\frac{U_{io} L_o}{v_o}\right)\left(\frac{\rho_o v_o^2}{p_o}\right) =$$

$$(D_I)(\gamma)(M^2), \quad (f) = \left(\frac{\mathcal{D}_o}{L_o^2 U_{io}}\right)\left(\frac{\rho_o g L_o}{p_o}\right)\left(\frac{U_{io} L_o}{v_o}\right) = (D_I)(\gamma)(M^2)/(\mathrm{Fr})(D_{II}).$$

This leaves (a), (b), (h), and (i) unidentified. However, we note that (i) = (a)/(D_{II}) = (b)(D_I). Only three new parameters are obtained: $\rho_o c_{po} T_o/p_o$, γ_o, and $\lambda_o T_o/p_o v_o L_o$. In more standard terminology we have

$$\left(\frac{p_o v_o L_o}{\lambda_o T_o}\right)\left(\frac{\rho_o c_{po} T_o}{p_o}\right)\left(\frac{\mathcal{D}_o}{L_o^2 U_{io}}\right)\left(\frac{U_{io} L_o}{v_o}\right) = \frac{\rho_o c_{po} \mathcal{D}_o}{\lambda_o} = \mathrm{Le}\ (\text{Lewis number}),$$

and

$$\left(\frac{p_o}{\rho_o c_{po} T_o}\right)\left(\frac{\rho_o v_o^2}{p_o}\right)\left(\frac{\gamma_o}{2}\right) = \frac{v_o^2/2}{c_{po} T_o/\gamma_o} = \Phi\ .$$

A final list of the nine independent dimensionless groups we have found is

$$\text{(a)}\ \gamma_o \qquad \text{(d)}\ Sc'_{io} = \frac{\mu_o}{D'_{io}} \qquad \text{(g)}\ Fr_{k,o} = \frac{v_o^2}{gL_{k,o}}$$

$$\text{(b)}\ Re_k = \frac{\rho_o v_o L_{ko}}{\mu_o} \qquad \text{(e)}\ Pr = \frac{c_{p,o}\mu_o}{\lambda_o} \qquad \text{(h)}\ D_{I,k,r} = \frac{L_{ko}U_{r,o}}{v_o} \qquad \text{(A)}$$

$$\text{(c)}\ Sc_{ijo} = \frac{\mu_o}{\rho_o \mathbb{D}_{ijo}} \qquad \text{(f)}\ M_o = \sqrt{\frac{\rho_o v_o^2}{\gamma_o p_o}} \qquad \text{(i)}\ \Phi = \frac{v_o^2/2}{c_{po}T_o/\gamma_o}$$

where the Schmidt number $(Sc) = (D_{II})/(Re)(D_I)$ replaces D_{II}, and the Prandtl number $(Pr) = (Sc)(Le)$ replaces Le. The indices k may run from 1 to ξ where there are ξ characteristic lengths and the indices i and j may run from 1 to ν for a ν-component mixture. There are exactly $(\nu^2+\nu)/2$ independent Sc since $\mathbb{D}_{ij} = \mathbb{D}_{ji}$.

Furthermore, the multiplicity of the groups in the set (A) may be even greater if other multiple characteristic values exist, (e.g., we could have more than one v_o or T_o, etc.). Sometimes these additional values are expressed in a form somewhat different from the quantities given in (A). For instance for two different characteristic lengths we must consider the two Reynolds numbers $Re_1 = \rho_o v_o L_{o1}/\mu_o$, $Re_2 = \rho_o v_o L_{o2}/\mu_o$. One could just as well consider the quantities Re_1 and L_{o1}/L_{o2}, which saves writing but may create the illusion that we have created a new type of similarity group given by L_{o1}/L_{o2} (which may really be considered as the ratio of Re_1 and Re_2). We will find that throughout the literature we will run into many such varieties of different appearing dimensionless groups and it must be realized that they all are expressible as combinations of the members of the set (A) utilizing, perhaps, different characteristic parameters.

One important group of this type is designated as D_{III} (Damköhler's third similarity group). This is given by

$$D_{IIIo,i,k} = \Delta h_{io} U_{io} L_k / v_o c_{p,o} T_o$$

where Δh_{io} is the characteristic heat per unit mass released in the i^{th} reaction, and $c_{p,o}$ is the specific heat of the frozen mixture under the characteristic conditions. It is hard to see at first that this has any relation to the members of the set (A). However, in a reacting mixture there are two types of characteristic specific heats, which might be defined as: $c_{p,o,1} T_o = \Delta h_{io}$, and $c_{p,o,2} = c_{p,o}$. Then by means analogous to those in the previous paragraph we can construct the ratio $c_{p,o,1}/c_{p,o,2} = \Delta h_{io}/c_{p,o} T_o$ (which might be considered the ratio of two Prandtl numbers, i.e., it is directly related to the similarity groups previously derived). Then it is seen that

$$D_{IIIo} = (c_{p,o,1})(D_I)/(c_{p,o,2})$$

or the group D_{III} has no new fundamental significance. However, it will often be convenient to refer to this quantity when discussing scaling problems where chemical reaction is present. Note that if the reaction specific heat had been included in our original list of dimensional dependent quantities, D_{III} would have naturally occurred as the tenth similarity parameter during the analysis.

In the next section the same situation occurs when a radiation heat flux is considered. This case is easily handled by defining a new characteristic λ_o in a manner analogous to the above definition of a new characteristic specific heat.

It can be shown that for special cases it is quite convenient to simplify the heat flux problem by defining

$$q = - (\lambda + \lambda_{ch})/\nabla T$$

where λ_{ch} is an effective thermal conductivity coefficient which includes the effects of chemical reaction (6). From eqs. 1 and 18 λ_{ch} is given by

$$\lambda_{ch} = \sum_{i=1}^{\nu} \sum_{j=1}^{\nu} \frac{C_T^2}{\rho} D_{ij} W_i W_j h_i \frac{dx_j}{dT} . \qquad (20)$$

Although the expression has been validated approximately by experiment (10) we gain nothing in our similarity analysis by introducing this expression into the energy equation. As seen previously the more complicated expression for the enthalpy transport due to diffusion gave rise to no new similarity groups. However, in special cases λ_{ch} may be a useful concept for scaling.

III. SIMILARITY PARAMETERS FOR GAS MIXTURES INCLUDING RADIATION TRANSPORT

To consider radiation effects, we want to exhibit separately those parameters specifically relating to them. We must consider the following effects:

1. Included in the pressure considered in the momentum and energy equations is the internal force $\vec{f}_{ra}$, the radiation force per unit volume.

2. Included in the heat flux vector $\vec{q}$ is the contribution of the radiation heat flux vector $\vec{F}_{ra}$, the radiant energy per unit area per second.

These two new quantities enter the conservation equations in a manner analogous to quantities previously defined (i.e., pressure and heat flux). It is therefore expected that the dimensionless quantities that could arise from their introduction will still be of the form of those in the set (A). Indeed we will see that such is the case. However, in order to scale a radiative system we must know the precise dependence of $\vec{f}_{ra}$ and $\vec{F}_{ra}$ upon such variables as T, p, ρ, etc. It may turn out then that in the formulation of $\vec{f}$ and $\vec{F}$ in terms of the dependent variables, new quantities arise giving a series of new dimensionless groups. In the three different radiation models we consider below, two new important similarity groups arise in the first two models, whereas only one appears in the last formulation.

From the conservation equations we can expect quantities analogous to the Mach number and the Prandtl number to arise from the introduction of the radiation. These would correspond to a new

characteristic pressure $p'_o = f_{ra,o} L_o$ and a new characteristic thermal conductivity $\lambda_o = F_{ra,o} L_o / T_o$. The new versions take the form

$$\frac{\rho_o v_o^2}{\gamma_o f_{ra,o} L_o} \quad , \quad \frac{c_{po}/\mu_o T_o}{F_{ra,o} L_o} \quad .$$

However, it is useful to note that these quantities are strictly related because

$$\vec{f} = \int_o^\infty \frac{k_{L,\nu,T}}{c} \vec{F}_\nu \, d\nu \tag{21}$$

where

$k_{L,\nu,T}$ = spectral absorption coefficient/unit length,

c = velocity of light,

$\vec{F}_\nu \, d\nu$ = radiation flux with frequency between ν and $\nu + d\nu$.

Let us define $\vec{F}^* = \vec{F}/F_{ra,o}$ or $d\vec{F} = F_o d\vec{F}^*$, $k^* = k_{L,\nu,T}/k_o$, $\vec{f}^* = \vec{f}/f_{ra,o}$; noting that $d\vec{F} = \vec{F}_\nu \, d\nu$, it follows that

$$\vec{f} = \vec{f}^* f_{ra,o} = \frac{F_{ra,o} k_o}{c} \int_\nu k^* \, d\vec{F}^* \quad . \tag{22}$$

Therefore, we may always choose

$$f_{ra,o} = F_{ra,o} k_o / c \quad . \tag{23}$$

At first sight it would appear that we have just interchanged the variable, $\vec{f}$, for another new variable, $k_{L,\nu,T}$, and have not accomplished anything. However, when we attempt to develop an expression for $F_{ra,o}$ in terms of the independent variables, the parameter $k_{L,\nu,T}$ will appear

in a new dimensionless group. Hence we would then have three groups to consider. By expressing $\vec{f}$ in terms of $k_{L,\nu,T}$ and $\vec{F}$, we reduce the number of similarity groups to two in the general case.

The two groups defined above now become

$$\frac{\rho_o v_o^2 c}{\gamma_o F_{ra,o} k_o L_o} \quad , \quad \frac{c_{po} \mu_o T_o}{F_{ra,o} L_o} \quad .$$

Now the most general case of a radiating system will be considered, viz., the case of a gas with arbitrary opacity. Later, the special cases of gases nearly transparent or opaque will be investigated.

A. Arbitrary Opacities

The radiant flux at a location $\vec{x}_1$, $\vec{F}(\vec{x}_1)$, is computed in a manner similar to that described in Ref. 3, p. 722 and Ref. 7, p. 380. Figure 1 shows the geometric setup for calculating the radiant flux emitted at $\vec{x}_2$ into the solid angle $d\Omega$ terminating at our point of observation, $\vec{x}_1$. The quantity, $x_{12} = |\vec{x}_1 - \vec{x}_2|$.

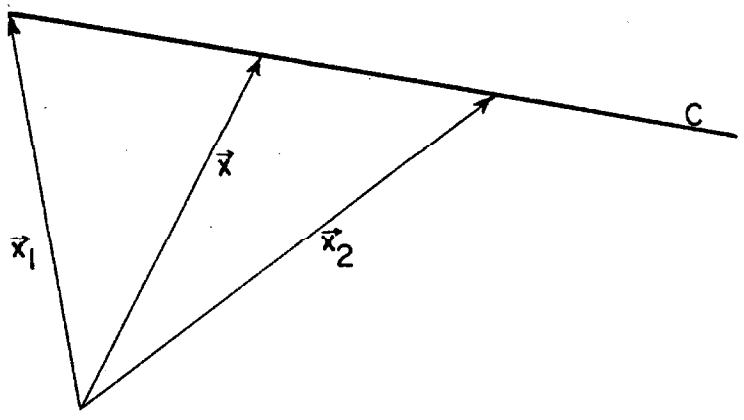

Fig. 1. Schematic diagram showing the definitions of $\vec{x}_1$, $\vec{x}$, $\vec{x}_2$, and C.

The spectral intensity emitted at $\vec{x}_2$ into the solid angle $d\Omega$ falls off as $(1/x_{12})^2$, irrespective of reabsorption. Then the total spectral flux emitted in direction $\vec{x}_1 - \vec{x}_2$ is

$$R^o_{\nu,\, T(\vec{x}_2)}\, k_{L,\, \nu,\, T(\vec{x}_2)} \left[\frac{\vec{x}_1 - \vec{x}_2}{x_{12}} \right] \frac{dV_2}{4\pi x_{12}^2}$$

where

dV_2 = volume element at $\vec{x}_2$,

$R^o_{\nu,\, T(\vec{x}_2)}$ = spectral radiance of a black body at temperature $T(\vec{x}_2)$

$$= \frac{2\pi h\nu^3}{c^2} \frac{1}{\exp\left[h\nu/kT(\vec{x}_2)\right] - 1} .$$

Including reabsorption, the expression for the spectral flux gains the additional term

$$\exp\left[-\int_o^{x_{12}} k_{L,\, \nu,\, T(\ell)}\, d\ell \right],$$

where we integrate along C in Fig. 1. The total flux at $\vec{x}_1$ is then given by

$$\vec{F}(\vec{x}_1) = 2 \int_o^{\infty} \int_V R^o_{\nu,\, T(\vec{x}_2)} k_{L,\, \nu,\, T(\vec{x}_2)} \left[\frac{\vec{x}_1 - \vec{x}_2}{x_{12}} \right] \frac{1}{4\pi x_{12}^2}$$

$$\times \exp\left[-\int_o^{x_{12}} k_{L,\, \nu,\, T(\ell)} d\ell \right] dV_2\, d\nu . \qquad (24)$$

To write this equation in dimensionless form as a function only

of reduced variables requires the introduction of a similarity group

$$Bu_{\nu,T} = k_{L,\nu,T}L \tag{25}$$

which is called the Bouguer number.† It is essentially the ratio of two characteristic lengths as k has the dimensions of $(\text{length})^{-1}$. However, it will be convenient to consider this as a new group originating through the introduction of a new parameter $k_{L,\nu,T}$ into the original list of variables in Sec. I. Let us define $k^*_{L,\nu,T} = k_{L,\nu,T}/k_o$, $\nu^* = \nu/\nu_o$ where $\nu_o = kT_o/h$, $dV_2^* = dV_2/L_o^3$, $x^* = x/L_o$:‡

$$\vec{F}(\vec{x}) = \vec{F}^* F_{ra,o} = \frac{k^4 T_o^4 Bu_o}{h^3 c^2} \int_o^\infty \int_{V^*} \frac{\vec{x}_1^* - \vec{x}_2^*}{x_{12}^{*3}} \frac{1}{e^{\nu^*/T^*} - 1}$$

$$\times \exp\left[-\int_o^{x_{12}^*} (Bu)_o k^* d\ell^*\right] k^* dV^* d\nu^* , \tag{26}$$

or we can choose

$$F_{ra,o} = \frac{k^4 T_o^4 Bu_o}{h^3 c^2} . \tag{27}$$

The equation for $F_{ra,o}$ may be substituted into the previously given expressions for the similarity groups yielding the quantities

$$\frac{\rho_o v_o^2 c h^3 c^2}{\gamma_o k^4 T_o^4} , \quad \frac{c_{po} \mu_o T_o h^3 c^2}{L_o k^4 T_o^4}$$

†Pierre Bouguer (1698-1756) was a French pioneer in radiation transfer studies. The Bouguer number was named in the USSR (8, 9).

‡From now on, a "k" without a subscript will be Boltzmann's constant.

where we have used the fact that $k_o L_o = Bu_o$ and is independently held constant. But the ratio of these two groups is

$$\frac{c_{po}\mu_o T_o \gamma_o}{\rho_o v_o^2 c L_o} = \left(\frac{v_o}{c}\right) \frac{\gamma_o^2}{2\Phi_o Re_o} \quad . \tag{28}$$

Therefore, if we consider c to be a characteristic velocity, the two radiation groups are not independent, and only one of them need be considered for a scaling process.

We further observe that the fact that c acts as a characteristic velocity leads to a severe restriction on the general scaling of a combined radiation and flow field. As c is a universal constant, we are required to keep <u>all</u> characteristic velocities constant, i.e., scaling is impossible with respect to velocity. However, the significance of c as a characteristic velocity is probably related to the comparison of the rate of radiation transport to the rate of convective energy transport. For all practical purposes the radiation transport rate can be considered infinite without a noticeable perturbation of the characteristics of the flow field. The finite time required for radiation transport would be important only for fluid flow velocities of the order of c. For non-relativistic flow fields, the characteristic velocity c can be ignored. If this is done, the addition of radiation to the scaling problem has introduced only two types of dimensionless groups.

The inability to reduce the energy flux equation to a simpler form than eq. 26 means that, to a reasonable approximation, it will be necessary to consider a continuum of Bouguer numbers corresponding

to the continuous range of frequency. This results in a severely restrictive scaling criterion which would be extremely difficult to satisfy. An attempt to change the physical size of a given system, keeping Bu constant, would require that k_{L,ν,T_o} change according to eq. 25, i.e.,

$$k_{L,\nu,T_o} L_o = \text{constant}, \quad \text{for all } \nu . \tag{29}$$

This requirement is the result of the fact that integrations over the volume and the frequency in eq. 26 cannot be uncoupled. This is obvious from the mathematical structure of eq. 26; physically it is a result of the important and significant fact that the integral depends upon the distribution of temperature throughout the entire region of interest; therefore, in general, it is impossible to define a "mean linear absorption coefficient" that could be defined in terms of local conditions. Therefore, for scaling in the general case of arbitrary opacities, eq. 29 must hold. In the special cases considered below it will be possible to define a mean absoprtion coefficient which can be tabulated.

If scaling is desired without change of temperature, it may be possible to satisfy even the very restrictive condition, $(Bu)_o$ = constant for all frequencies. This will be demonstrated in Secs. VI - VIII where specific expressions are assumed for k_ν.

B. Diffusion Approximation

The diffusion approximation applies to a gas system which is highly absorbing with respect to radiation. The continuous absorption and emission of photons on a microscopic scale is analogous to the diffusion of the photons through the gas. It is not surprising, therefore,

that this model yields quantities similar to those that would be derived if the photons were considered billiard balls bouncing through the medium, i.e., quantities analogous to those in the kinetic theory of gases are obtained. After manipulation of eq. 24 the energy flux can be expressed in the following form (10)

$$\vec{F} = - \lambda_{ra} \nabla T \tag{30}$$

where

$$\lambda_{ra} = \frac{16\sigma T^3}{3\bar{k}_{L, Ro}}$$

Here σ is the Stefan-Boltzmann constant and the quantity $\bar{k}_{L, Ro}$ is the Rosseland mean absorption coefficient which is defined by

$$\bar{k}_{L, Ro} = \frac{\int_o^\infty \left(\frac{dB_\nu^o}{dT} \right) d\nu}{\int_o^\infty \frac{1}{k_{L, \nu, T}} \left(\frac{dB_\nu^o}{dT} \right) d\nu} \tag{31}$$

where B_ν^o = the black body spectral steradiancy. (7).

The radiation similarity groups take the form

$$Pr' = c_{po} \mu_o / \lambda_{ra, o} \tag{32}$$

where

$$\lambda_{ra, o} = \sigma T_o^3 / k_o,$$

and

$$Bu = k_{L, Ro} L_o .$$

The diffusion approximation results in a specific equation for the radiation force, viz. (10)

$$f = - (16\sigma T^3/3c)\nabla T \tag{33}$$

which leads to

$$f_o = \sigma T_o^4/cL_o \, . \tag{34}$$

Using this, one constructs a parameter that is commonly found in the literature

$$\mathcal{R} = \frac{4\sigma T_o^4/c}{\rho_o v_o^2/2} \tag{35}$$

which, as previously indicated, is not independent of Pr'. This group directly shows the relative energy per unit volume carried by the radiation and the fluid flow under the characteristic conditions.

The quantity Bu is no longer a function of frequency and, from eq. 31, it is determined only by local conditions. Therefore, if the temperature dependence of $\overline{k}_{L, Ro}$ is known and is a simple function of T, it may be possible to scale the radiation field with respect to temperature, impossible in the case of a gas with arbitrary opacity (Sec. III, A).

C. Transparent Gases

The opposite extreme to the above is that of a nearly transparent gas. By "nearly transparent" we mean that for all important frequencies, $k_{L, \nu, T} L \ll 1$, so that terms of the form $[1 - \exp(- k_{L, \nu, T} x)]$ can be expanded and set equal to $k_{L, \nu, T} x$ to a good approximation. The

energy transfer by radiation is again characterized by a single linear absorption coefficient, $\overline{k}_{L,P\ell}$, the Planck absorption coefficient, defined by (10)

$$\overline{k}_{L,P\ell} = \frac{\pi}{\sigma T^4} \int_o^\infty k_{L,\nu,T} B_\nu^o \, d\nu \, . \tag{36}$$

However, we have incorporated another simplification into the case of a transparent gas. Reabsorption of the radiation in this case is neglected; hence there will be no radiation pressure acting on the gas. Therefore there will be no characteristic force associated with this model. This condition is inherent in the model and is not an additional assumption.

For the case of the transparent gas, the divergence of the radiation flux, which would be the quantity appearing in the energy conservation equation, is given by (10)

$$\nabla \cdot \vec{F} = \int \epsilon_\nu \, d\nu = 4\sigma T^4 \overline{k}_{L,P\ell} \tag{37}$$

where

$$\epsilon_\nu = 4\pi k_{L,\nu,T} B_\nu^o \, .$$

It is again seen that the divergence of the radiation flux depends only upon local conditions and therefore scaling with respect to temperature is theoretically possible, as in the case of the diffusion approximation. Specifically we must keep the radiation Prandtl number constant. Introducing the usual reduced variables into eq. 37, we find

$$\nabla^* \cdot \vec{F}^* \left(\frac{F_{ra,o}}{L_o} \right) = 4\sigma T_o^4 k_o T^{*4} k^{*4} \, , \tag{38}$$

or we may choose $F_{ra,o}$ as

$$F_{ra,o} = \sigma T_o^4 k_o L_o \, . \tag{39}$$

The previously derived similarity group becomes

$$\frac{c_{po}\mu_o}{\sigma T_o^3 k_o L_o^2} \, .$$

Furthermore, this is the only similarity parameter that arises when the transparent gas assumption is valid.

Again a somewhat different group is common in the literature. This is ordinarily denoted by Γ where

$$\Gamma_o = \frac{\sigma T_o^4 \bar{k}_{L,Pl,o} L_o}{\rho_o v_o c_{po} T_o} \, . \tag{40}$$

It is easily verified that Γ is related to the basic quantities we have found by multiplying Γ by Re_o. The Γ may be thought of as representing the ratio of the radiative energy loss, from the system per unit area, to the rate of convective enthalpy transport per unit area, evaluated under the characteristic conditions. The parameter Γ plays an important role, for instance, in problems of stellar turbulence (11).

Still another similarity group is sometimes associated with the case of a radiating gas. This is the so-called Boltzmann number, Bo, where

$$Bo = \frac{\sigma T_o^3}{\rho_o v_o c_{po}} = \frac{\Gamma_o}{Bu_o} \, . \tag{41}$$

To summarize the three radiation cases considered, the scaling criteria are the following:

A. Arbitrary opacities

The groups

$$\frac{\rho_o v_o^2 c^3 h^3}{\gamma_o k^4 T_o^4}\ ,\quad {}^{k}L,\nu,\ T_o\ {}^{L}o \quad (\text{all } \nu)$$

must be kept constant. Scaling with respect to T is impossible.

B. Diffusion approximation

The groups

$$Pr'_o = \frac{c_{po}\mu_o}{\lambda_{ra,o}}\ ,\quad \bar{k}_{L,Ro}L_o$$

must be kept constant.

C. Transparent gas

The single group

$$\Gamma_o = \frac{\sigma T_o^4 \bar{k}_{L,P\ell,o} L_o}{\rho_o v_o c_{po} T_o}$$

must be kept constant.

IV. EXAMPLES OF SCALING PROBLEMS

Let us identify by the subscripts H and M a large-scale system and the model, respectively. Furthermore, let

$$n_\eta = \frac{\eta_{o;H}}{\eta_{o;M}}$$

denote the scaling parameter for the physical variable η.

A. Scaling of Flow in Transparent Gas for Gas Burner

Suppose it is desired to build a model of a large gas burner and determine its operating characteristics. Assume that the flow velocities are small, i.e., the kinetic energy in the flow field is negligible compared to the enthalpy transport. Then the two groups M and Φ of the set (A) may be neglected. The remaining seven groups plus Γ must be held constant. Temperature will not be scaled, i.e., $n_T = 1$.

We now choose as independent variables the quantities T_o, L_o, ρ_o, and v_o, and will try to express the similarity criteria in terms of n_T, n_L, n_v, and n_ρ. This is seen to be possible from Sec. I where it was assumed that all our variables could be expressed in terms of four independent quantities.

If the flame mixture had a constant composition we could assume that the quantities μ, λ, and $\rho\mathfrak{D}_{ij}$ are all proportional to $T^{1/2}$ and independent of ρ. For a reacting mixture we may have a composition change and this simple dependence is no longer valid for the cases of μ and λ. However, it can be assumed that the deviation from this law will be small unless ionization takes place (12). Then it is not a bad

assumption to set $n_\mu = n_\lambda = n_\rho \Phi_{ij} = n_T^{1/2} = 1$. Assume $k_{L,\nu,T}$ is proportional to ρ, $n_k = n_\rho$.

There will be an appreciable region of non-equilibrium in the flame. From classical chemical kinetics (5)

$$\frac{\partial C_i}{\partial t} = (\nu_i'' - \nu_i') k_f \prod_{j=1}^{n} (C_j)^{\nu_j'} \tag{42}$$

where ν', ν'' are the pertinent stoichiometric coefficients, k_f is the reaction rate constant, and C is the molar concentration. The order of the reaction is defined by

$$\mathcal{O} = \sum_{j=1}^{n} \nu_j' . \tag{43}$$

Therefore at constant temperature, eq. 42 may be written in a reduced form as

$$\frac{\partial(\rho_i^*/W_i^*)}{\partial t^*} \left(\frac{U_{io}\rho_o}{w_o} \right) = (\nu_i'' - \nu_i') k_f \left[\prod_{j=1}^{n} (\rho_j^*/W_j^*) \right] \left(\frac{\rho_o}{W_o} \right)^{\mathcal{O}} . \tag{44}$$

It is now apparent that the ratio of characteristic frequencies is given by $n_{U_i} = n_\rho^{\mathcal{O}-1}$ for $n_T = n_W = 1$.

In the following statement of similarity criteria, we assume that the flame is characterized by a single reaction which may be considered to go to completion, i.e., the recombination kinetic equation may be ignored. In such a manner, we are free to change the pressure (density) over a wide range without affecting the total heat released during the reaction. This is, of course, a physically realistic assumption.

All the quantities appearing in the similarity groups to be considered have been expressed in terms of our four independent variables. The non-trivial scaling conditions become

$$n_{Re} = 1 = n_\rho n_v n_L ,$$

$$n_{D_I} = 1 = n_L n_\rho^{\mathfrak{G}-1} n_v^{-1} ,$$

$$n_\Gamma = 1 = n_L n_v^{-1} .$$

These will all be satisfied if

$$\mathfrak{G} = 1,$$

$$n_v = n_L,$$

and

$$n_\rho = n_L^{-1/2} .$$

Hence scaling is possible only for the unrealistic case of a first order chemical reaction. Also gas injection velocities must be scaled down and the density increased as the square root of the scaling.

B. Scaling of Flow in Transparent Gas for Uncoupled Radiative and Convective Energy Transport

Consider the same problem as above with the additional condition that the radiation constitutes only a small perturbation on the flow field. It may be important to require invariance of the chemical composition profile and of the absolute value of the radiant energy emission rate per unit area of reaction front. In this case, it is pertinent to demand invariance of the Bouguer numbers, rather than Γ. The new condition is

$$n_{Bu} = 1 = n_\rho N_L \, .$$

Together with the constancy of Re and D_I this condition may be satisfied for

$$\Theta = 2, \quad n_v = 1, \quad n_\rho = n_L^{-1} \, .$$

Hence if the size of the system is to be reduced, the operating pressure must be increased proportionally. Scaling is possible only for the important case of second-order, overall rate processes.

V. SCALING PARAMETERS FOR RADIANT ENERGY EMISSION FROM ISOBARIC AND ISOTHERMAL SYSTEMS FOR ARBITRARY OPACITIES AND VARIOUS SPECTRAL LINE AND MOLECULAR BAND MODELS

For isothermal systems at the temperature T, the emitted steradiancy may be calculated from the equation

$$B(T) = \frac{1}{\pi}\int R_{\omega}^{o}\left[1 - \exp(-P_{\omega}X)\right]\, d\omega\,.$$

The results of these calculations are summarized in Table 1a for selected spectral line shapes and in Table 1b for selected vibration-rotation band models.

From the data listed in Tables 1a and 1b, we may draw the following important conclusions:

1. For transparent gases, the steradiancy is directly proportional to ρL irrespective of the spectral line contour or of the band model.
2. The important scaling parameter is ρL at all optical depths for isolated Doppler-broadened lines, and for all band models in which the spectral line structure is effectively smeared out.
3. The steradiancy is proportional to $\sqrt{\rho^2 L}$ at moderate to large optical depths (a) for isolated, collision-broadened lines, (b) for isolated lines with combined collision and Doppler broadening falling in the "square-root region" of the curves of growth. Also for statistical distributions of the lines described under (a) and (b) $\sqrt{\rho^2 L}$ is the important scaling parameter.

Table 1a. Radiation Scaling Rules for Selected Spectral Line Shapes, Isothermal Emitters

Assumed Line Contour	Function of Density (ρ) and Geometrical Length (L) Which Assures Constancy of the Line Radiancy	Restrictive Conditions	Basic Equation(s) or Figures
pure natural line broadening	ρL^* $\sqrt{\rho L}^*$	$(SX/2\pi b) < (2/\pi)$ $(SX/2\pi b) > (2/\pi)$	Eq. (4-28) Eq. (4-29) for constant b
pure collision broadening	ρL^* $\sqrt{\rho^2 L}^*$	$(SX/2\pi b) < (2/\pi)$ $(SX/2\pi b) > (2/\pi)$	Eq. (4-28) Eq. (4-29) for $b \propto p$
pure Doppler broadening	ρL^* ρL $\sqrt{\ln (P'X)}^* = \sqrt{\ln (P' R_g T \rho L)}^*$	$P'X \ll 1$ none $\ln (P'X) \gg 1$	 Eq. (4-8) Eqs. (4-10), (4-11)
combined Doppler and collision broadening	ρL^* $\sqrt{\rho^2 L}^*$	$P_\omega X \ll 1$ for all ω "square-root region" of the curves of growth where $P'X$ is sufficiently large to make R_L independent of the line contour near the line center for all values of $\underline{a}$	Eq. (4-35) Fig. 4-6
first-order Stark broadening	$\rho L n_e^*$	$P_\omega X \ll 1$ for all ω	Eqs. (3-48), (3-48a)

(Notes on following page.)

Table 1a (Continued)

Notes: (a) Quantities identified with an asterisk indicate that the line radiancy is directly proportional to the specified function of ρ and L; without asterisk, constancy of the line radiancy is determined by the specified function of ρ and L although no proportionality exists.

(b) Equation and figure numbers refer to the book Quantitative Molecular Spectroscopy and Gas Emissivities by S. S. Penner, Addison-Wesley Publishing Co., Reading, Mass., 1959. (Ref. 7)

(c) P_ω = spectral absorption coefficient at the wave number ω (in cm^{-1}-$atmos^{-1}$); X = optical depth (in cm-atmos); S = integrated absorption of a spectral line (in cm^{-2}-$atmos^{-1}$); b = dispersion semi-half-width of a spectral line (in cm^{-1}); P' = maximum value of the spectral absorption coefficient at the line center for a spectral line with pure Doppler broadening; n_e = number of electrons per unit volume.

Table 1b. Radiation Scaling Rules for Selected Vibration-rotation Band Models, Isothermal Emitters

Assumed Band Model	Function of Density (ρ) and Geometrical Length (L) Which Assures Constancy of the Band Radiancy	Restrictive Conditions	Basic Equation(s)
non-overlapping spectral lines	applicable results for isolated spectral lines (see Table 1a)	the assumed line contour applies for all of the spectral lines which determine the total band radiancy	applicable equations as listed in Table 1a
rectangular box model	ρL^*	$(\alpha X/\Delta\omega) \ll 1$	Eqs. (11-25), (11-26)
	ρL	none	Eqs. (11-25), (11-26)
just overlapping line model	ρL^*	$P_\omega X \ll 1$ for all ω	Eq. (11-50)
	ρL	none	Eq. (11-49)
	$\sqrt{\ln (C\alpha X/\Delta\omega)}^*$, C = Euler's constant	$(\alpha X/\Delta\omega) \rightarrow \infty$, rotational fine structure smeared out	Eq. (11-143) et seq.
statistical distribution of collision-broadened lines	ρL^*	$(\bar{S}X/2\pi b) \ll 1$ and $(\bar{S}X/\delta^*) \ll 1$	Eq. (11-120a)
	ρL	$(\bar{S}X/2\pi b) \ll 1$	Eq. (11-120a)
	$\sqrt{\rho^2 L}$	$(\bar{S}X/2\pi b) \gg 1$	Eq. (11-120b)
statistical distribution of Doppler-broadened lines	ρL^*	$P_\omega X \ll 1$ for all ω: $(\bar{S}X/\delta^*) \ll 1$	Eqs. (11-118), (4-8)
	ρL	none	Eqs. (11-118), (4-8)
statistical distribution of spectral lines with combined Doppler and collision broadening	ρL^*	$P'X \ll 1$ and $\bar{S}X/\delta^* \ll 1$	Eq. (11-118) and Fig. 4-6
	$\sqrt{\rho^2 L}$	square-root region of the curves of growth for all important contributing spectral lines	Eq. (11-118) and Fig. 4-6
all other band models	ρL^*	$P_\omega X \ll 1$ for all ω	

Table 1b (Continued)

Notes: (a) Quantities identified with an asterisk indicate that the band radiancy is directly proportional to the specified function of ρ and L; without asterisk, constancy of the band radiancy is determined by the specified function of ρ and L although no simple proportionality exists.

(b) Equation and figure numbers refer to the book Quantitative Molecular Spectroscopy and Gas Emissivities by S. S. Penner, Addison-Wesley Publishing Co., Reading, Mass., 1959. (Ref. 7)

(c) P_ω = spectral absorption coefficient at the wave number ω (in cm^{-1}-$atmos^{-1}$);

X = optical depth (in cm-atmos);

α = integrated absorption of a vibration-rotation band (in cm^{-2}-$atmos^{-1}$);

$\Delta\omega$ = effective width of a vibration-rotation band (in cm^{-1});

$\overline{S}$ = constant value of the integrated absorption for each of the spectral lines contributing to the statistical distribution (in cm^{-2}-$atmos^{-1}$);

b = dispersion semi-half-width of the spectral lines (in cm^{-1});

δ^* = mean spacing of spectral lines (in cm^{-1});

P' = maximum value of P_ω at the line center for a spectral line with pure Doppler broadening.

VI. RADIATIVE SCALING PROPERTIES FOR REPRESENTATIVE TEMPERATURE PROFILES

The integral of eq. 24 for the spectral steradiancy B_ν is the formal solution to the linear, first-order differential equation

$$\frac{dB_\nu}{ds^*} = L_o k_\nu (B_\nu^o - B_\nu) \tag{45}$$

where $s^* = s/L_o$ is the distance along the line of sight, and L_o is a characteristic length of the system. Equation 45 has been integrated numerically by means of a fourth order Runga-Kutta method for representative temperature profiles. The temperature profiles are represented by the expressions

$$T = (T_{max} - T_o)(1 - |s^* - 1|^m) + T_o, \quad m = 1, 2, 4. \tag{46}$$

The specified temperature profiles are sketched in Fig. 2.

For local thermodynamic equilibrium, we find for diatomic emitters, to the harmonic-oscillator and rigid-rotator approximation, the following relation for collision broadening:

$$k_\nu = \frac{c^2}{8\pi^2 \nu_o^2} A_{u\to\ell} \left(\frac{p}{kT_o}\right) \frac{\sigma_o}{b_o} \left(\frac{T_o}{T}\right)^{3/2} [1 - \exp(-u_o T_o/T)] g_u$$

$$\times [1 - \exp(-h\nu_o/kT)][\exp(-E_\ell/kT)] \left\{1 + [(\nu - \nu_o)^2/(b_o^2 T_o/T)]\right\}^{-1} \tag{47}$$

Here ν_o is the frequency at the center of the emitted spectral line; $A_{u\to\ell}$ is the Einstein coefficient for spontaneous emission for the

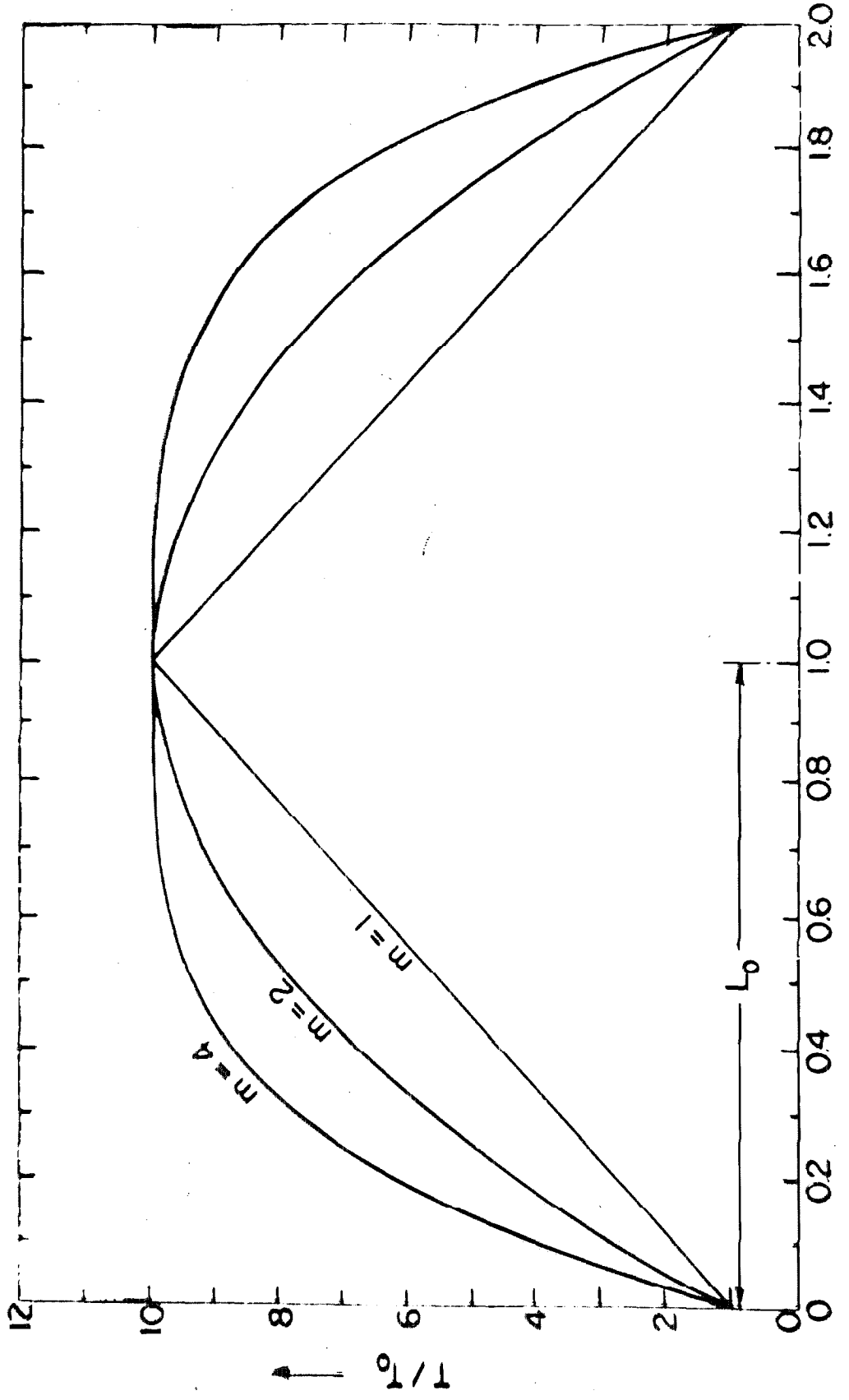

Fig. 2. Representative temperature profiles described by eq. 46 for m = 1, 2 and 4.

transition producing the given spectral line; g_u is the statistical weight of the upper energy level involved in the transition; p/kT_o represents the number of molecules per unit volume at the pressure p and at the reference temperature T_o with k denoting the Boltzmann constant; $\sigma_o = hcB/kT_o$ where B is the appropriate rotational constant for the rigid rotator; b_o is the spectral line semi-half-width at the pressure p and at the reference temperature T_o and we have assumed that $b = b_o\sqrt{T_o/T}$ at the constant pressure p; $u_o = h\nu_e/kT_o$ where ν_e represents the normal vibration frequency of the diatomic molecule (harmonic oscillator); E_ℓ = energy of the lower state above the zero-point energy.

For Doppler-broadened lines, we find

$$k_\nu = \frac{c^2}{8\pi\nu_o^2} A_{u\to\ell}\, g_u \left(\frac{p}{kT_o}\right) \frac{\sigma}{b_{D,o}} \left(\frac{\ln 2}{\pi}\right)^{1/2} \left(\frac{T_o}{T}\right)^{5/2} [1-\exp(-u_o T_o/T)]$$

$$\times[1-\exp(-h\nu_o/kT)][\exp(-E_\ell/kT)] \exp\left[-(\ln 2)\left(\frac{\nu-\nu_o}{b_{D,o}}\right)^2 \frac{T_o}{T}\right] \qquad (48)$$

where the Doppler half-width under reference conditions is given by

$$b_{D,o} = \left(\frac{2kT_o \ln 2}{mc^2}\right)^{1/2} \nu_o .$$

Numerical integration of eq. 45 using eqs. 46, 47, and 48 yields values for the emitted steradiancy. These values are shown in Figs. 3, 4, and 5 for the R3 (v = 0, J = 3 → v = 1, J = 4) line of HF. For this line in case of dispersion broadening, $b_o/c = 0.132p$ cm^{-1} (p in atmos) whereas for Doppler-broadening we have used $b_o/c = 5.85 \times 10^{-3}$ cm^{-1}. The reference optical depth is defined as $\tau_o = (L_o/\pi b_o)\int k_{\nu,o} d\nu$ ($k_{\nu,o}$ = absorption coefficient evaluated at T_o),

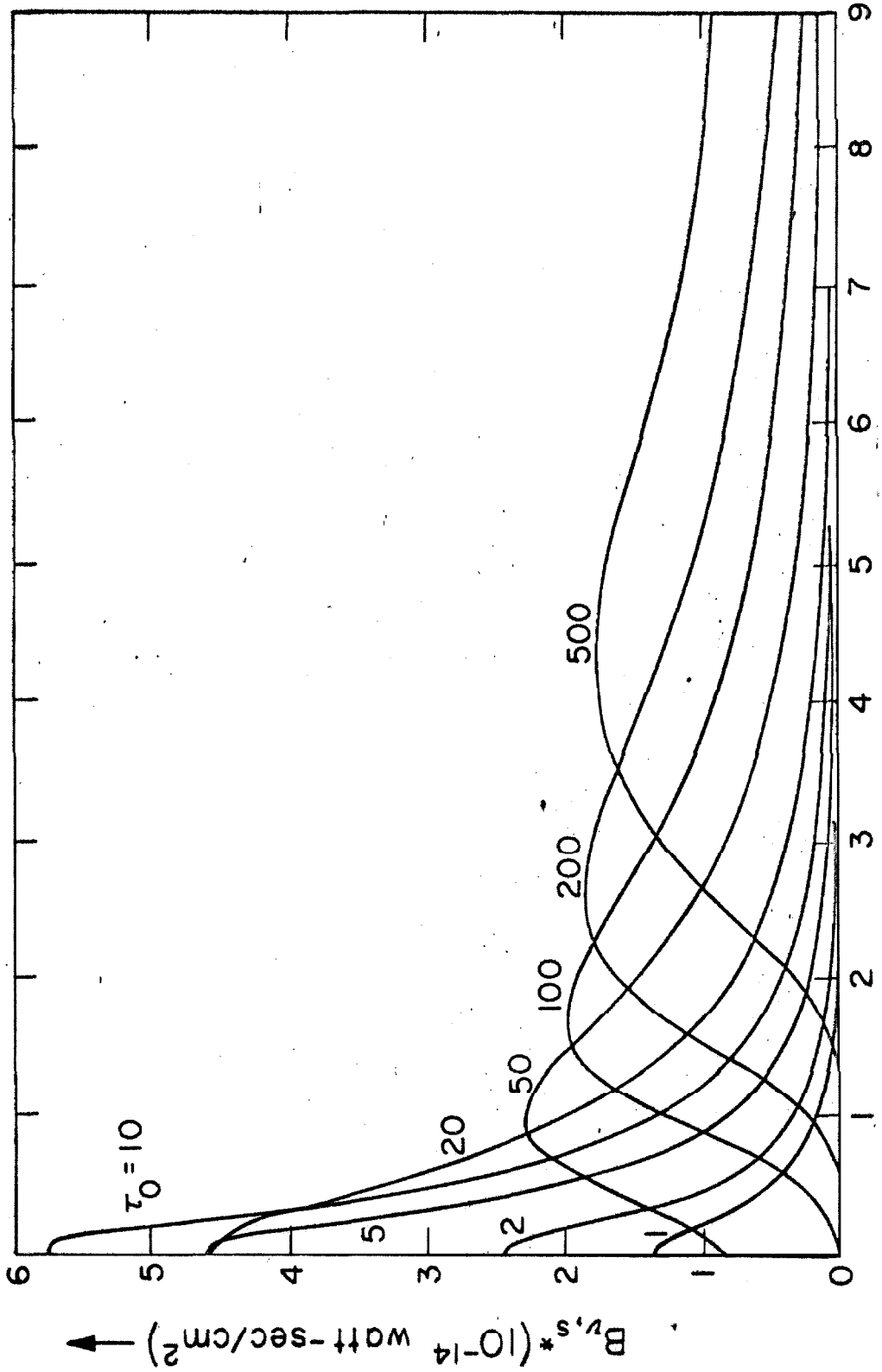

Fig. 3. The spectral steradiancies B_{ν,s^*} for m = 2 for the R3 line of HF at $s^* = 2$ as a function of $(\nu - \nu_0)/b_0$ for dispersion broadening and various values of the reference optical depth τ_0.

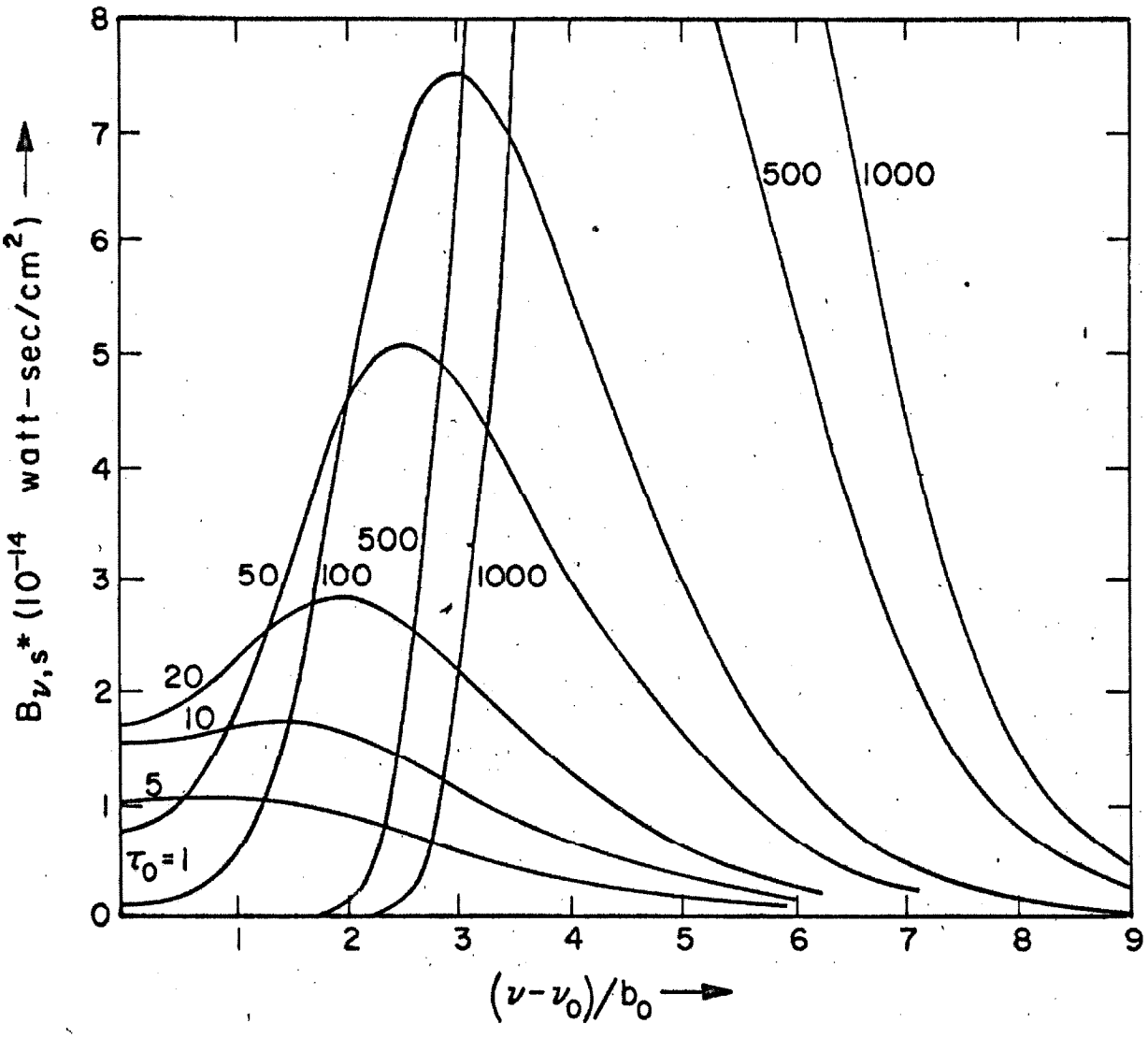

Fig. 4. The spectral steradiancies B_{ν, s^*} for m = 2 for the R3 line of HF at $s^* = 2$ as a function of $(\nu - \nu_0)/b_0$ for pure Doppler broadening and various values of the reference optical depth τ_0.

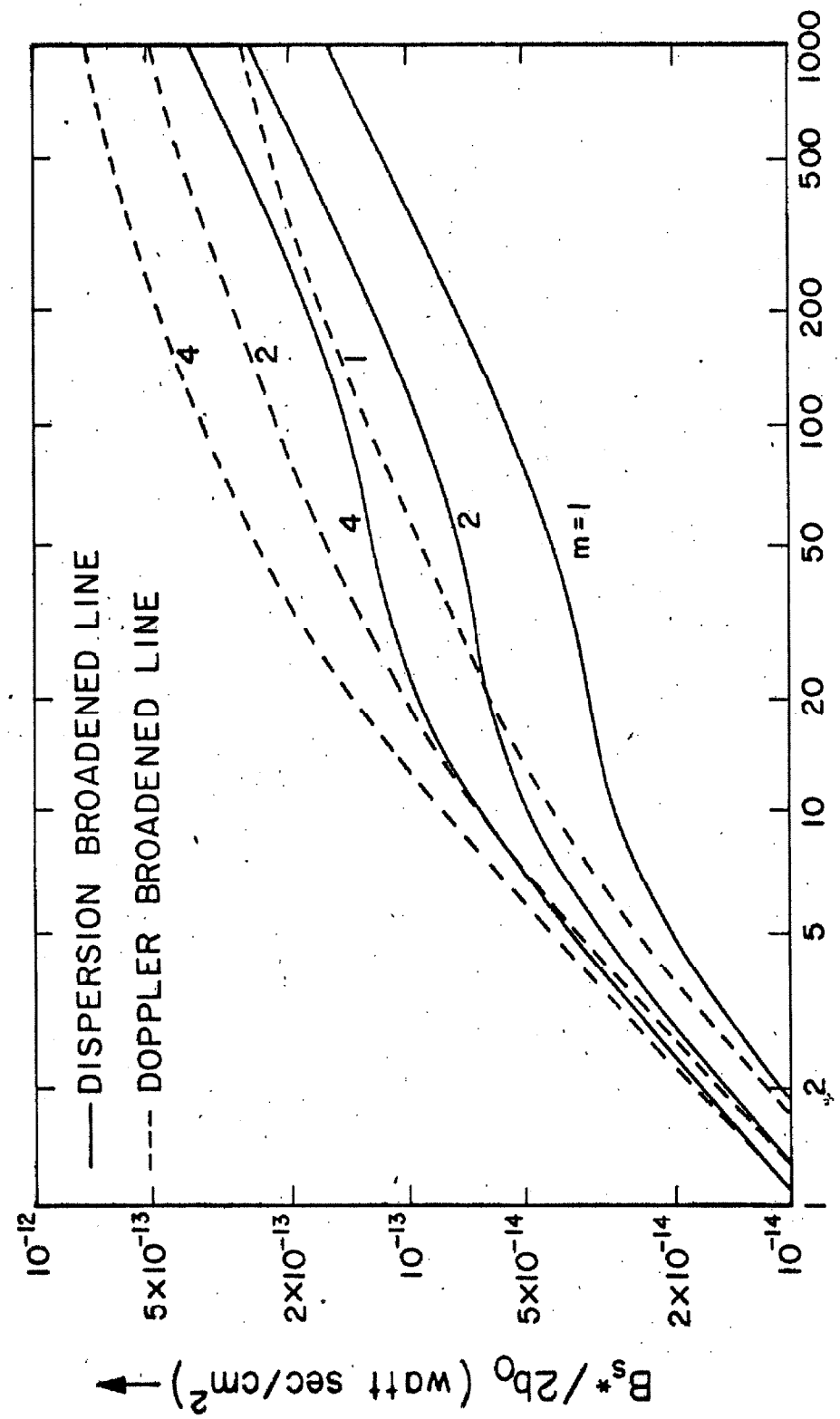

Fig. 5. The total steradiancy divided by $2b_o$ ($\equiv B_{g*}/2b_o$) at $s^* = 2$ as a function of τ_o for the dispersion- and Doppler-broadened R3 line of HF, $T_o = 300\ ^oK$, $T_{max} = 3000\ ^oK$, for various values of m in eq. 46.

$B_{\nu, s*}$ is the spectral steradiancy at $s^* = 2$, and B_{s*} represents the integrated steradiancy at $s^* = 2$ for the entire line.

Reference to Fig. 5 shows that Doppler and dispersion broadening produce the same total steradiancy B_{s*} for the case under consideration for large values of τ_o provided that $b_{o, \text{dispersion}} \simeq 2b_{o, \text{Doppler}}$, i.e., for $p \simeq 0.1$ atm.

A. Dispersion-Broadened Line

Examination of Fig. 3 shows that the R3 line of HF retains a typical dispersion contour until τ_o becomes greater than about 10, when self-reversal becomes important. Hence $\tau_o \simeq 10$ may be said to define the upper limit of the transparent gas regime. From Fig. 5 it is seen that the pressure and length dependence of the steradiancy for $\tau_o \lesssim 10$ is

$$B_{s*} \propto \rho_o L_o , \tag{49}$$

i.e., it is the same as for an isothermal transparent gas. In general, $\tau_o = 10$ corresponds to a small physical length for a strong spectral line. For the R3 line of HF, the value of L_o at $\tau_o = 10$ is about 0.015 cm.

The center of the line is essentially completely self-absorbed for $\tau_o \simeq 100$. Figure 5 shows that $\tau_o \gtrsim 100$

$$B_{s*} \propto \sqrt{\rho_o^2 L_o} , \tag{50}$$

which is the same as for the Eddington-Barbier approximation or for the isothermal case for large optical depths. For a strong line, the

transition to the regime described by eq. 50 occurs at a small physical length ($\simeq$ 0.15 cm for R3 line of HF). In Sec. VI, D below, the lower boundary of this regime will be found analytically.

B. Doppler-Broadened Line

The plot in Fig. 4 shows that self-reversal for the Doppler-broadened line becomes important for $\tau_o \simeq 5$. However, reference to Fig. 5 indicates that eq. 49 remains valid up to $\tau_o \simeq 10$ which, at p = 0.1 atmos., corresponds to $L_o \simeq 0.007$ cm for the R3 line of HF. For larger values of τ_o, however, the Doppler-broadened line does not approximate the behavior of the dispersion-broadened line, i.e., B does not become simply proportional to a power of L_o. Rather, B_{s*} becomes a weaker and weaker function of τ_o as saturation is approached.

The more complicated behavior of the Doppler-broadened line compared to the dispersion broadened line is the result of the fact that the Doppler line half-width increases with temperature while the dispersion line half-width decreases with temperature at constant pressure. *Hence, viewing a Doppler-broadened system at* $s^* = 2$, *the* radiation emitted from the higher temperature regions is "seen" at all optical depths since this radiation is not extensively reabsorbed.

C. Solution to the Radiant Transfer Equation for Large Optical Depths

We now derive a solution to the radiation transfer equation for large optical depths when scattering may be ignored. The basic radiation transfer equation may be written

$$\frac{dB_\nu}{ds^*} = - t_\nu B_\nu + t_\nu B_\nu^o \qquad (51)$$

where $t_\nu = L_o k_\nu$. For an optically thick gas, we expect the B_ν will be nearly equal to B_ν^o. We shall now find an iterative solution to eq. 51 which to the first order yields

$$B_\nu = B_\nu^o .$$

It then follows that

$$\frac{dB_\nu}{ds^*} = \frac{dB_\nu^o}{ds^*} .$$

Substituting this relation into eq. 51 and iterating (see Appendix B) we obtain, to the third order in $1/t_\nu$,

$$B_\nu = B_\nu^o - \frac{1}{t_\nu}\frac{dB_\nu^o}{ds^*} + \frac{1}{t_\nu^2}\left[\frac{d^2B_\nu^o}{ds^{*2}} - \frac{dB_\nu^o}{ds^*}\frac{d \ln t_\nu}{ds^*}\right]$$

$$- \frac{1}{t_\nu^3}\left[\frac{d^3B_\nu^o}{ds^{*2}} - 3\frac{d^2B_\nu^o}{ds^{*2}}\frac{d \ln t_\nu}{ds^*} - \frac{dB_\nu^o}{ds^*}\frac{d^2 \ln t_\nu}{ds^{*2}} + 2\frac{dB_\nu^o}{ds^*}\left(\frac{d \ln t_\nu}{ds^*}\right)^2\right]. \qquad (52)$$

The solution takes a more useful form if we make the following substitutions: let $\theta = u_o T/T_o$ and $x_\nu = - \theta'/t_\nu$ (where the prime indicates differentiation with respect to s^*). Equation 52 becomes now

$$B_\nu = B_\nu^o \left\{ 1 + \left[\frac{d \ln B_\nu^o}{d\theta} \right] x_\nu + \left[\left(\frac{d \ln B_\nu^o}{d\theta} \right)^2 + \frac{\theta''}{\theta'^2} \frac{d \ln B_\nu^o}{d\theta} + \frac{d^2 \ln B_\nu^o}{d\theta^2} \right.\right.$$

$$\left. - \left(\frac{d \ln B_\nu^o}{d\theta} \right) \left(\frac{d \ln t_\nu}{d\theta} \right) \right] x_\nu^2 + \left[\frac{\theta'''}{\theta'^3} \frac{d \ln B_\nu^o}{d\theta} + 3 \frac{\theta''}{\theta'^2} \frac{d^2 \ln B_\nu^o}{d\theta^2} \right.$$

$$+ \frac{d^3 \ln B_\nu^o}{d\theta^3} + \left(\frac{d \ln B_\nu^o}{d\theta} \right)^3 + 3 \frac{d \ln B_\nu^o}{d\theta} \left(\frac{\theta''}{\theta'^2} \frac{d \ln B_\nu^o}{d\theta} + \frac{d^2 \ln B_\nu^o}{d\theta^2} \right)$$

$$- 3 \left(\frac{d \ln B_\nu^o}{d\theta} \right)^2 \left(\frac{d \ln t_\nu}{d\theta} \right) - 3 \frac{d \ln t_\nu}{d\theta} \left(\frac{\theta''}{\theta'^2} \frac{d \ln B_\nu^o}{d\theta} + \frac{d^2 \ln B_\nu^o}{d\theta^2} \right)$$

$$\left. \left. - \frac{d \ln B_\nu^o}{d\theta} \left(\frac{\theta''}{\theta'^2} \frac{d \ln t_\nu}{d\theta} \frac{d^2 \ln t_\nu}{d\theta^2} \right) + 2 \left(\frac{d \ln B_\nu^o}{d\theta} \right) \left(\frac{d \ln t_\nu}{d\theta} \right)^2 \right] x_\nu^3 \right\} . \tag{53}$$

In the following discussion we will be concerned with rotation-vibration spectra and will assume $E_\ell = 0$ (i.e., transitions occur to the ground state) and $h\nu_o/kT_o = u_o$ (which is nearly true for vibration-rotation transitions). These assumptions are actually not essential in the analysis. Now

$$B_\nu^o = \frac{C}{e^{u_o^2/\theta} - 1} \tag{54}$$

$$t_\nu = \tau_o \left(\frac{u_o}{\theta} \right)^{3/2} \left[1 - e^{-u_o^2/\theta} \right]^2 \left[1 - e^{-u_o} \right]^{-2} \frac{1}{1 + \Gamma\theta/u_o} , \tag{55}$$

where

$$C \equiv \frac{2h\nu_o^3}{c^2} \qquad \text{and} \qquad \Gamma = \left(\frac{\nu - \nu_o}{b_o} \right)^2 .$$

In order to simplify the calculations, we now assume that

$$\exp(h\nu_o/kT) = \exp(u_o^2/\theta) >> 1 \tag{56}$$

in the temperature and frequency regions of interest. Then eqs. 54 and 55 become

$$B_\nu^o \simeq C \exp(-u_o^2/\theta) , \tag{57}$$

and

$$t_\nu \simeq \tau_o \left(\frac{u_o}{\theta}\right)^{3/2} \frac{1}{1 + \theta\Gamma/u_o} . \tag{58}$$

We again choose the temperature profile

$$\theta = u_o[10 - 9(s^* - 1)^m] \tag{59}$$

corresponding to $T = 300\,^oK$ at $s^* = 2$ and $T_{max} = 3000\,^oK$ at $s^* = 1$. Substituting eqs. 57 and 59 into eq. 53, we obtain the steradiancy at the line center received at $s^* = 2$ (i.e., at the point of observation). The result is

$$B_{\nu_o} = B^o_{\nu_o}\left\{1 + x_{\nu_o} + \left[1 - \frac{1}{u_o}\left(\frac{m-1}{9m} + \frac{1}{2}\right)\right]x^2_{\nu_o} + \left[1 - \frac{3}{u_o}\left(\frac{m-1}{9m} + \frac{1}{2}\right) + \frac{1}{u_o^2}\left(\frac{(m-1)(m-2)}{81m^2}\right)\right]x^3_{\nu_o}\right\} . \tag{60}$$

It is apparent that, after N iterations,

$$B_{\nu_o} = B^o_{\nu_o} \sum_{n=0}^{N} a_n x^n_{\nu_o} \tag{61}$$

where[†]

$$a_n = 1 - O\left(\frac{1}{u_o}\right) . \tag{62}$$

[†] $O\left(\frac{1}{u_o}\right) \equiv$ of order $\left(\frac{1}{u_o}\right)$.

Hence an upper limit for B_{ν_o} is

$$B_{\nu_o} = B^o_{\nu_o} \sum_{n=0}^{\infty} x^n_{\nu_o} = \frac{B^o_{\nu_o}}{1-x_{\nu_o}} \quad , \quad x_{\nu_o} < 1 \, , \tag{63}$$

where $x_{\nu_o} = 9u_o m/\tau_o$.

The values of B_{ν_o} at the line center are listed in Table 2 for the R3 line of HF as calculated by numerical integration of eq. 45 compared with those calculated by eqs. 60 and 63.

The prediction derived from eq. 63 that B_{ν_o} depends, in the totally absorbing region, mainly upon the ratio m/τ_o (i.e., upon x_ν) is substantiated by the data of Table 2 (see, in particular, the values for $m/\tau_o = 1/500 = 2/1000$ and $m/\tau_o = 2/500 = 4/1000$). Therefore, *the steeper the temperature profile near the point of observation,* the greater is the required thickness of the system to give the same intensity of radiation.

The solution found here is useful whenever optically thick gases are considered. Specifically, we shall use it for deriving the diffusion approximation (Appendix A), evaluating the Eddington-Barbier approximation in the limit of an optically thick gas (Sec. VIII, B), and for the determination of the lower bound for the $\sqrt{\rho^2 L}$ dependence of the steradiancy of a pressure broadened spectral line (Sec. VI, D).

D. Determination of the Lower Bound for the $\sqrt{\rho^2 L}$ Dependence of the Steradiancy of a Pressure-Broadened Line

For a pressure-broadened, strong spectral line and a representative temperature profile, the steradiancy is proportional to $\sqrt{\rho_o^2 L_o}$ for all but relatively small characteristic lengths. It is obviously of

Table 2. Spectral Steradiancy at the Line Center for the R3 line of HF and a Representative Temperature Profile (Dispersion-broadened Line)

m	τ_o	x_{ν_o}	B_{ν_o} (10^{-19} watt-sec/cm^2)		
See eq. 59	Reference optical depth	See eq. 63	Results obtained by an exact numerical integration	Results from the truncated series, eq. 60	Results from the upper limiting expression, eq. 63
1	1000	0.179	0.083	0.082	0.082
1	500	0.358	0.105	0.103	0.105
2	1000	0.358	0.105	0.103	0.105
2	500	0.716	0.209	0.173	0.237
4	1000	0.716	0.208	0.171	0.237
4	500	1.432	3.12	0.480	-

interest to determine a general criterion for the applicability of this type of ρ-L dependence in order to facilitate consideration of various spectral lines and temperature profiles. From representative numerical calculations, it was found (see Sec. VI, A) that the steradiancy becomes proportional to $\sqrt{\rho_o^2 L_o}$ at the same time that the line center displays total absorption. This has been noted previously for isothermal systems (13). We now use the solution to the radiant transfer equation, derived in the previous section, to define the condition for the center of a spectral line to correspond to a large optical depth where eq. 61 is valid.

It is apparent that, as $N \rightarrow \infty$, the series given by eq. 61 has a radius of convergence $R \geq 1$.[†] However, we may now obtain a conservative estimate of the lower bound of the region of $\sqrt{\rho^2 L}$ dependence of the steradiancy by setting

$$R = 1 = 9\, u_o m/\tau_{o_{\ell b}},$$

i.e., we assume that the line center is totally absorbed for $x_{\nu_o} < R$ or $\tau_o > \tau_{o_{\ell b}}$. Actually, we would expect that the real lower bound may be somewhat lower as the a_n in eq. 61 really are less than unity. Reference to Fig. 5 indicates that for $m = 1$, $\tau_{o_{\ell b}} \simeq 100$. From eq. 64 we find the value $\tau_{o_{\ell b}} = 179$ for the lower bound, which is in agreement with our rough estimate.

Consider a temperature profile which behaves similar to the one considered above and, near the point of observation, is given by

[†] If a_n in eq. 61 = 1, then $R = 1$.

$$\frac{T}{T_o} = a - \lambda(s^* - 1)^m \qquad (65)$$

rather than by eq. 59. Here a, λ, and m are arbitrary constants adjusted so that at $T = T_o$, $s^* = 2$ = the point of observation. Then, (see eq. 64)

$$\tau_{o_{\ell b}} = \lambda u_o m \, . \qquad (66)$$

Once $\tau_{o_{\ell b}}$ is known, we may determine the least value of $2L_o$ (the physical width of the radiating system) for which $B_{s*} \propto \sqrt{\rho^2 L}$ for any given vibration-rotation line of a diatomic molecule.† Conversely, if the physical system is given, one may find the minimum matrix elements (or Einstein coefficients) for which $B_{s*} \propto \sqrt{\rho^2 L}$ in a given spectral band. In such a way one may determine if the total steradiancy of a system of isolated pressure-broadened spectral lines is proportional to $\sqrt{\rho^2 L}$. The detailed behavior of the temperature profile is needed only near the point of observation.

The preceding statements are, of course, still based on the assumed truth of the observation that the start of the region of $\sqrt{\rho^2 L}$ dependence on B_{s*} and the absorption of the line center are concurrent.

E. Radiant Energy Transfer from High-temperature, non-isothermal, Air

Recent calculations by Breene and Nardone (14) of the spectral absorption coefficient of high temperature air have been used to

† Specifically, $\tau_o \equiv L_o \left[\frac{c^2 A_{u \to \ell} g_u \sigma_o}{8\pi^2 \nu_o^2 k T_o} \right] \frac{p}{b_o} \left[1 - \exp(-u_o) \right]^{-1} \left[1 - \exp\left(\frac{-h\nu_o}{kT_o} \right) \right]^{-1}$.

determine the radiant energy emitted from a non-isothermal air system. For the computing machine calculations, the spectral data for $p = 1$ atm and $T = 3000^{\circ}$, 4000°, 6000° and $9000\ ^{\circ}K$ served as input data; for intermediate temperatures, logarithmic interpolation was used to obtain the values of the absorption coefficient. The data were obtained from Figs. 43, 44, 46, and 49 of Ref. 14 by interpolating between the appropriate density values and dividing by the geometric factor of 1.8. Figure 6 shows the values of k_ν that were used as input data in the IBM 7090 program for $T = 4000^{\circ}$, 6000°, and $9000\ ^{\circ}K$, reference to Fig. 6 shows that a large degree of spectral resolution was retained.

1. Calculations for a Parabolic Temperature Profile

In the following analysis a parabolic temperature profile (see eq. 46 with $m = 2$) was used with the temperature range extending from 3000° to $9000\ ^{\circ}K$. The temperature profile is given by

$$T = T(s^*) \tag{67}$$

where $s^* = s/s_o$ and s_o is the physical width of the system. Hence the optical depth is given by

$$\tau_\nu = \int_o^{s_o} k_\nu(T)\, ds = s_o \int_o^1 k_\nu(s^*)\, ds^* \tag{68}$$

The function τ_ν/s_o is shown in Fig. 7 for the specified temperature profile. From Fig. 7, the optical depth for any frequency or physical width of the radiating air system may be determined.

In the isothermal case, the gas would be considered transparent for $\tau < 0.3$. It is to be expected that, for the non-isothermal case, the

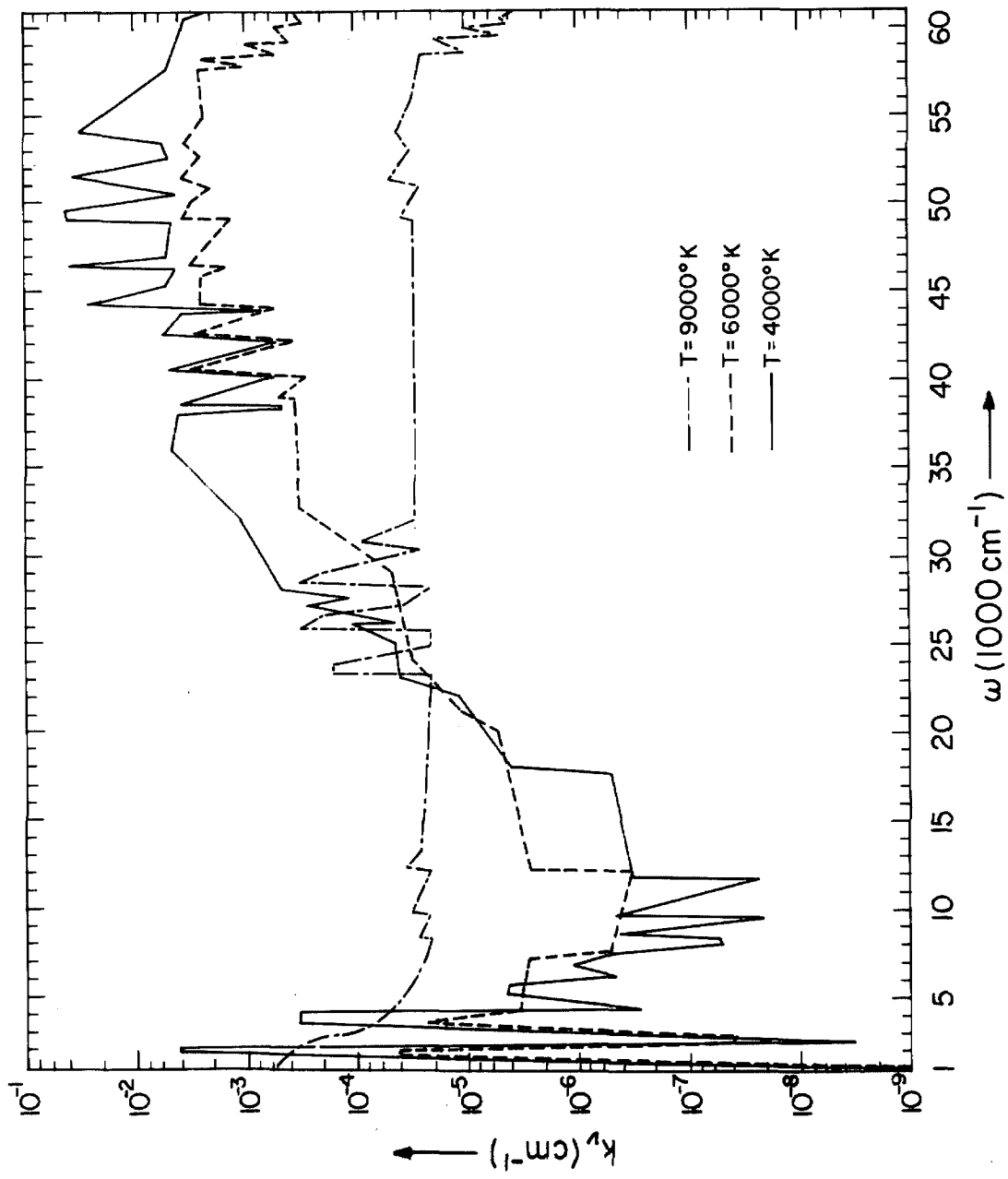

Fig. 6. The spectral linear absorption coefficient for air at p = 1 atm as a function of temperature and frequency. The data were obtained from Figs. 44, 46, and 49 of Ref. 14.

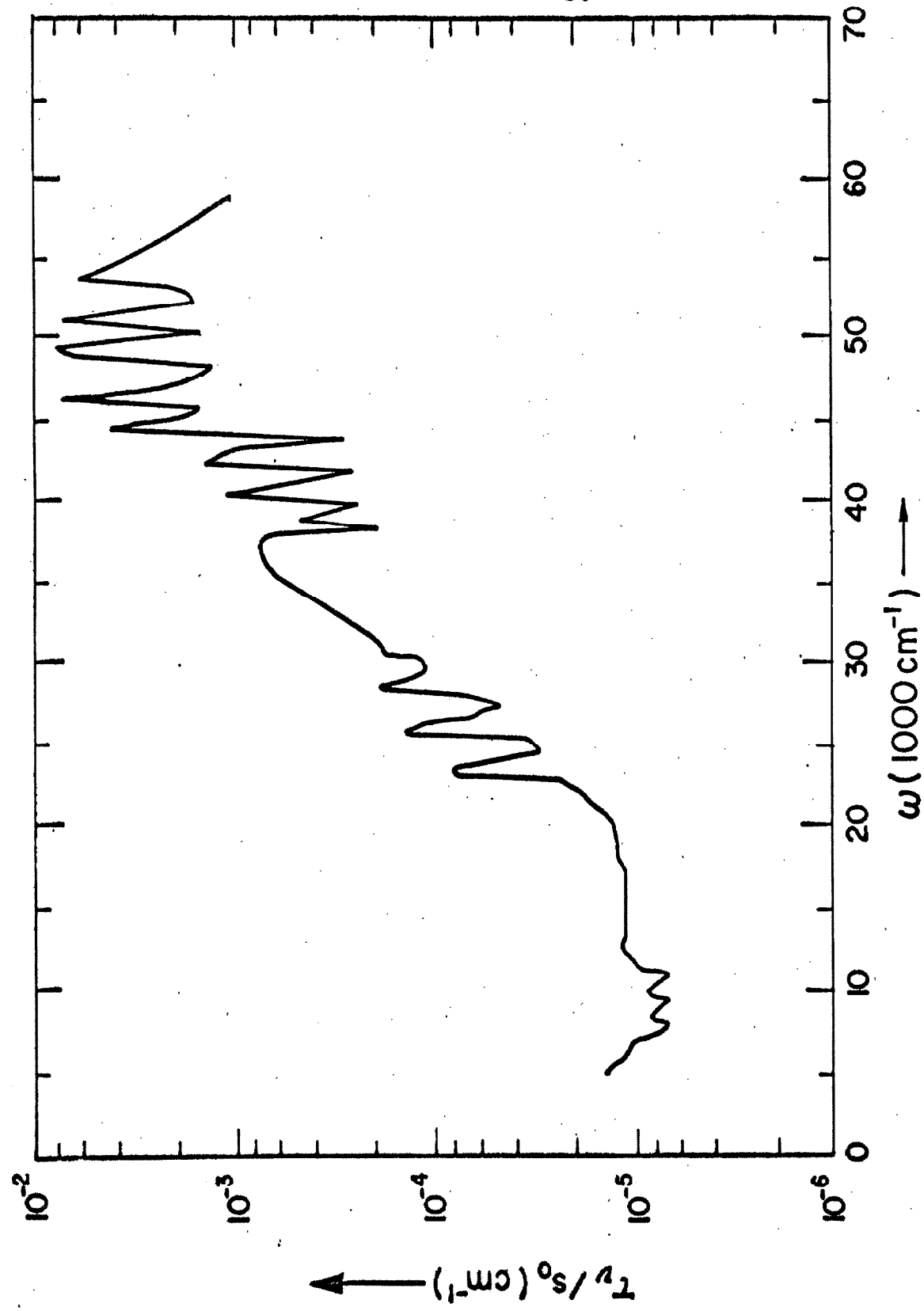

Fig. 7. The function $\int_o^1 k_\nu(s^*)\, ds^* = \tau_\nu/s_o$ for air at p = 1 atm for the parabolic temperature profile described in the text.

limiting value of τ should not differ greatly from this value. As may be seen in Fig. 7, τ_ν has maxima at $\omega = 46,500$ and $49,500\ cm^{-1}$. The effects of increasing s_o are, therefore, first apparent at these wave numbers. For $s_o = 60$ cm, the value of τ_ν at $\omega = 46,500$ and $49,500\ cm^{-1}$ is about 0.4, which is close to the expected value for transition from the transparent gas region. Figure 8 shows the value of the spectral steradiancy emitted from hot air for $s_o = 2$ cm and 60 cm. As expected, the spectral distributions are generally similar with some differences occurring near $\omega = 46,500$ and $49,500\ cm^{-1}$. Furthermore, the integrated steradiances from $5000\ cm^{-1}$ to $56,000\ cm^{-1}$ are $0.450\ watt/cm^2$ and $13.3\ watt/cm^2$ for $s_o = 2$ cm and 60 cm, respectively, i.e., roughly in the expected ratio of 1:30 for transparent gases. The most important contributors to the spectral structure shown in Fig. 8 are, for $5000\ cm^{-1} < \omega < 12,500\ cm^{-1}$, the first positive system of N_2; for $23,000\ cm^{-1} < \omega < 32,000\ cm^{-1}$, the first negative system of N_2^+; for $40,000\ cm^{-1} < \omega < 53,000\ cm^{-1}$, the gamma system of NO.

In Fig. 9, the high frequency values of $B_\nu(0)$ for $s_o = 2000$ cm are contrasted with $1000\ B_\nu(0)$ for $s_o = 2$ cm for the specified temperature profile. If the gas were transparent, these curves would coincide, as is actually the case for wave numbers less than about $30,000\ cm^{-1}$. The strong absorption bands at higher frequencies are produced by the strong NO gamma system which is of primary importance in the cooler gas regions. The integrated steradiancy for the wavenumber region from $5000\ cm^{-1}$ to $56,000\ cm^{-1}$ is $345\ watt/cm^2$, i.e.

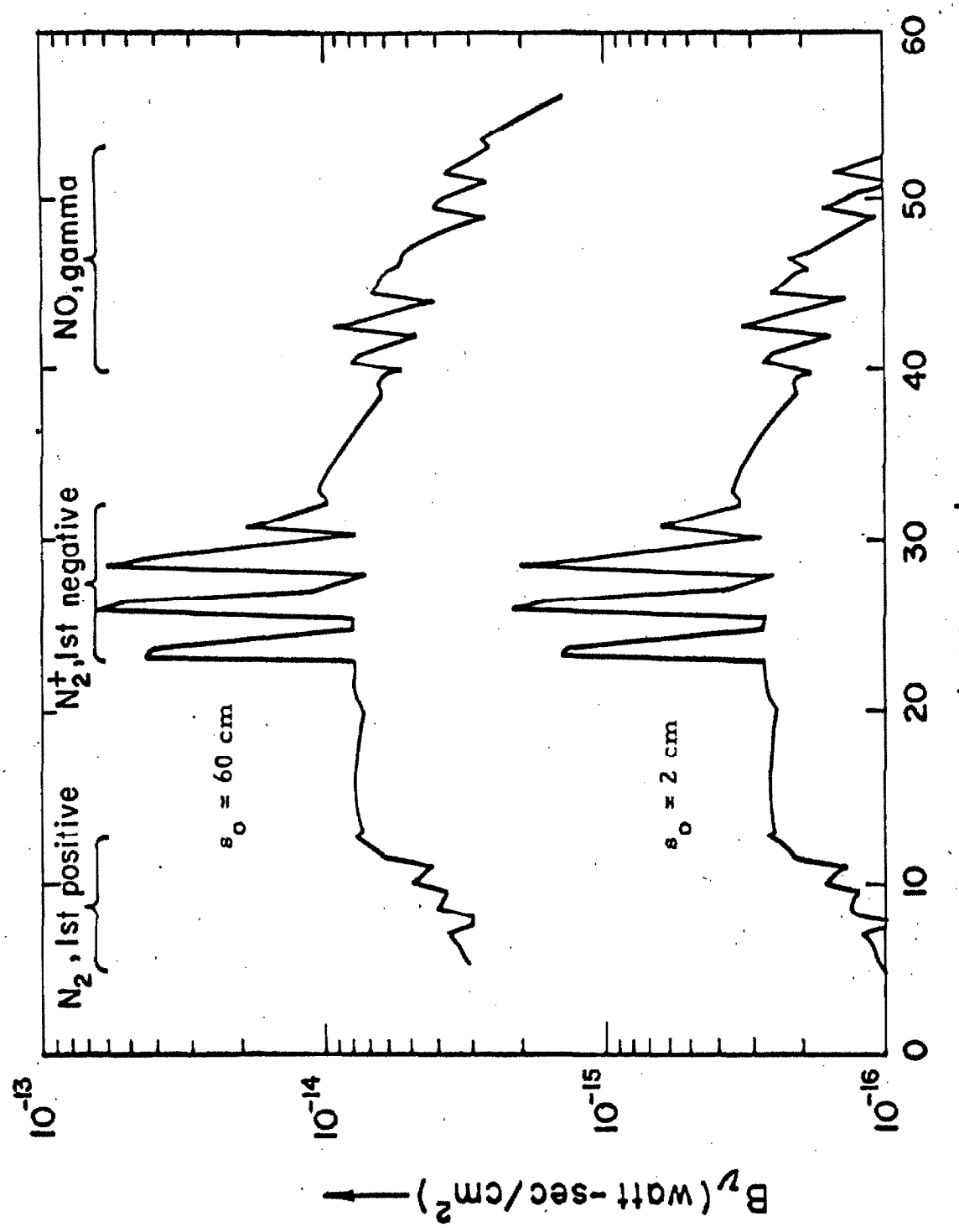

Fig. 8. The spectral steradiancy $B_\nu(0)$ emitted from air at p = 1 atm for the parabolic temperature profile described in the text. Curves for s_o = 2 and 60 cm are given and the dominant radiating systems are identified.

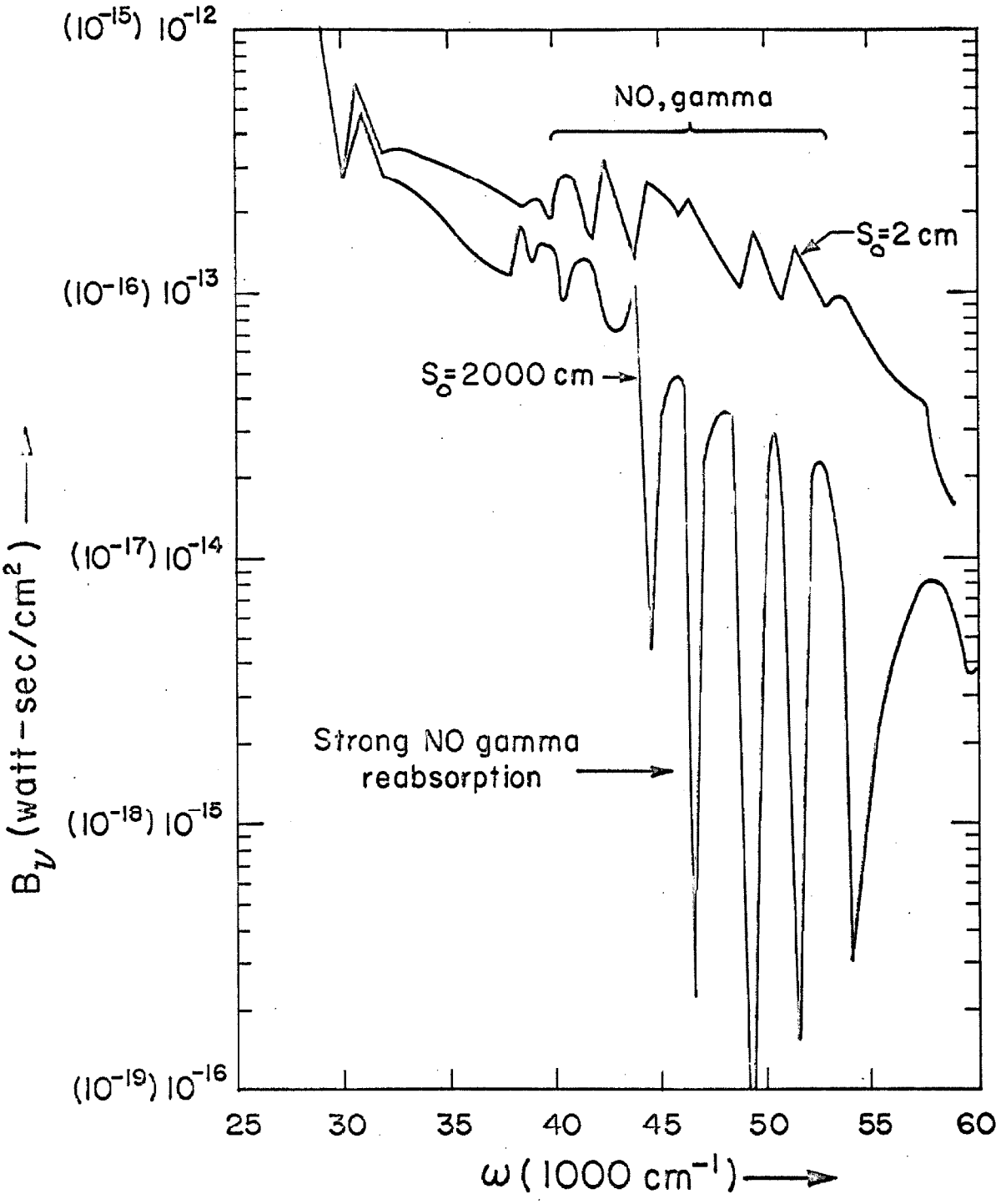

Fig. 9. The spectral steradiancy $B_\nu(0)$ emitted from air at p = 1 atm for the parabolic temperature profile described in the text. The scale in parentheses refers to the $s_o = 2$ curve.

$$[B(0),\ s_o = 2000\ \text{cm}]/[B(0),\ s_o = 2\ \text{cm}] = 345/0.450 = 789.$$

It is interesting to compare the exact calculations of $B(0)$ with an estimate obtained using the Planck mean absorption coefficient and computing $B(0)$ from the expression

$$B(0) = \bar{k}_{L,\,P\ell}(\sigma/\pi)\bar{T}_g^4 s_o \tag{69}$$

where $\bar{k}_{L,\,p\ell}$ denotes again the Planck mean absorption coefficient and $\bar{T}_g$ is an appropriate average temperature of the gas. We take $\bar{T}_g = 7500 \pm 1000\ ^oK$, since we expect the higher temperatures to be weighted more heavily for transparent gases and the parabolic temperature profile. Using appropriate data from Ref. 15, we find that $\bar{k}_{L,\,P\ell} \simeq 1\times 10^{-4}\ \text{cm}^{-1}$ † and $B(0)/s_o = 0.57 \pm 50\%$, which is in fair agreement with the result derived from exact calculations, viz., $B(0)/s_o = 0.225$.

2. Calculations for a Reentry Vehicle

The heated gas behind the shock wave in the stagnation region of a reentry vehicle may be considered to be isothermal if the thermal layer thickness is small and non-equilibrium effects are unimportant. In this case, radiant energy transfer calculations are easily performed since k_ν is constant along the optical path. However, the thickness

† At 8000 °K, a pressure of 1 atm corresponds to $\rho/\rho_o \simeq 10^{-7/4}$ (see Ref. 16). Logarithmic interpolation between calculated values (15) at $T = 8000\ ^oK$ gives $\bar{k}_{L,\,P\ell} = 1.0\times 10^{-4}\ \text{cm}^{-1}$. Because $\bar{k}_{L,\,P\ell}$ varies strongly with temperature, the use of this value of $\bar{k}_{L,\,P\ell}$ in the calculations of $B(0)$ can only be expected to provide an order-of-magnitude estimate.

of the thermal layer ($\equiv d_T$) is proportional to the square root of the vehicle nose radius whereas the shock detachment distance ($\equiv d_S$) is directly proportional to the nose radius. It is therefore to be expected that, even for rather low reentry velocities, the non-isothermal temperature profile of the heated air will become important for sufficiently small nose radii.

In the following representative calculations, we have chosen a stagnation pressure of 1 atm and a stagnation enthalpy of 10,000 cal/g, corresponding to an equilibrium temperature for the shocked air of 8550 ^{o}K. These conditions apply to a reentry vehicle at about 30,000 ft/sec at an altitude of 100,000 ft. The wall temperature of the reentry vehicle was chosen to be 2000 ^{o}K.

Figure 10 shows the temperature profile used in the numerical calculations of the emitted radiation. It is based upon calculations for the stagnation region of a reentry vehicle using the real gas properties of air (17). The radiant energy transfer to the missile wall has been calculated using again the data of Breene and Nardone (14). The results are shown in Fig. 11 which gives the spectral steradiancy emitted in a direction toward the wall. Also shown are the data of Fig. 8 for a parabolic temperature profile and a geometrical thickness of $s_o = 2$ cm multiplied by 0.075 for the purpose of comparison. Calculation of the optical depth again indicates that the maximum values of τ_ν occur at $\omega = 46,500$ and $49,500$ cm^{-1} where $\tau_\nu = 7 \times 10^{-5}$ for the temperature profile of Fig. 10. Since the air is optically thin at all of the frequencies considered, the steradiancy is obtained from the integral

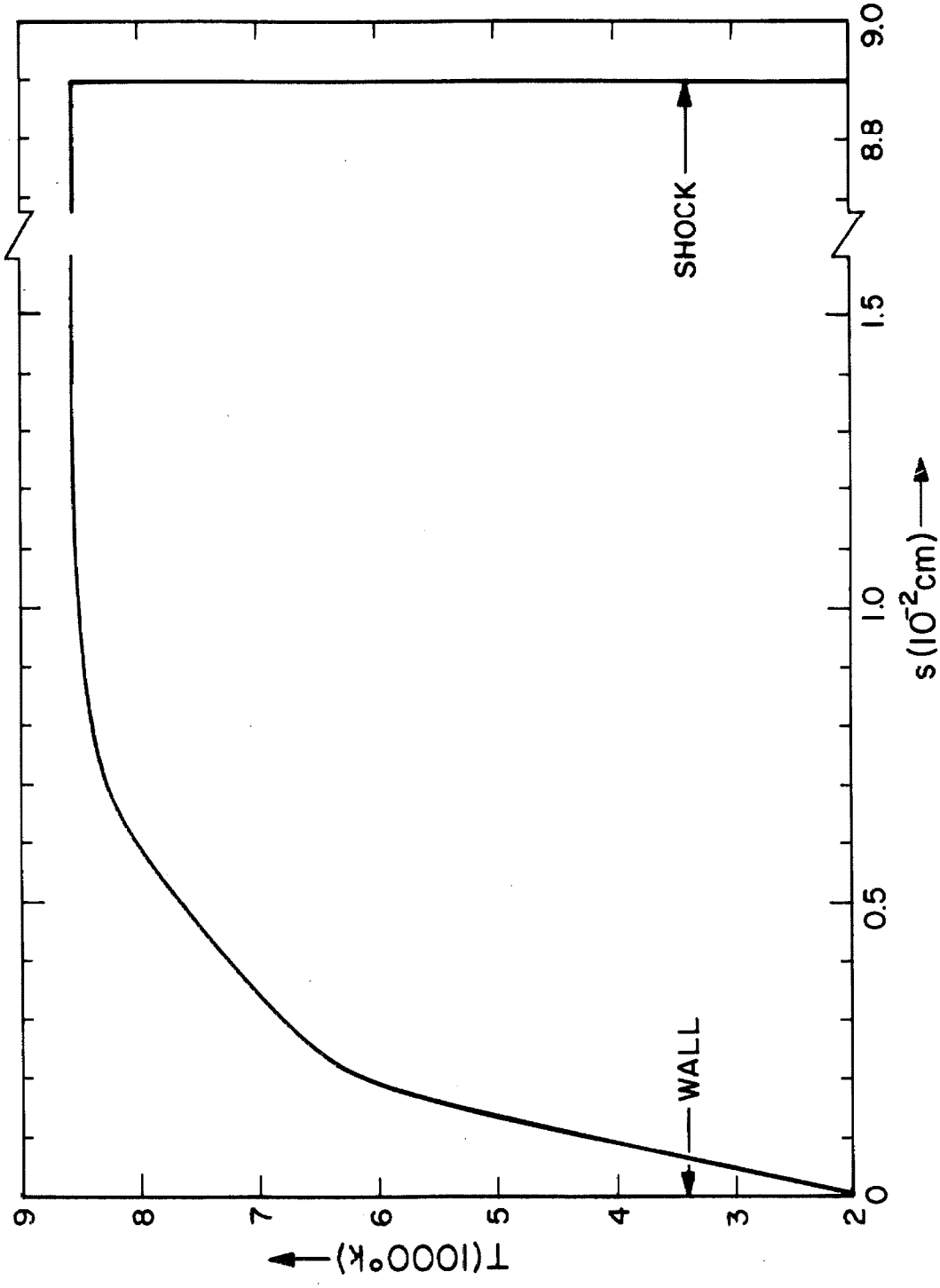

Fig. 10. The air temperature as a function of the distance from the wall at the stagnation point of a reentry vehicle with a 1 cm nose radius; reentry velocity = 30,000 ft/sec at an altitude of 100,000 ft.

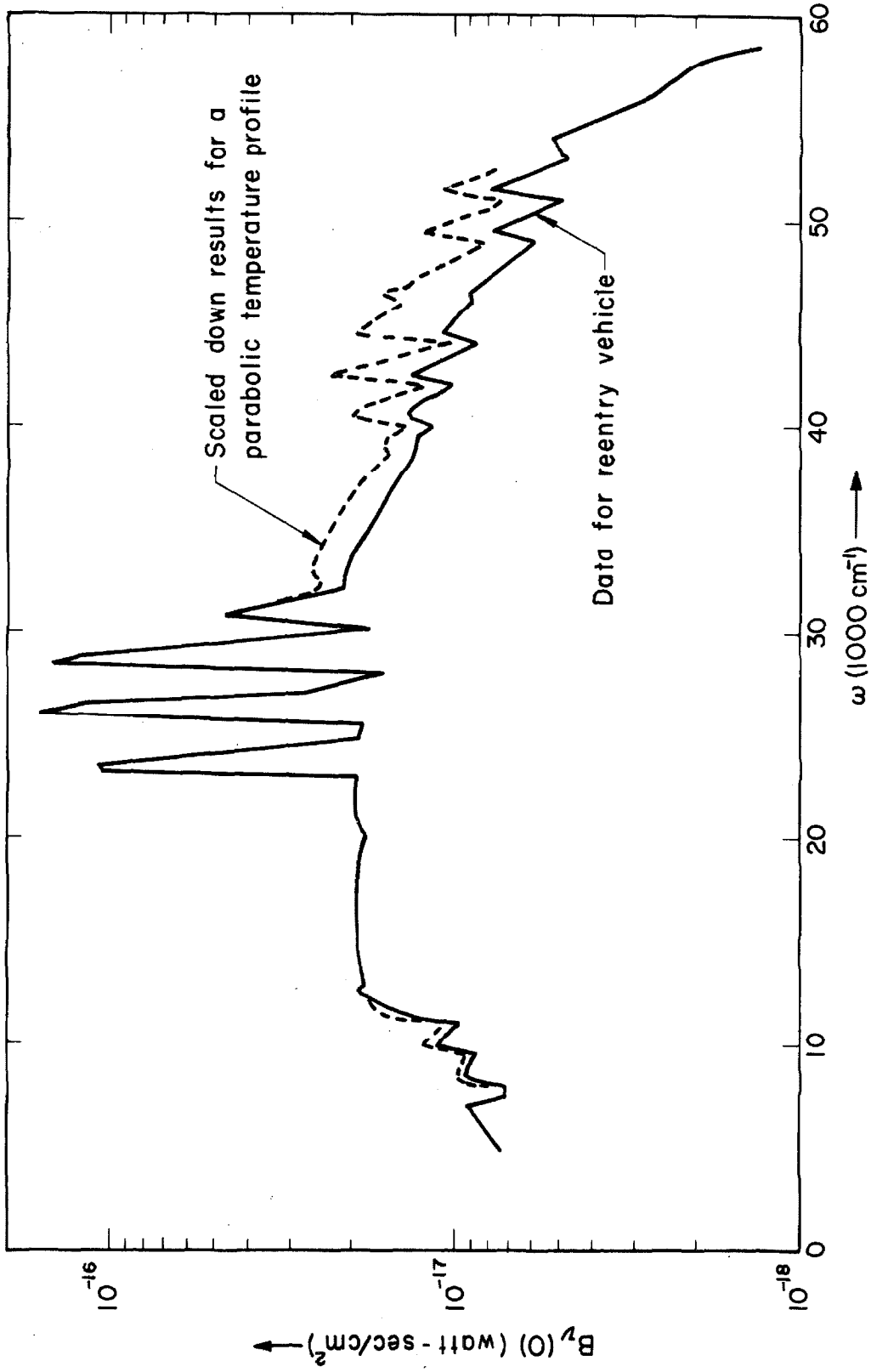

Fig. 11. The spectral steradiancy $B_\nu(0)$ incident on the wall of a reentry vehicle with a 1 cm nose radius; velocity = 30,000 ft/sec at 100,000 ft. The dashed line corresponds to 0.075 $B_\nu(0)$ for a parabolic temperature profile of width 2 cm.

$$B_\nu(s) = \int_o^s k_\nu B_\nu^o \, ds \ . \tag{70}$$

It is then apparent that the absolute value of the steradiancy incident on the wall is equal to the incident on the shock front, assuming that the radiant energy from the wall itself may be neglected. Furthermore, because of the transparency of the heated air, we may assume that $B_\nu(0,\theta) = B_\nu(0,0)/\cos\theta$ where θ is the angle of the incident radiation measured with respect to the normal to the wall. Hence the flux to the wall becomes

$$F_\nu(0) = \int_{\Omega/2} \frac{B_\nu(0,0)}{\cos\theta} \cos\theta \, d\Omega = 2\pi B_\nu(0,0) \tag{71}$$

and $F(0) = 2\pi \int B_\nu(0,0) \, d\nu$.

Our calculations give a value for the integrated steradiancy from 5000 to 56,000 cm^{-1} of 3.03×10^{-2} watt/cm^2, or the total radiant heat delivered to the wall is $F(0) = 0.19$ watt/cm^2 = 0.116 Btu/ft^2 sec. Under the given reentry conditions, the total heat flux to the wall due to thermal conduction (17) is about 4000 Btu/ft^2 sec.

VII. SCALING PARAMETERS FOR RADIANT ENERGY EMISSION FROM ISOBARIC BUT NON-ISOTHERMAL SYSTEMS IN THE EDDINGTON-BARBIER APPROXIMATION

One of the classical approaches to the theoretical calculation of radiant energy emission from non-isothermal systems is exemplified by the Lundblad series development for the solar photosphere (Ref. 11, pp. 109-115, 382-384) (18,19).

The spectral steradiancy at the frequency ν and at the optical depth $\tau_\nu = 0$, corresponding to the geometrical length $s = 0$, in the direction θ' (see Fig. 12), is given by the relation

$$B_\nu(0,\theta') = \int_o^\infty B_\nu^o(\tau_\nu) \left\{ \exp\left[-\tau_\nu \sec\theta' \right] \right\} (\sec\theta')\, d\tau_\nu$$

$$= \int_o^\infty B_\nu^o(s) \left\{ \exp\left[-\int_o^s k_{L,\nu}(s')\, ds' \right] \right\} k_{L,\nu}(s)\, ds \qquad (72)$$

where B_ν^o is the blackbody steradiancy for local thermodynamic equilibrium at the optical depth $\tau_\nu = \cos\theta' \int_o^s k_{L,\nu}(s')\, ds'$ corresponding to the geometric length s, along the beam of the emitting system, for a spectral linear absorption coefficient $k_\nu \equiv k_{L,\nu}$.

If $B_\nu^o(\tau_\nu)$ is developed in a (Lundblad) power series in τ_ν, viz.,

$$B_\nu^o(\tau_\nu) = \sum_{i=0}^{\infty} a_i \tau_\nu^i , \qquad (73)$$

then

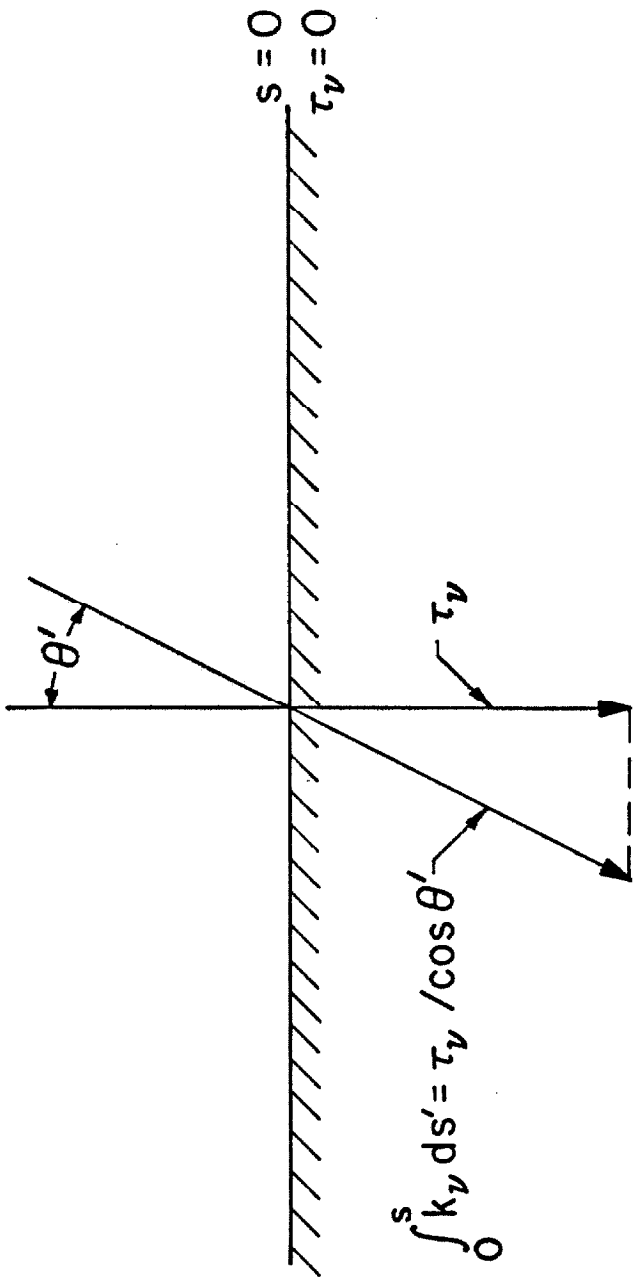

Fig. 12. Schematic diagram showing the geometric configuration discussed in the text.

$$B_\nu(0,\theta') = \sum_0^\infty a_i \cos^i\theta' \int_o^\infty y^i e^{-y} dy = \sum_0^\infty a_i i! \cos^i\theta' \qquad (74)$$

where the substitution $y = \tau_\nu \sec\theta'$ has been used. Comparison of eqs. 73 and 74 shows that

$$B_\nu(0,\theta') = B_\nu^o(T_{\tau_\nu = \cos\theta'}) \text{ for } a_i = 0 \text{ if } i \geq 2, \qquad (75)$$

i.e., if only the first two terms are used (Eddington-Barbier approximation) in the power series given in eq. 73. The physical interpretation of eq. 75 is the following: the spectral steradiancy at $\tau_\nu = 0$, observed at an angle θ', for a non-isothermal system is identically equal to the numerical value of the spectral blackbody steradiancy $B_\nu^o(T_{\tau_\nu=\cos\theta'})$ at the optical depth $\tau_\nu = \cos\theta'$ or at the geometrical length defined by $\int_o^s k_{L,\nu}\, ds' = 1$,† provided only two terms are used in the power series expansion shown in eq. 73.

It is interesting to consider the possible temperature profiles for selected spectral line shapes that are consistent with the statements

$$\begin{aligned} B_\nu^o(\tau_\nu) &= a_o + a_1\tau_\nu = a_o + a_1\cos\theta' \int_o^s k_\nu(s')\, ds' \\ &= B_\nu^o(0) + \left[B_\nu^o(T_{\tau_\nu=\cos\theta'}) - B_\nu^o(0)\right] \int_o^s k_\nu(s')\, ds' \end{aligned} \qquad (76)$$

and

$$\int_o^s k_\nu(s')\, ds' = 1 . \qquad (77)$$

†Note that s is measured along the direction θ' shown in Fig. 12.

We assume a monotone variation of T and τ_ν with s (and thus also of τ_ν with T) and we impose the boundary condition $T = T_o$ at $\tau_\nu = s = 0$. Differentiation of eq. 76 with respect to T yields the differential equation

$$(\cos\theta')k_\nu(T)\frac{ds}{dT} = \frac{1}{a_1}\frac{dB_\nu^o}{dT} = \frac{1}{a_1}\frac{2h^2\nu^4}{c^2}\frac{1}{kT^2}\frac{\exp(h\nu/kT)}{[\exp(h\nu/kT)-1]^2} \quad . \qquad (78)$$

It is now possible to specify $k_\nu(T)$ for various spectral line profiles belonging to various assumed atomic or molecular emitters. We may then integrate eq. 78 in order to find s as a function of T. Finally, eq. 77 may be used to obtain the proper value of s, and hence of T, for which $B_\nu(0,\theta') = B_\nu^o$ (T for $\int_o^s k_\nu(s')\,ds' = 1$).

In the analysis presented in eqs. 72 to 78, it has been assumed that the quantities a_1 are independent of τ_ν. For an emitting system with structure, this statement can be true only spectrally, i.e., a different value of a_1 must be chosen at a different frequency <u>for any specified temperature dependence on geometrical length.</u> The implications of this fact may be clarified by referring to the schematic diagram shown in Fig. 13. The temperature profile must, of course, be independent of frequency in any physically meaningful problem. However, the physical location s and the temperature T at which eq. 77 is satisfied is strongly dependent on frequency. In the near line wing at the frequency $\nu_o + \Delta\nu_1$, the integral condition of eq. 77 will be met for small values of s and T; on the other hand, in the far wings of spectral lines where $\nu = \nu_o + \Delta\nu_2$, much larger values of s, and hence of T, are required (compare Fig. 13). In other words, the

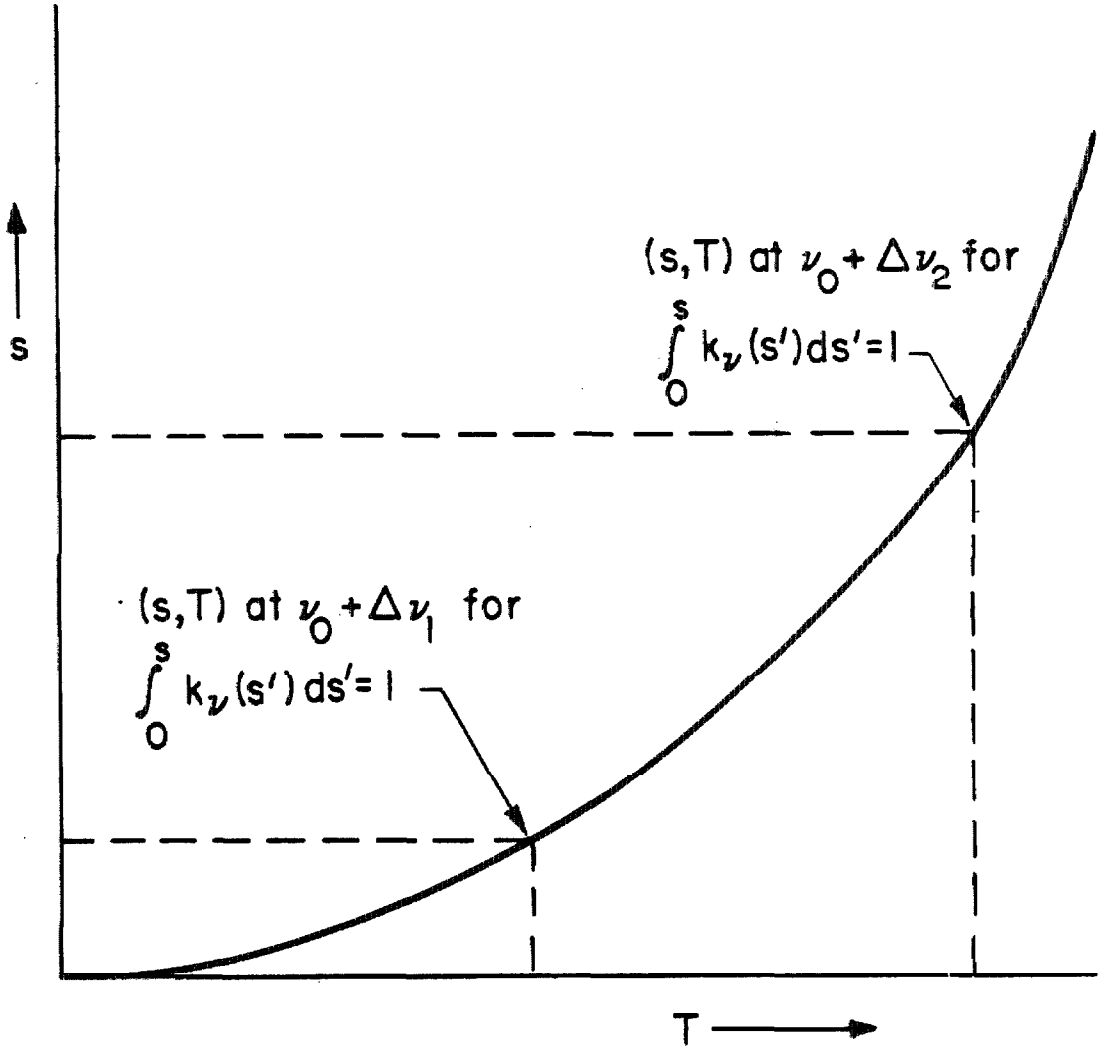

Fig. 13. Schematic diagram showing the relation between temperature T and distance s for a specified angle θ'. The values of s and T required to satisfy eq. 77 are shown for the representative frequencies $\nu_0 + \Delta\nu_1$ in the near wing and $\nu_0 + \Delta\nu_2$ in the far wing of a line.

contributions to $B_\nu(0, \theta')$ calculated according to eq. 75 arise from regions of different temperature at different locations for different frequencies in such a way that the far line wings will make relatively larger contributions since they may be "seen" at greater geometrical depths and, correspondingly, at higher temperatures.

Since a_1 may vary with frequency, it will prove to be convenient to introduce a frequency dependence for a_1 deliberately in such a way as to allow a universal representation of a reduced distance variable (which is a function of ν) as a function of T.

A. Isolated Spectral Lines Belonging to Diatomic Emitters with Collision Broadening

From eqs. 78 and 47 we obtain the following differential equation (after approximating ν in eq. 78 by ν_o):

$$ds = \frac{\mathcal{C}}{\cos\theta'} \frac{b_o}{a_1} \left(\frac{T_o}{T}\right)^{1/2} \frac{\exp(-h\nu_o/kT)}{[1 - \exp(-h\nu_o/kT)]^3} \frac{\exp(E_\ell/kT)}{[1 - \exp(-u_o T_o/T)]} \times \left[1 + \frac{(\nu - \nu_o)^2}{b_o^2 (T_o/T)}\right] dT \qquad (79)$$

where

$$\mathcal{C} = \frac{16\pi^2 h^2}{c^4 k} \frac{kT_o}{p} \frac{\nu_o^6}{\sigma_o T_o^2 g_u A_{u\to\ell}} \qquad (80)$$

1. The Limiting Case $h\nu_o/kT \ll 1$, $u_o T_o/T \ll 1$, $(h\nu_o - E_\ell)/kT \ll 1$

For $h\nu_o/kT \ll 1$, $u_o T_o/T \ll 1$, $(h\nu_o - E_\ell)/kT \ll 1$, eq. 79 becomes, after integration between the limits $s = 0$ at $T = T_o$ and s, T,

$$s \simeq \frac{\mathcal{G}'}{\cos\theta'}\left(T^{9/2} - T_o^{9/2}\right) + \frac{\mathcal{B}'}{\cos\theta'}\left(T^{11/2} - T_o^{11/2}\right), \tag{81}$$

where

$$\mathcal{G}' = \frac{2}{9}\,\frac{\mathcal{G}(b_o/a_1)}{u_o(h\nu_o/kT_o)^3 T_o^{7/2}}\,,$$
$$\mathcal{B}' = \frac{2}{11}\,\frac{\mathcal{G}(b_o/a_1)}{u_o(h\nu_o/kT)^3 T_o^{9/2}}\left(\frac{\nu-\nu_o}{b_o}\right)^2. \tag{82}$$

2. The Limiting Case $h\nu_o/kT \gg 1$, $u_o T_o/T \gg 1$

For $h\nu_o/kT \gg 1$, $u_o T_o/T \gg 1$, and with $z \equiv (h\nu_o - E)/kT$ eq. 79 becomes

$$ds \simeq -\frac{\mathcal{G}}{\cos\theta'}\frac{b_o}{a_1}T_o\left(\frac{h\nu_o - E_\ell}{kT_o}\right)^{1/2} z^{-3/2} e^{-z}\left[1 + \left(\frac{\nu-\nu_o}{b_o}\right)^2 \times \frac{h\nu_o - E_\ell}{kT_o}\,z^{-1}\right] dz\,. \tag{83}$$

Integrating again from $s = 0$ to $T = T_o$ and $z = z_o \equiv (h\nu_o - E)/kT_o$ to s, z, we find now that

$$(\cos\theta')s \simeq \mathcal{G}\frac{b_o}{a_1}T_o\left(\frac{h\nu_o - E_\ell}{kT_o}\right)^{1/2} I_1 + \mathcal{G}T_o\frac{b_o}{a_1}\left(\frac{h\nu_o - E_\ell}{kT_o}\right)^{3/2}\left(\frac{\nu-\nu_o}{b_o}\right)^2 I_2 \tag{84}$$

where

$$I_1 = -\int_{z_o}^{z} z^{-3/2} e^{-z} dz, \qquad I_2 = -\int_{z_o}^{z} z^{-5/2} e^{-z}\, dz\,. \tag{85}$$

In order to evaluate I_1 and I_2, it is convenient to write the identity

$$-\int_{z_o}^{z} z^{-n} e^{-z} dz = -\int_{\infty}^{z} z^{-n} e^{-z} dz + \int_{\infty}^{z_o} z^{-n} e^{-z}\, dz \quad \text{for} \quad n = \frac{3}{2} \text{ or } \frac{5}{2}, \tag{86}$$

where the second integral appearing on the right-hand side of eq. 86 is negligibly small compared to the first for z_o much larger than z. But

$$-\int_{\infty}^{z} z^{-3/2} e^{-z} dz = 2\frac{e^{-z}}{\sqrt{z}} - 2\Gamma(\tfrac{1}{2})\left\{1 - \frac{\Gamma_z(\frac{1}{2})}{\Gamma(\frac{1}{2})}\right\} \tag{87}$$

where $\Gamma(\frac{1}{2})$ is the complete gamma function of argument $\frac{1}{2}$ and $\Gamma_z(\frac{1}{2})$ is the incomplete gamma function of z of argument $\frac{1}{2}$. Making use of the notation of Pearson (20), the preceding expression may be rewritten in the form

$$-\int_{\infty}^{z} z^{-3/2} e^{-z} dz = 2\left\{\frac{e^{-z}}{\sqrt{z}} - \sqrt{\pi}\left[1 - I\left(\frac{z}{\sqrt{0.5}} - 0.5\right)\right]\right\}. \tag{88}$$

With the available tables of the incomplete Γ-function (20), which gives values to seven significant figures, eq. 88 can only be evaluated for $z < 9$. For $z > 9$, the integrals may be evaluated either numerically or else by using a simple approximation procedure.

Integrating by parts twice yields the expression

$$-\int_{\infty}^{z} z^{-n} e^{-z} dz = z^{-n} e^{-z} + \frac{n}{z}\int_{\infty}^{z} z^{-n} e^{-z} dz + \int_{\infty}^{z} \frac{n}{z^2}\left(\int_{\infty}^{z} z^{-n} e^{-z} dz\right) dz. \tag{89}$$

For sufficiently large values of z, eq. 89 reduces to

$$-\int_{\infty}^{z} z^{-n_e-z}\,dz \simeq \frac{z^{-n_e-z}}{[1+(n/z)]} \tag{90}$$

or, in somewhat cruder approximation

$$-\int_{\infty}^{z} z^{-n_e-z}\,dz \simeq z^{-n_e-z}\,. \tag{91}$$

Results obtained by using eqs. 90 and 91, and also by using eq. 88 together with tabulated values of the incomplete gamma function (20), are plotted in Figs. 14a and 14b. These data, together with eqs. 84, 85 and 86 yield the desired temperature profile. For $h\nu_o/kT \ll 1$, the dependence of T on s is easily computed by using eq. 81.

Reference to eqs. 81 and 84 shows that the temperature profile depends on the frequency. At the line center, however, $\beta' = 0$. Therefore s may be computed as a universal function of T for $h\nu_o/kT_o \ll 1$. Similarly, for $h\nu_o/kT_o \gg 1$, the second term in eq. 84 vanishes and $(\cos 0')s/\{G(b_o/a_1)T_o[(h\nu_o-E_\ell)/kT_o]^{1/2}\} = I_1$, which has been plotted in Figs. 14a and 14b for the special cases $z_o = \infty$ and $z_o = 20$; in Figs. 15a to 15c, the corresponding temperature profiles are shown for $z_o = 20$, $T_o = 300\,^{o}K$.

In the line wings, the first terms of eqs. 81 and 84 become negligibly small. Hence reduced temperature profiles are again determined in terms of easily computed quantities or in terms of I_2.

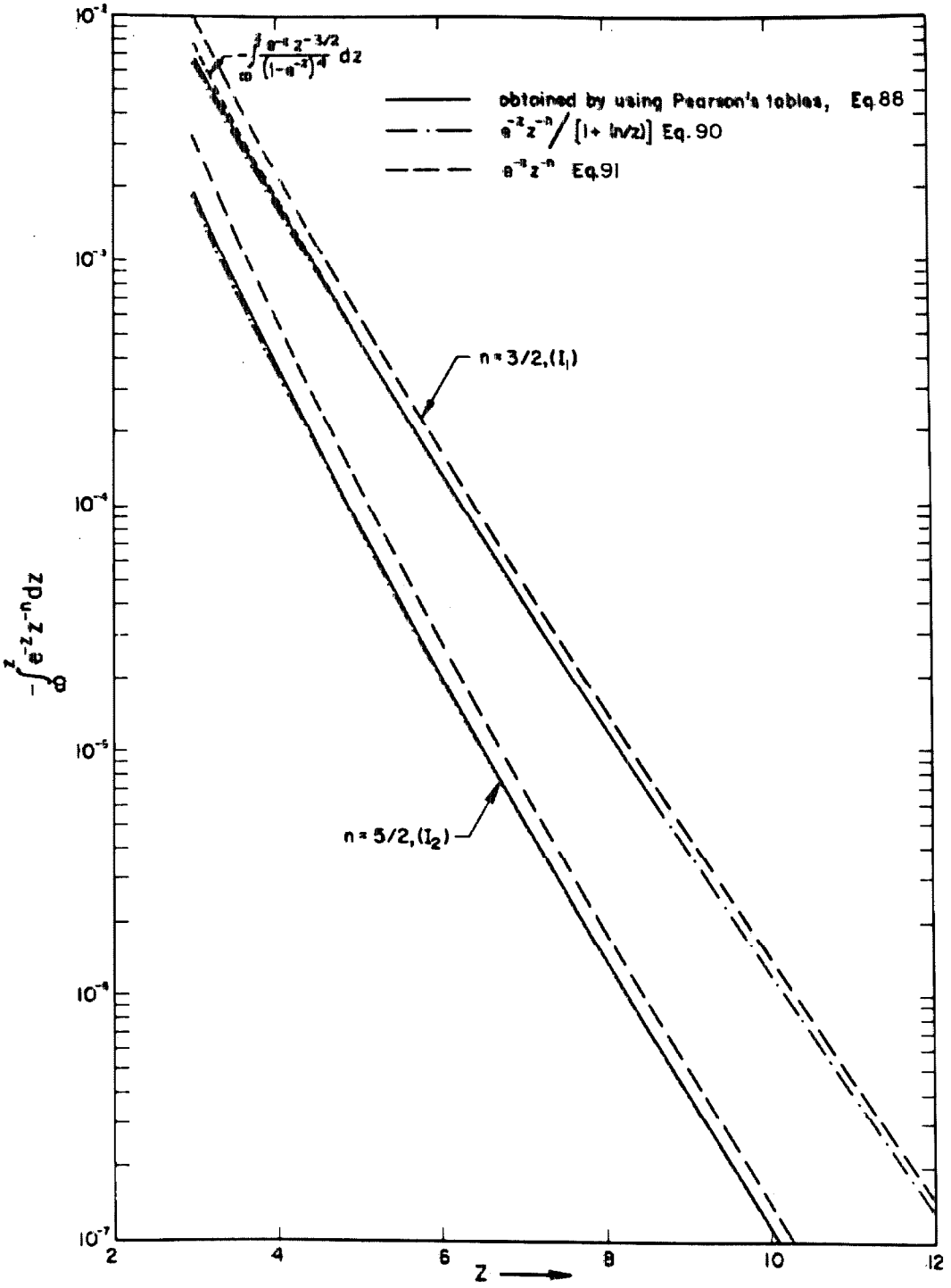

Fig. 14a. The quantity $-\int_{\infty}^{z} e^{-z} z^{-n} dz$ as a function of z for $3 \leq z \leq 12$. For comparison also $-\int_{\infty}^{z} \frac{e^{-z} z^{-3/2}}{(1-e^{-z})^4} dz$ is plotted, which determines s(T) for z of the order of 1 (see eq. 79).

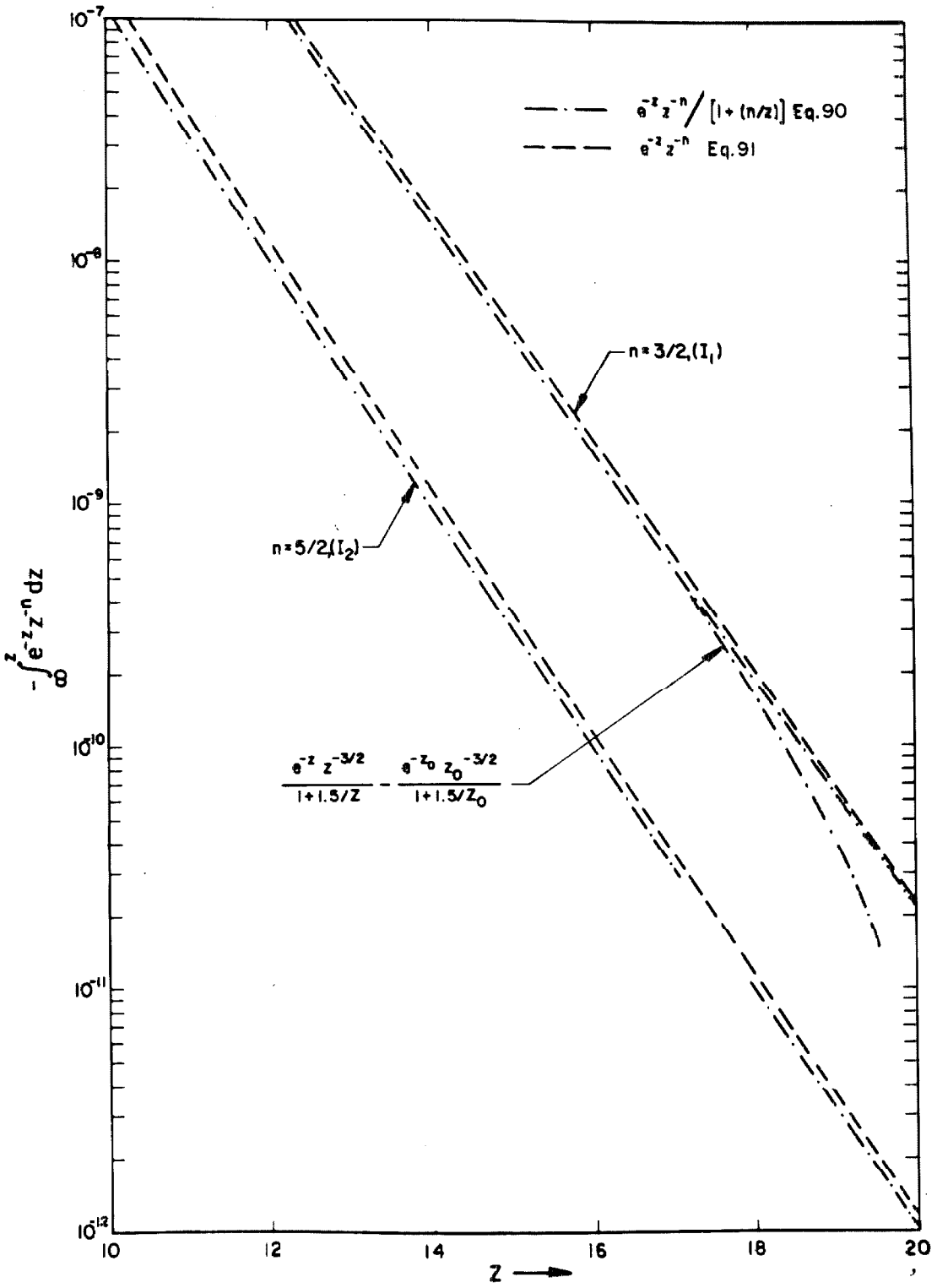

Fig. 14b. The quantity $-\int_{\infty}^{z} e^{-z} z^{-n} dz$ as a function of z for $10 \leq z \leq 20$ ($z_0 = 20$).

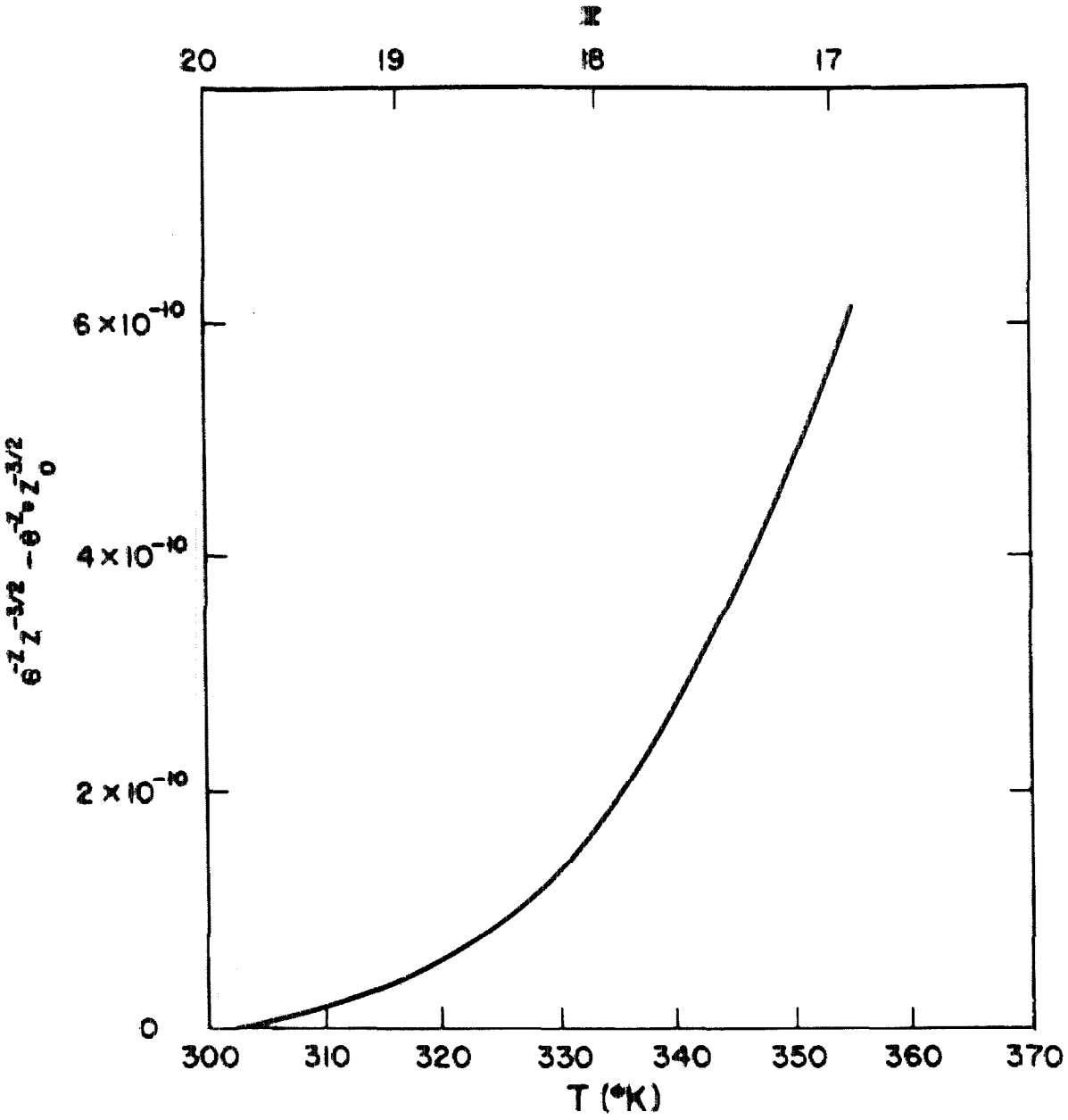

Fig. 15a. A plot of the first approximation to I_1 (see eq. 91) as a function of T and z (for $z_o = 20$, $T_o = 300\ ^oK$, $E_\ell = 0$).

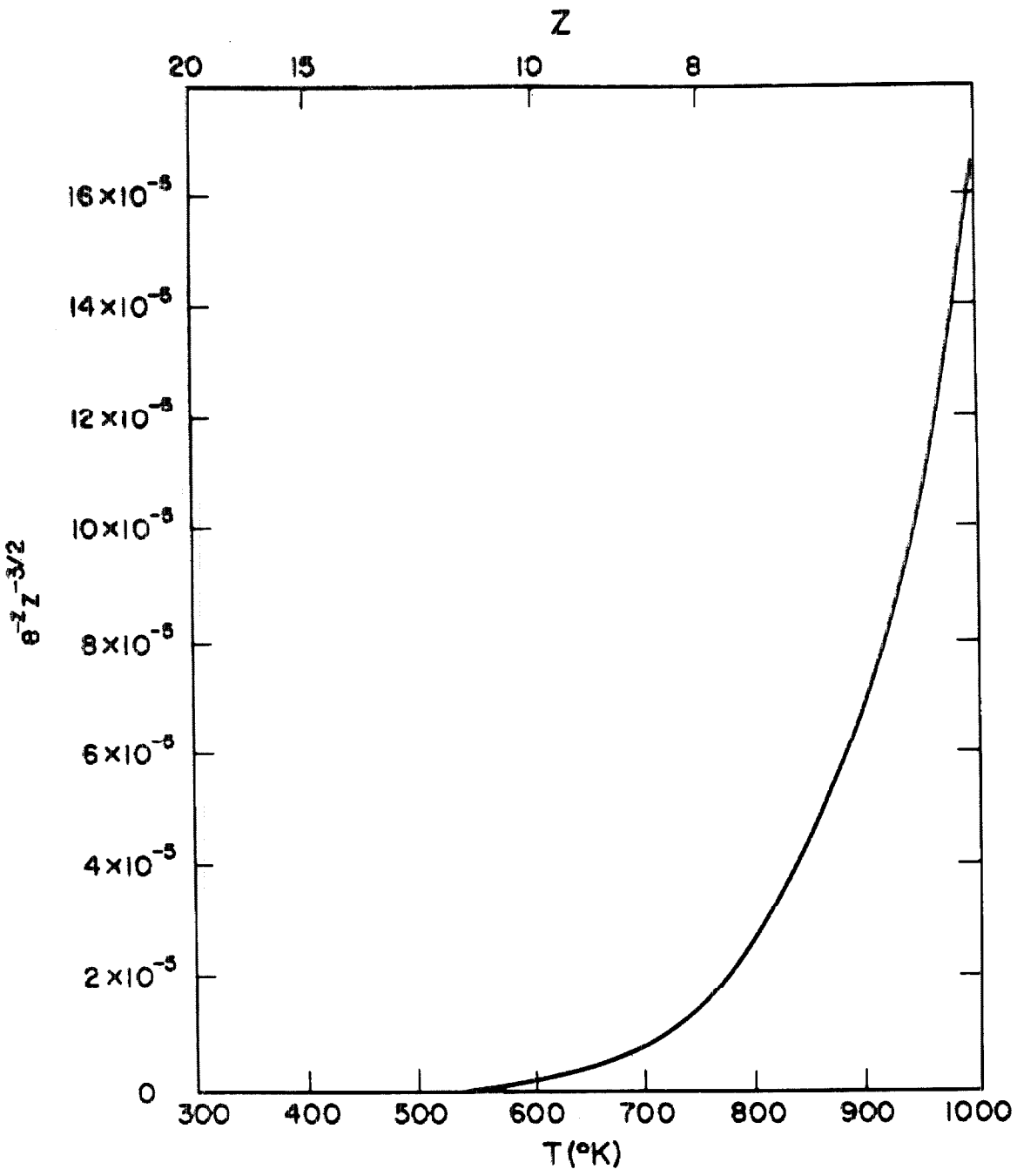

Fig. 15b. A plot of the first approximation to I_1 (see eq. 91) as a function of T and z (for $z_o = 20$, $T_o = 300\,^{o}K$, $E_\ell = 0$). The contribution of the term $e^{-z_o} z_o^{-3/2}$ to I_1 is negligibly small.

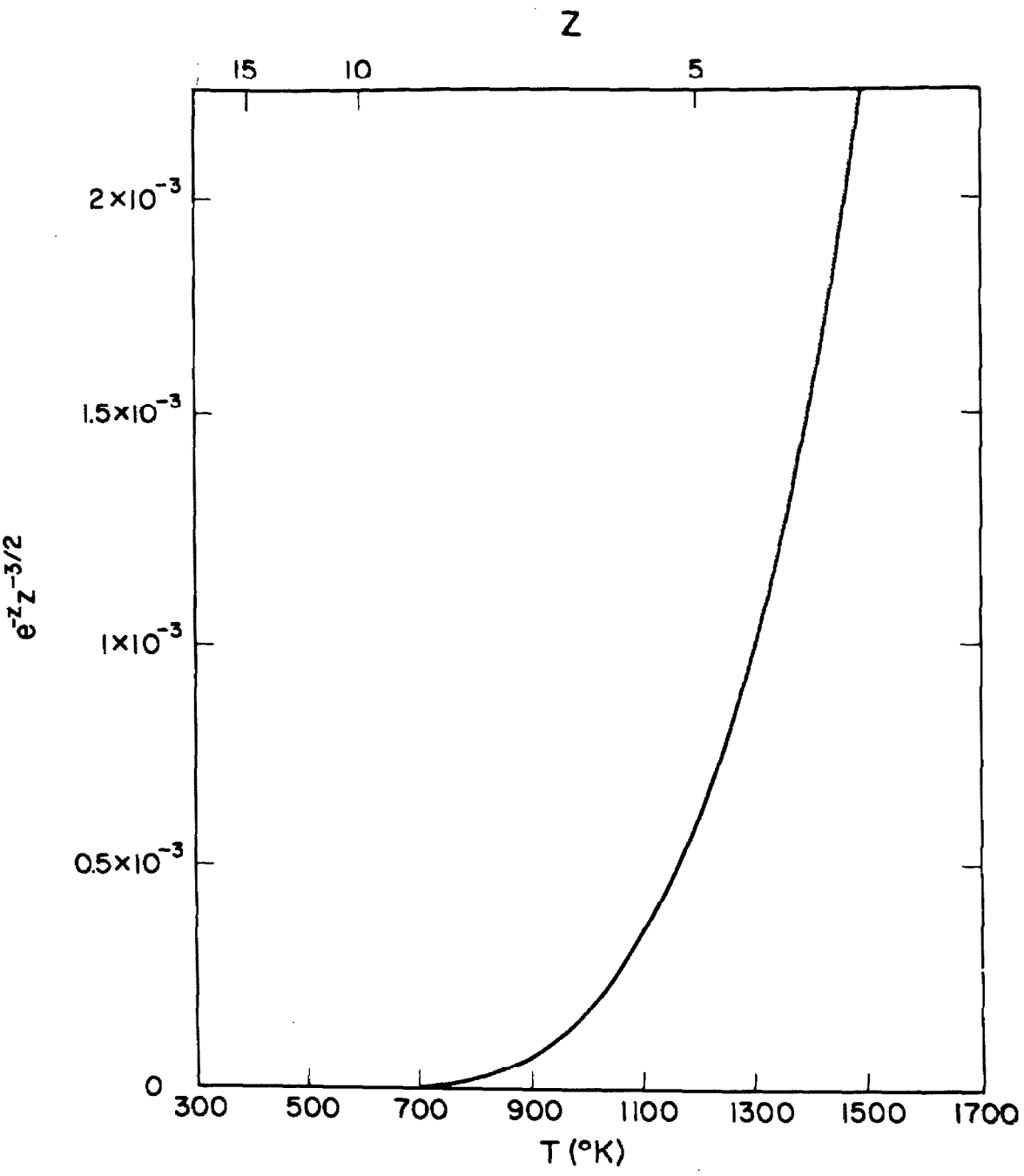

Fig. 15c. A plot of the first approximation to I_1 (see eq. 91) as a function of T and z (for $z_o = 20$, $T_o = 300\ ^oK$, $E_\ell = 0$). The contribution of the term $e^{-z_o} z_o^{-3/2}$ to I_1 is negligibly small.

3. Determination of Steradiancy $B(0,\theta)$ for $h\nu_o/kT_o \gg 1$, $u_o T_o/T \gg 1$

If a temperature profile is specified which differs from I_1 or I_2 by at most a constant factor, then the steradiancy $B(0,\theta)$ may be calculated for suitable frequency regions. From eq. 75 it is apparent that

$$B(0,\theta) = \int_o^\infty B_\nu^o(T_{\tau_\nu=\cos\theta'})\, d\nu \,, \tag{92}$$

where $B_\nu^o(T_{\tau_\nu=\cos\theta'})$ is the blackbody steradiancy at that location where $\tau_\nu/\cos\theta' = 1$. According to eq. 76,

$$a_1 = \left[B_\nu^o(T_{\tau_\nu=\cos\theta'}) - B_\nu^o(T_o) \right] / \cos\theta' \,. \tag{93}$$

Let us consider the temperature profile $(\cos\theta')s = L_1 l_1$, where the characteristic length L_1 is a constant. Close to the line center, eqs. 84 and 93 lead to the relation

$$B_\nu^o(T_{\tau_\nu=\cos\theta'}) - B_\nu^o(T_o) = \frac{\mathcal{C}}{L_1} b_o \left(\frac{h\nu_o - E_\ell}{kT_o} \right)^{1/2} T_o \cos\theta' \,. \tag{94}$$

Next we introduce eq. 94 into eq. 92 and integrate from $\nu_o - \Delta\nu_c$ to $\nu_o + \Delta\nu_c$, where $\Delta\nu_c$ is sufficiently small to justify use of the first term only in eq. 84. In this manner we obtain

$$\int_{\nu_o-\Delta\nu_c}^{\nu_o+\Delta\nu_c} B_\nu^o(T_{\tau_\nu=\cos\theta'})\, d\nu \simeq 2\, \frac{\mathcal{C} T_o}{L_1} b_o \left(\frac{h\nu_o - E_\ell}{kT_o} \right)^{1/2} \Delta\nu_c \cos\theta' , \tag{95}$$

where $B_\nu^o(T_o)$ has been neglected. The contribution of the term in eq. 86, which has been neglected in eq. 95, is close to $(\Delta\nu_o/b_o)^2$.

Let us now consider a temperature profile $(\cos\theta')s = L_2 I_2$ and investigate only the contribution of the wings in eq. 84. Then, proceeding as before,

$$B_\nu^o(T_{\tau_\nu=\cos\theta'}) = \frac{\mathcal{C}}{L_2} b_o T_o \left(\frac{h\nu_o - E_\ell}{kT_o}\right)^{3/2} \left(\frac{\nu-\nu_o}{b_o}\right)^2 \cos\theta' + B_\nu^o(T_o). \tag{96}$$

Introducing eq. 96 into eq. 92, we obtain the following integral

$$2\int_{\nu_o+\Delta\nu_w}^{\nu_o+\Delta\nu_w^u} B_\nu^o(T_{\tau_\nu=\cos\theta'})\,d\nu = \frac{2\mathcal{C}}{L_2} b_o^2 T_o \left(\frac{h\nu_o - E_\ell}{kT_o}\right)^{3/2} \cos\theta' \times \int_{\Delta\nu_w/b_o}^{\Delta\nu_w^u/b_o} \left(\frac{\nu-\nu_o}{b_o}\right)^2 d\left(\frac{\nu-\nu_o}{b_o}\right). \tag{97}$$

where $B_\nu^o(T_o)$ has been neglected.† The integration limit towards the center, $\nu_o+\Delta\nu_w$, must be chosen sufficiently large so that the first term in eq. 84 is negligibly small. The upper limit, $\nu_o + \Delta\nu_w^u$, must be consistent with the restriction that $\tau_\nu = \cos\theta'$ for all ν. Clearly the basic relation given in eq. 75 can only hold provided $T_{\tau_\nu=\cos\theta'} \leq T_{max}$, where T_{max} is the highest temperature of the system, i.e., the value of $\Delta\nu_w^u$ is determined by the expression

$$\frac{\Delta\nu_w^u}{b_o} \simeq \left[\frac{B_\nu^o(T_{max})L_2}{\mathcal{C} b_o T_o \cos\theta'}\left(\frac{kT_o}{h\nu_o - E_\ell}\right)^{3/2}\right]^{1/2}. \tag{98}$$

Hence eq. 97 becomes

† $B_\nu^o(T_o)$ may be neglected ordinarily unless $T \simeq$ constant or $\cos\theta' \simeq 0$.

$$2\int_{\nu_o+\Delta\nu_w}^{\nu_o+\Delta\nu_w^u} B_\nu^o(T_{\tau_\nu}=\cos\theta')d\nu \simeq \frac{2}{3}\frac{\mathcal{C}}{L_2} b_o^2 T_o \left(\frac{h\nu_o - E_\ell}{T_o}\right)^{3/2} \cos\theta'$$

$$\times \left\{\left[\frac{B_\nu^o(T_{max})L_2}{\mathcal{C}T_o b_o \cos\theta'}\left(\frac{kT_o}{h\nu_o - E_\ell}\right)^{3/2}\right]^{3/2} - \left(\frac{\Delta\nu_w}{b_o}\right)^3\right\} . \quad (99)$$

From eqs. 95 and 99 we may now determine the scaling parameters for the steradiancy. Since $\Delta\nu_c \propto b_o$ for a fixed ratio of the second term (which has been neglected) relative to the first term in eq. 84, we find

$$\int_{\nu_o-\Delta\nu_c}^{\nu_o+\Delta\nu_c} B_\nu^o(T_{\tau_\nu}=\cos\theta')\, d\nu \propto \frac{\rho_o}{L_1} \quad (100)$$

and

$$2\int_{\nu_o+\Delta\nu_w}^{\nu_o+\Delta\nu_w^u} B_\nu^o(T_{\tau_\nu}=\cos\theta')\, d\nu \propto \rho_o\sqrt{L_2} \quad \text{for } \Delta\nu_w \ll \Delta\nu_w^u . \quad (101)$$

The result given in eq. 101 is identical with the scaling parameter obtained for the wings of isothermal collision-broadened lines. This conclusion is consistent with Thomson's approximate considerations (21).

B. Isolated Spectral Lines Belonging to Diatomic Emitters with Doppler Broadening

From eqs. 78 and 48 we find that

$$ds = \frac{\mathcal{C}b_{D,o}}{a_1\cos\theta'}\left(\frac{1}{\pi \ln 2}\right)^{1/2}\left(\frac{T}{T_o}\right)^{1/2}\frac{\exp(-h\nu_o/kT)}{[1-\exp(-h\nu_o/kT)]^3}$$

$$\times \frac{\exp(E_\ell/kT)}{[1-\exp(-u_o T_o/T)]}\exp(\ln 2)\left[\left(\frac{\nu-\nu_o}{b_{D,o}}\right)^2\frac{T_o}{T}\right]dt \quad (102)$$

where $\mathcal{C}$ is given by eq. 80.

1. The Limiting Case $h\nu_o/kT \ll 1$, $u_o T_o/T \ll 1$, $(h\nu_o - E_\ell)/kT \ll 1$

Equation 102 becomes now

$$ds \simeq \frac{\mathcal{C} b_{D,o}}{a_1 u_o \cos\theta'} \left(\frac{kT_o}{h\nu_o}\right)^3 \left(\frac{1}{\pi \ln 2}\right)^{1/2} \left(\frac{T}{T_o}\right)^{9/2} \exp\left[(\ln 2)\left(\frac{\nu-\nu_o}{b_{D,o}}\right)^2 \frac{T_o}{T}\right] dT \,. \tag{103}$$

We define the region near the line center by the condition that the exponential term may be replaced by unity. In this case

$$(\cos\theta')s = \mathcal{C}''\left[(T/T_o)^{11/2} - 1\right] \tag{104}$$

where

$$\mathcal{C}'' = \frac{2}{11} \frac{\mathcal{C} b_{D,o} T_o}{u_o a_1} \left(\frac{1}{\pi \ln 2}\right)^{1/2} \left(\frac{kT_o}{h\nu_o}\right)^3 .$$

When the exponent is sufficiently large, the following approximation may be used:

$$(\cos\theta')s = \mathcal{B}'' \left\{ \exp\left[(\ln 2)\left(\frac{\nu-\nu_o}{b_{D,o}}\right)^2\right] - \left(\frac{T}{T_o}\right)^{13/2} \exp\left[(\ln 2)\left(\frac{\nu-\nu_o}{b_{D,o}}\right)^2 \frac{T_o}{T}\right] \right\} \tag{105}$$

where

$$\mathcal{B}'' = \frac{\mathcal{C} b_{D,o}}{u_o a_1 \ln 2} T_o \left(\frac{1}{\pi \ln 2}\right)^{1/2} \left(\frac{kT_o}{h\nu_o}\right)^3 \left(\frac{b_{D,o}}{\nu-\nu_o}\right)^2 .$$

2. The Limiting Case $h\nu_o/kT \gg 1$, $u_o T_o/T \gg 1$

Integration of eq. 102 yields the expression

$$(\cos\theta')_s = \frac{\mathcal{C} b_{D,o} T_o}{a_1} \left(\frac{1}{\pi \ln 2}\right)^{1/2} \left[\frac{h\nu_o}{kT_o} - \frac{E_\ell}{kT_o} - (\ln 2)\left(\frac{\nu-\nu_o}{b_{D,o}}\right)^2\right]^{3/2}$$

$$\times \left[- \int_{w_o}^{w} w^{-5/2} e^{-w}\, dw \right] \tag{106}$$

where

$$w = \left[\frac{h\nu_o}{kT_o} - \frac{E_\ell}{kT_o} - (\ln 2)\left(\frac{\nu-\nu_o}{b_{D,o}}\right)^2\right]\frac{T_o}{T} .$$

For $w > 0$, we may proceed as with the collision-broadened lines and the integral

$$I_2' = - \int_{w_o}^{w} w^{-5/2} e^{-w}\, dw \tag{107}$$

may be evaluated by using the methods of Sec. VII, A(2).

Having assumed $h\nu_o/kT_o \gg 1$, the frequency region for $w < 0$ occurs far out in the line wings and contributes relatively little to the total steradiancy.

3. Determination of Steradiancy $B(0,\theta)$ for $h\nu_o/kT \gg 1$, $u_o T_o/T \gg 1$, $(h\nu_o - E_\ell)/kT \gg 1$

The frequency dependence of ds/dT given in eq. 106 does not permit us to choose $a_1(\nu)$ in such a way that a reduced distance-temperature profile can be constructed. The difficulty is caused by the occurrence of a product of frequency- and temperature dependent terms in the exponential.

Near the line center, we may, however, calculate the radiant flux since the integral I_2' is determined almost entirely by its upper

limit w_{min} (corresponding to $T = T_{max}$) provided that $w_o - w_{min} \gtrsim 2$. This property of the integral has been discussed in Section VII, A(2). Introducing the additional restrictions

$$\left(\frac{\nu-\nu_o}{b_{D,o}}\right)^2 \ln 2 \ll \frac{k\nu_o - E_\ell}{kT_o}$$

and (108)

$$\left(\frac{\nu-\nu_o}{b_{D,o}}\right)^2 (\ln 2)\ \frac{T_o}{T_{max}} \ll 1,$$

eq. 106 becomes

$$s \simeq \frac{G b_{D,o} T_o}{a_1(\cos\theta')}\left(\frac{1}{\pi \ln 2}\right)^{1/2}\left(\frac{h\nu_o - E_\ell}{kT_o}\right)^{3/2} I_2'' \qquad (109)$$

where

$$I_2'' = -\int_\infty^z z^{-5/2} e^{-z}\, dz, \quad z = (h\nu_o - E_\ell)/kT\ ,$$

and z is independent of ν.

The inequalities in eq. 108 become, for typical fundamental vibration-rotation bands of diatomic molecules,

$$\left(\frac{\nu-\nu_o}{b_{D,o}}\right)^2 \ll 30$$

and

$$\left(\frac{\nu-\nu_o}{b_{D,o}}\right)^2 \ll 1.4\,\frac{T_{max}}{T_o}\ .$$

Hence, for large values of T_{max}/T_o, the correct integral is obtained for a frequency range that may be appreciably larger than $b_{D,o}$. On the other hand, for systems with small temperature gradients, we have

obtained a temperature profile that is appreciable only very close to the line center.

For the temperature profile $s(\cos\theta') = L_3 I_2$, we find, after integrating over the frequency range $\nu_o - \Delta\nu_D$ to $\nu_o + \Delta\nu_D$ (compare eq. 95), that

$$\int_{\nu_o-\Delta\nu_D}^{\nu_o+\Delta\nu_D} B_\nu(T_{\tau_\nu=\cos\theta'})\, d\nu = 2\left[\frac{\mathcal{C} b_{D,o} T_o}{L_3}\left(\frac{1}{\pi \ln 2}\right)^{1/2}\left(\frac{h\nu_o - E_\ell}{kT_o}\right)^{3/2} \times (\cos\theta')\right]\Delta\nu_D. \qquad (110)$$

In general, the integral represents only the contributions arising from a narrow frequency range near the line center. Since it is reasonable to assume that $\Delta\nu_D$ is proportional to $b_{D,o}$, the radiancy for this frequency range near the line center is inversely proportional to $\rho_o L_3$.

C. Gray Body

With

$$k_\nu(T) = \bar{k} = \text{constant},$$

integration of eq. 78 leads to the expression

$$s(\cos\theta') = \frac{1}{a_1 \bar{k}} \frac{2h\nu^3}{c^2}\left[\frac{1}{\exp(h\nu/kT)-1} - \frac{1}{\exp(h\nu/kT_o)-1}\right]. \qquad (111)$$

In certain regions of frequency and temperature, eq. 111 reduces to a universal relation between s and T.

1. The Special Case $h\nu/kT_o \ll 1$

Equation 111 now reduces to

$$s(\cos\theta') = \frac{2k\nu^2}{a_1\bar{k}c^2}(T - T_o) . \tag{112}$$

Hence, for

$$s(\cos\theta') = \bar{L}(T - T_o) , \tag{113}$$

eqs. 92 and 93 lead to

$$\int_{\nu_1}^{\nu_2} B_\nu(0,\theta)\,d\nu = \int_{\nu_1}^{\nu_2} B_\nu^o(T_o)\,d\nu + \frac{2k}{3\bar{L}\bar{k}c^2}(\nu_2^3 - \nu_1^3)(\cos\theta') , \tag{114}$$

and if $T \gg T_o$, then $\int_{\nu_1}^{\nu_2} B_\nu(0,\theta)\,d\nu \propto (\rho_o\bar{L})^{-1}$; the scaling parameter is $\rho_o\bar{L}$.

2. The Special Case $h\nu/kT_o \gg 1$, $h\nu/kT \ll 1$

In eq. 112, T replaces $(T - T_o)$ and the preceding results apply.

3. The Special Case $h\nu/kT_o \gg 1$, $h\nu/kT \gg 1$

In this case there is no s-T curve which is independent of ν.

VIII. APPLICATION OF THE EDDINGTON-BARBIER APPROXIMATION TO DISPERSION- AND DOPPLER-BROADENED SPECTRAL LINES FOR AN ARBITRARY TEMPERATURE PROFILE

We have seen in Section VI that the adoption of the Eddington-Barbier (EB) approximation is equivalent to specifying a particular temperature profile through a gas, e.g. the profiles shown in Figs. 15-a, b, c for the Lorentz-broadened lines. We now calculate the error in the radiant energy transfer which results from using the EB approximation with a temperature profile other than the one required theoretically. In the discussion below, we consider the temperature profile given by eq. 46. Numerical calculations will again be performed for the R3 line in the vibration-rotation spectrum of HF. The angle θ' defined in Fig. 12 will be taken equal to zero so that the statement of the EB approximation is the following: the spectral steradiancy emitted at $s = 2L_o$ is approximately equal to the black body steradiancy evaluated at $s = \bar{s}$ where

$$\tau = \int_{\bar{s}}^{2L_o} k_\nu(s)\, ds = 1 \quad . \tag{115}$$

A. Evaluation of the Spectral Steradiancy Using the Eddington-Barbier Approximation

Elementary arguments show that two types of profiles are to be expected. For sufficiently small optical depths, $\bar{s} < L_o$ at the line center; therefore, the spectral profile of the emitted line will be a maximum at the line center and may become undefined in the line wings since the value of $\bar{s}$ required in eq. 115 actually becomes less than zero. For

sufficiently large optical depths, $\bar{s} > L_o$ at the line center and the emission profile will peak in the line wings at a frequency determined by the requirement specified in eq. 115. At this frequency peak, the EB approximation implies that the steradiancy will be equal to the black body steradiancy evaluated at the maximum temperature in the temperature profile, a physically unreasonable result.

Although the qualitative shapes of the spectral line are similar to the exact contours given in Figs. 3 and 4, it is apparent that the EB approximation can be valid only in isolated spectral regions and can not give accurate results over the whole spectral range. In Figs. 16 to 19 the line shapes are shown as calculated both by using exact formulas and by using the EB approximation for dispersion- and Doppler-broadened lines for various values of τ_o. The total steradiancies $(B/2b_o)$ found by integrating over frequency for the spectral lines shown in Figs. 16 to 18 are listed in Table 3. It is seen that, in general, the EB approximation is not a useful procedure for calculating accurately the total steradiancy of spectral lines for typical temperature profiles.

B. *The Limit of Optically Thick or Optically Thin Systems*

The Eddington-Barbier approximation was developed for astrophysical applications. It was not intended for use in optically thin gases and, in fact, is undefined in that limit. However, we now show that the EB approximation is valid for the large optical depths which may be encountered at the centers of a spectral lines.

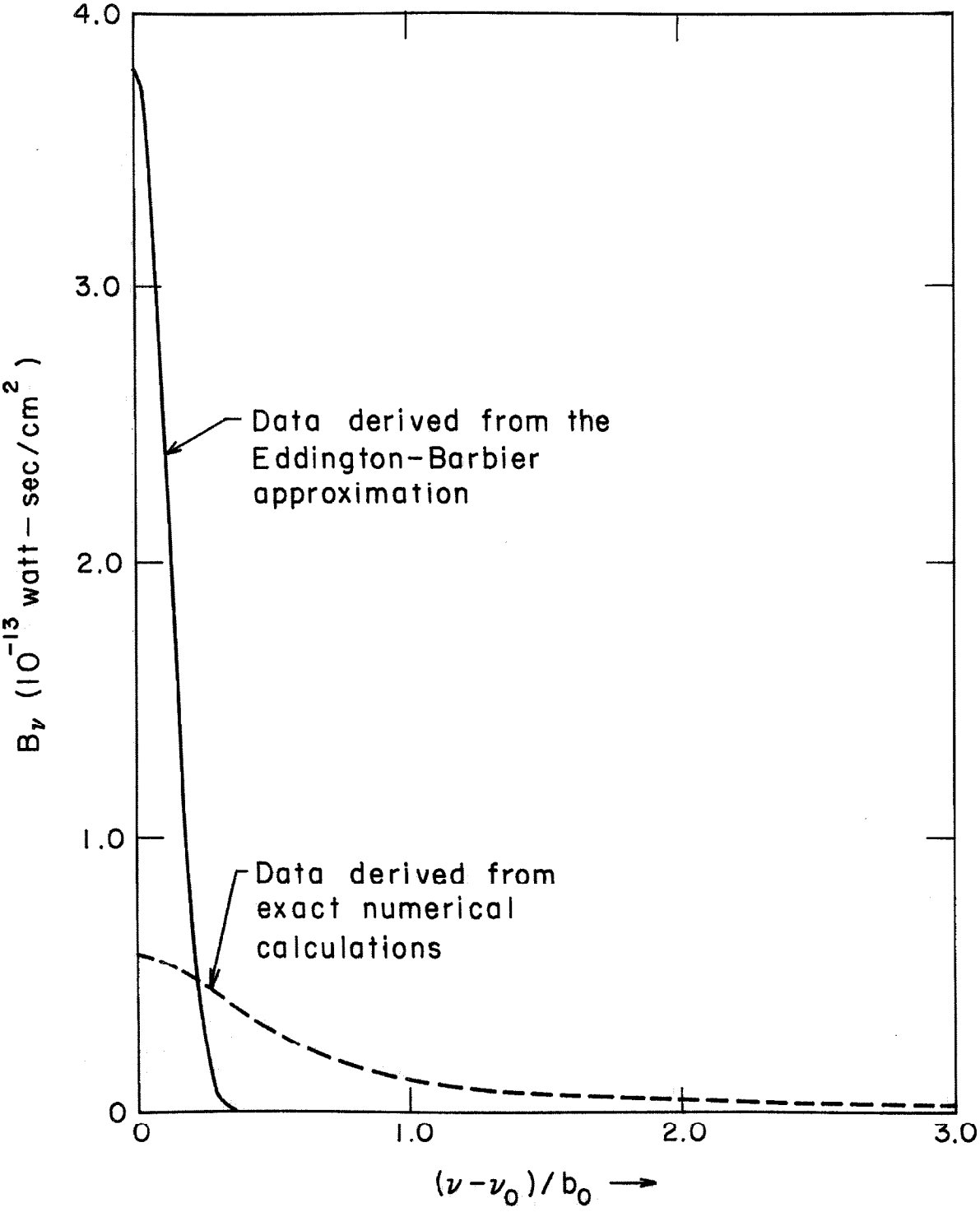

Fig. 16. The exact spectral steradiancies for the R3 line of HF are compared with results derived from the Eddington-Barbier approximation. A dispersion contour was used; m = 2 and $\tau_0 = 10$.

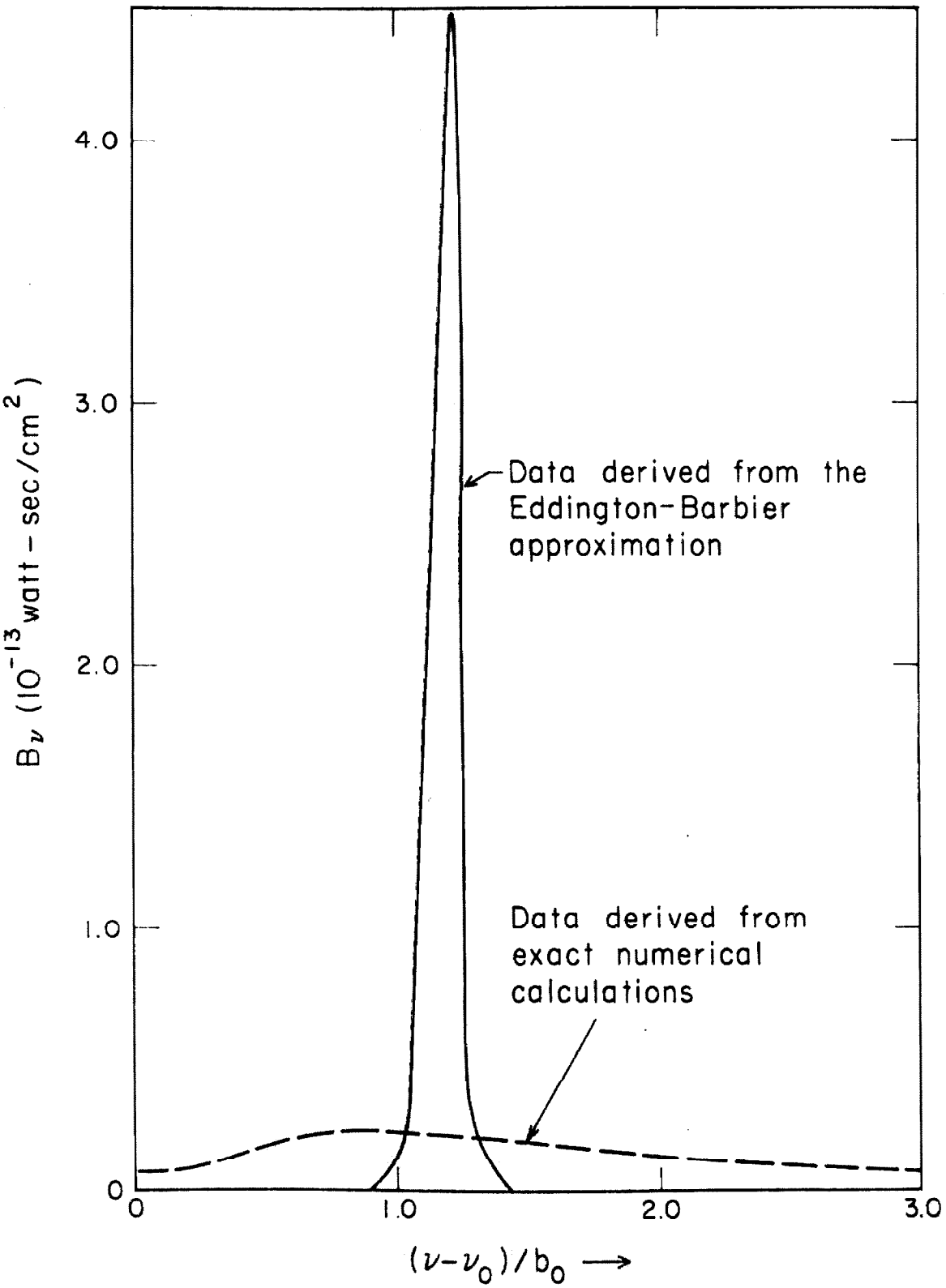

Fig. 17. The exact spectral steradiancies for the R3 line of HF are compared with results derived from the Eddington-Barbier approximation. A dispersion contour was used; m = 2 and $\tau_0 = 50$.

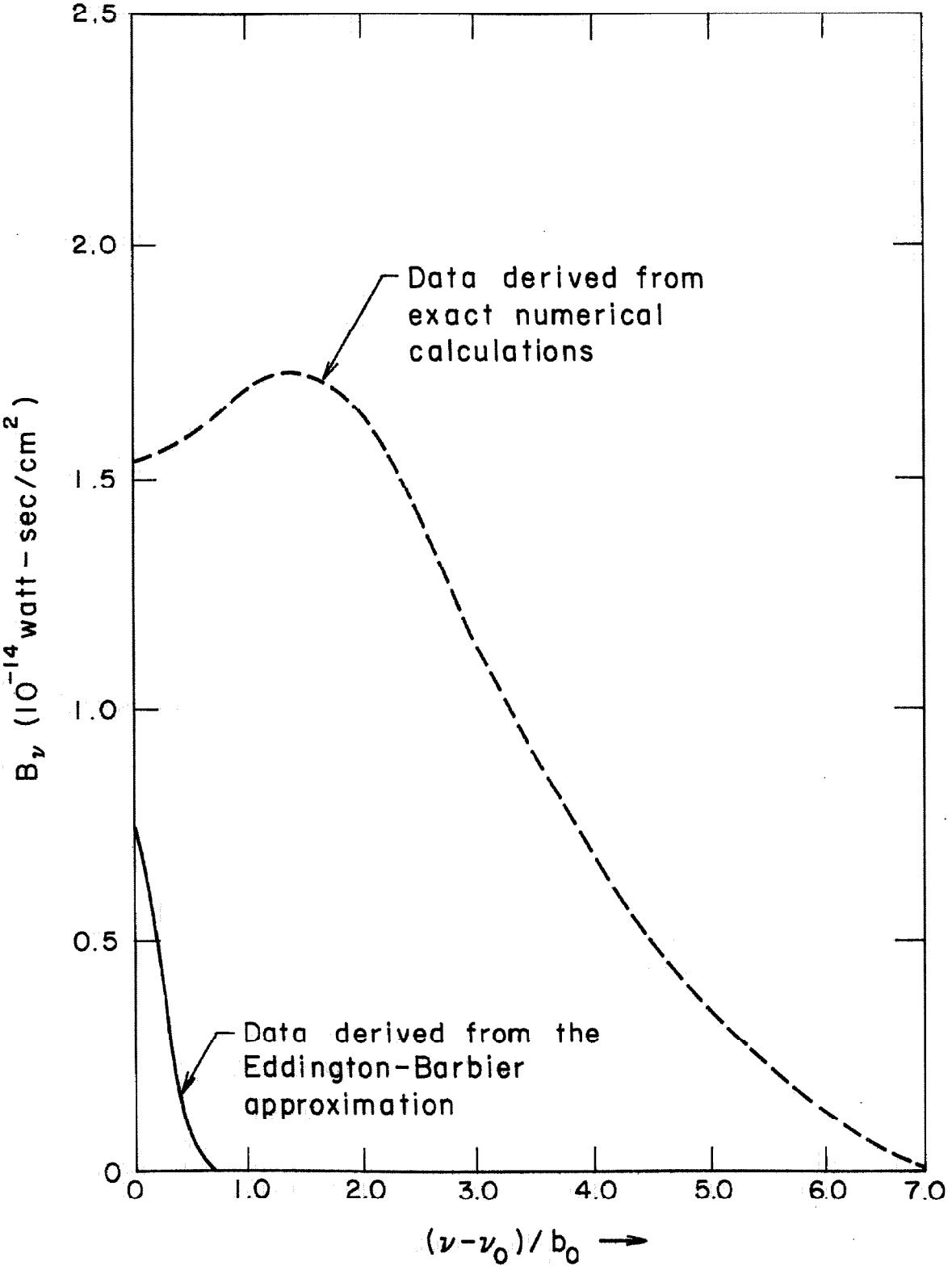

Fig. 1. The exact spectral steradiancies for the R3 line of HF are compared with results derived from the Eddington-Barbier approximation. A Doppler contour was used; m = 2 and $\tau_0 = 10$.

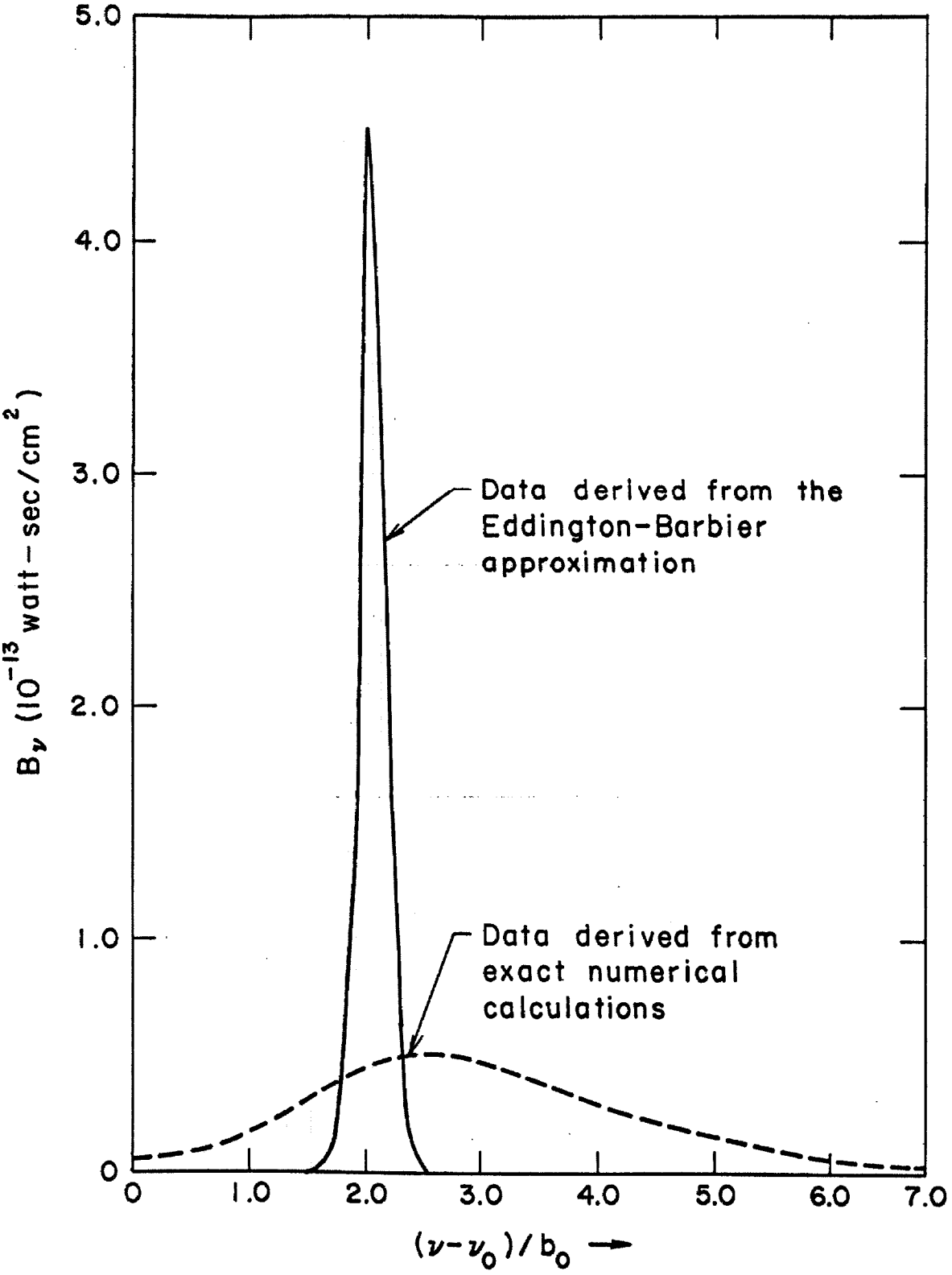

Fig. 19. The exact spectral steradiancies for the R3 line of HF are compared with results derived from the Eddington-Barbier approximation. A Doppler contour was used; m = 2 and $\tau_0 = 50$.

Table 3. Total Steradiancy for the R3 line of HF and a Representative Temperature Profile

m	τ_o		$B/2b_o$ (10^{-14} watt-sec/cm^2)	
See eq. 59	Reference optical depth	Type of Broadening	Results obtained by an exact numerical integration	Results obtained using the Eddington-Barbier approximation
2	10	Dispersion	4.80	5.68
2	50	Dispersion	7.57	4.92
2	10	Doppler	6.49	0.21
2	50	Doppler	17.13	11.94

Equation 52 may be rewritten as

$$B_\nu = B_\nu^o - \frac{1}{k_\nu}\frac{dB_\nu^o}{ds} + \frac{1}{k_\nu^2}\left[\frac{d^2B_\nu^o}{ds^2} - \frac{dB_\nu^o}{ds}\frac{d\ln k_\nu}{ds}\right]$$

$$- \frac{1}{k_\nu^3}\left[\frac{d^3B_\nu^o}{ds^3} - 3\frac{d^2B_\nu^o}{ds^2}\frac{d\ln k_\nu}{ds} - \frac{dB_\nu^o}{ds}\frac{d^2\ln k_\nu}{ds^2} + 2\frac{dB_\nu^o}{ds}\left(\frac{d\ln k_\nu}{ds}\right)^2\right] + \ldots \tag{116}$$

This equation is useful for large optical depths and leads directly to the diffusion approximation (see Appendix A). For large optical depths, the condition defined by eq. 115 will be satisfied for $\bar{s}$ only slightly less than $2L_o$, or

$$\bar{s} = 2L_o - \Delta s\ , \tag{117}$$

where Δs is small. For sufficiently opaque gases, B_ν^o and k_ν may be expanded in appropriate Taylor series. Thus

$$k_\nu(s) = k_\nu(2L_o) + (s - 2L_o)\frac{\partial k_\nu}{\partial s}\bigg|_{2L_o} + \ldots \tag{118}$$

and

$$B_\nu^o(\tau{=}1) = B_\nu^o(2L_o) - \Delta s\frac{\partial B_\nu^o}{\partial s}\bigg|_{2L_o} + \frac{\Delta s^2}{2}\frac{\partial^2 B_\nu^o}{\partial s^2}\bigg|_{2L_o} + \ldots \tag{119}$$

Neglecting third order terms in Δs, we obtain from eqs. 115, 117, and 118 the following results:

$$\Delta s \simeq \frac{1}{k_\nu} + \frac{1}{2}\frac{\partial \ln k_\nu}{\partial s}\Delta s^2\ ,$$

and

$$\Delta s^2 \simeq \frac{1}{k_\nu^2}\left(1 + \frac{1}{k_\nu}\frac{\partial \ln k_\nu}{\partial s}\Delta s^2\right) \simeq \frac{1}{k_\nu^2}\ ,$$

where the terms are evaluated at $s = 2L_o$. Substituting the above relations into eq. 119, we obtain

$$B_\nu^o(\tau=1) = B_\nu^o - \frac{1}{k_\nu}\frac{\partial B_\nu^o}{\partial s} + \left(\frac{1}{2}\right)\frac{1}{k_\nu^2}\left[\frac{\partial^2 B_\nu^o}{\partial s^2} - \frac{dB_\nu^o}{ds}\frac{d \ln k_\nu}{ds}\right] + \ldots \qquad (120)$$

where terms on the right-hand side are evaluated at $s = 2L_o$. To first order in $1/k_\nu$, eq. 120 agrees with eq. 116; however, the second order term is lower than that of eq. 116 by a factor of (1/2). We may conclude that as a gas becomes optically thick, the EB approximation becomes valid for any temperature profile and spectral absorption coefficient.

It is interesting to compare the results of the EB approximation for the steradiancy at the line center with those calculated by other means and presented in Table 2 in Sec. VI (C). The new results are given in Table 4. It can be seen that the EB approximation is less accurate than the method used in the previous section and that the results derived from the EB approximation are too low, as predicted by eq. 120.

We know from the analysis of Sec. VII that the EB approximation is exact for a temperature profile such that the Lunblad series, eq. 73, is terminated after two terms, i.e.

$$B_\nu^o(s) = a_o + a_1\int^s k_\nu \, ds. \qquad (121)$$

In order for eq. 120 to reduce to eq. 116 it is necessary that the third term vanish, or

Table 4. Spectral Steradiancy at the Line Center for the R3 Line of HF and a Representative Temperature Profile (Dispersion-Broadened Line)

m	τ_o	x_{ν_o}	B_{ν_o} (10^{-19} watt-sec/cm^2)	
See eq. 59	Reference optical depth	See eq. 63	Results obtained by an exact numerical integration	Results obtained by using the Eddington-Barbier approximation
1	1000	0.179	0.083	0.082
1	500	0.358	0.105	0.097
2	1000	0.358	0.105	0.098
2	500	0.716	0.209	0.139
4	1000	0.716	0.208	0.139
4	500	1.432	3.12	0.277

$$\frac{\partial^2 B_\nu}{\partial s^2} = \frac{\partial B_\nu^o}{\partial s} \frac{\partial \ln k_\nu}{\partial s} \tag{122}$$

One may easily check that eq. 121 is a solution to eq. 122. If an additional term is kept in the Lunblad series, one may determine that eq. 122 is not satisfied so that the second order term remains, but the third order term in eq. 116 vanishes. It is apparent that if n terms are kept in the Lunblad series, the analysis leading to eq. 120 will yield equations for the steradiancy accurate through the n^{th} term for a general temperature profile. Furthermore these equations will have the same terms in the expansion as does eq. 116, the exact solution, even past the n^{th} term except for a numerical factor. These conclusions are proved in Appendix B.

IX. RELATIVE IMPORTANCE OF THERMAL CONDUCTION AND RADIATION FOR ENERGY TRANSPORT IN STATIONARY HEATED AIR

Rather than employing the dimensionless groups of radiation gas dynamics derived in Sec. III, we may estimate directly the ratio of conductive to radiative energy transport in heated air in order to gain some insight into the conditions under which radiative energy transport becomes important in stationary systems. This procedure is used in the following computations. It should be noted that the results are directly applicable to flow problems with radiant energy transport only in the Rosseland (diffusion) limit since, in this case, the radiative and conductive heat transfer coefficients are additive. In the transparent gas limit, the important similarity group Γ (which measures the ratio of radiative energy loss from the system per unit surface area to the free stream rate of enthalpy transport per unit area) is the more meaningful parameter in gas-dynamic studies.

A. Heat Transfer Parameters

In the diffusion approximation, the ratio of heat transfer by thermal conduction to heat transfer by radiation is given by the relation

$$a_1 = \frac{3\lambda}{16\sigma T^3 \overline{\ell}_{L,Ro}} \quad ; \tag{123}$$

for transparent gases, this ratio is

$$a_2 \simeq \frac{(1/L)\lambda(\vee T)}{4\sigma T^4 \overline{k}_{L,P\ell}} \tag{124}$$

Here λ = coefficient of thermal conductivity, σ = Stefan-Boltzmann constant, T = absolute temperature, $\bar{\ell}_{L, Ro}$ = Rosseland mean free path, L = characteristic length, ∇T = typical temperature gradient, and $\bar{k}_{L, P\ell}$ = Planck mean absorption coefficient.

Values of $\bar{\ell}_{L, Ro}$ and $\bar{k}_{L, P\ell}$ have been obtained from the data listed in Ref. 22 where only the continuum contributions† to the spectral absorption coefficient of air were used. The coefficients of thermal conductivity for temperatures below 2eV were taken from the work of Peng and Pindroh (23), who used a shielded coulomb potential for electron-ion interactions. These estimates for λ are considered to be more accurate than those derived earlier by Hansen (24). For temperatures of 2eV and higher, the thermal conductivity of the electron gas is the dominant contribution to the total thermal conductivity. The coefficient of thermal conductivity was assumed to be given by the formula (25)

$$\lambda = \frac{80k^3(2k/m\pi)^{1/2}T^{5/2}\delta_T}{\pi e^4 \bar{z} \ln\left[9k^4T^4/4e^6\pi\bar{z}^2P_e(1+\bar{z})\right]}$$

† The method of Seaton [M. J. Seaton, Thermal inelastic collision processes, Rev. Mod. Phys. 30, 979-989 (1958)] which has been discussed also by Zhigulev, et al. [V. N. Zhigulev, Ye. A. Romishevskii, and V. K. Vertushkin, Role of radiation in modern gas dynamics, AIAA J. 1, 1473-1485 (1963) translated from Inzhenernii Zhurnal 1, 60-83 (1961)] has been shown to give results that do not differ greatly from those calculated by using a simple, approximate procedure described in Sec. X. At elevated temperatures and low densities, the line radiation becomes important and cannot properly be neglected.

where k = Boltzmann's constant, T = absolute temperature, δ_T = transport coefficient calculated numerically as a function of $\bar{z}$ in Ref. 25,† e = electronic charge, $\bar{z}$ = mean ion charge = $\Sigma n_i z_i^2 / \Sigma n_i z_i$, P_e = electron partial pressure, and n_i = concentration of particles with charge z_i. The expression for λ applies in the presence of D.C. current in a completely ionized gas. For partially ionized gases, corrections to the Spitzer and Härm relation may be found in Ref. 26 but these can be shown to be unimportant for our purposes.

Numerically, the equation for λ becomes

$$\lambda = \frac{2.465 \times 10^6 \theta^{5/2} \delta_T}{\bar{z} \log_{10}\left[\frac{2.401 \times 10^{20} \theta^3}{\bar{z}^2 \bar{m}(1+\bar{z}) N} \right]} \quad \frac{\text{erg}}{\text{cm-sec}^{\circ}\text{K}} \tag{125}$$

where θ = temperature in eV, $\bar{m}$ = mean particle charge = $\Sigma n_i z_i / \Sigma n_i$, and N = particle concentration = $5 \times 10^{19} \rho/\rho_o$ (where ρ is the mass density and $\rho_o = 1.293 \times 10^{-3}$ g/cm^3). If an electric field builds up sufficiently to restrain the flow of electric current, the values of λ from eq. 125 should be multiplied by 0.4. Values of λ for air, as calculated from eq. 125 (for $T \geq 2$eV) and taken from Ref. 23 (for $T < 2$eV) are shown in Fig. 20 as a function of temperature and density. In many practically important problems, eq. 125 is known to yield values for the total thermal conductivity that are good to within about a factor of two.

In Table 5 are listed the values used for λ, $\bar{\ell}_{L, Ro}$, and $\bar{k}_{L, P\ell}$ and the parameters a_1 and $a_2 L/\nabla T$ calculated from eqs. 123 and 124.

† The coefficient δ_T is obtained by interpolation from Table III of Ref. 25.

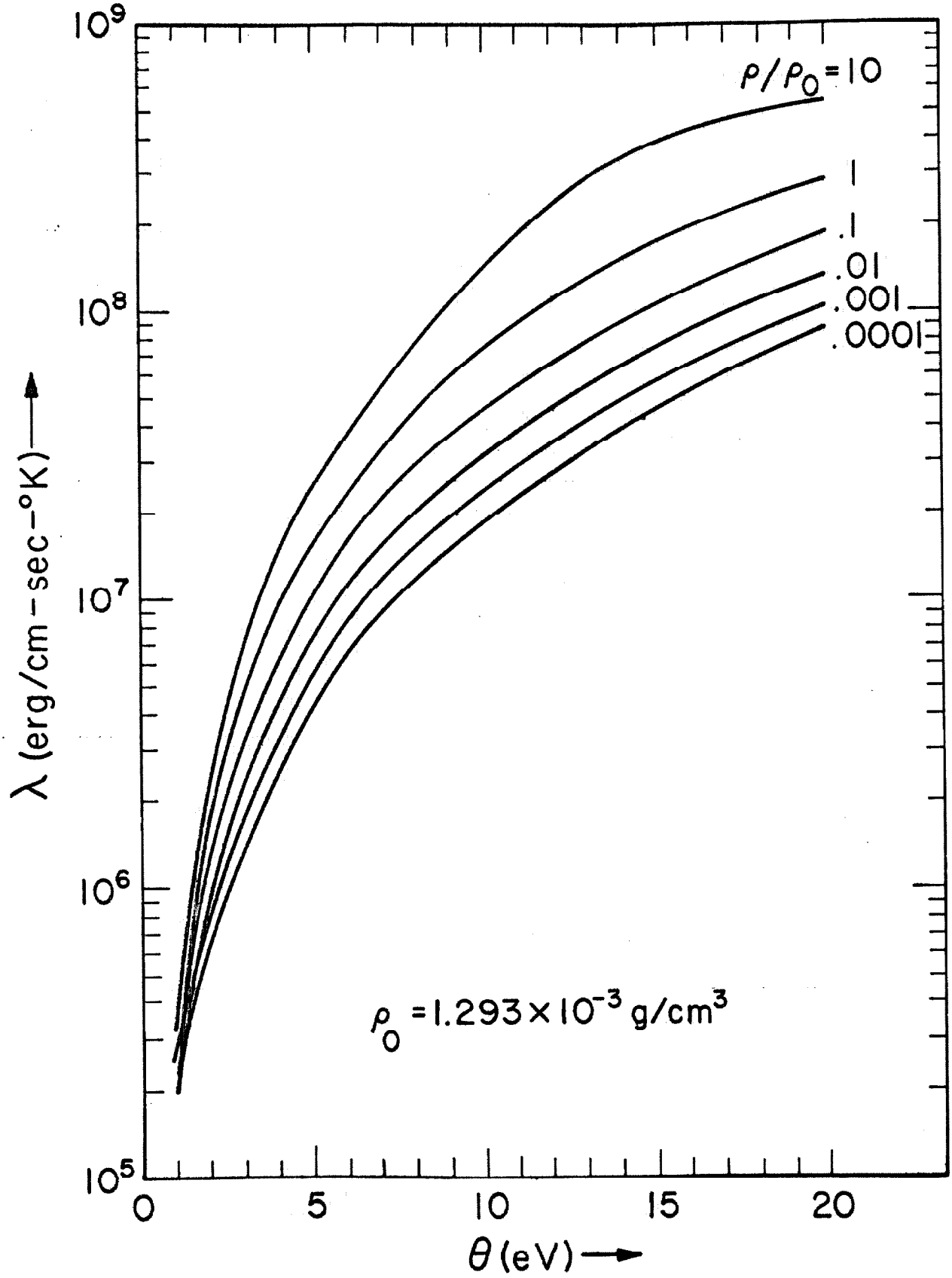

Fig. 20. The coefficient of thermal conductivity for air at temperatures to 230,000 °K for various densities. Data below 2eV were taken from Ref. 23; data above 2eV were calculated from eq. 3.

Table 5. Heat Transfer Parameters for High-Temperature Air

θ (eV)	$\log_{10}(\rho/\rho_o)$	λ[†] (erg/cm-sec°K)	$\bar{\ell}_{L,Ro}$[‡] (cm)	a_1	$k_{L,P\ell}$[§] (cm^{-1})	$\bar{\ell}_{L,P\ell}$ (cm)	$a_2 L/\nabla T$ (cm^2/°K)
0.7	1	2.30^{+5}	5.5^{+1}	2.6^{-5}	1.0	1.0	2.3^{-7}
	0	3.00^{+5}	1.1^{+3}	1.7^{-6}	4.0^{-2}	2.5^{+1}	7.6^{-6}
	-1	3.17^{+5}	1.5^{+4}	1.3^{-7}	3.0^{-3}	3.3^{+2}	1.1^{-4}
	-2	1.609^{+5}	2.0^{+5}	5.0^{-9}	1.7^{-4}	5.9^{+3}	9.6^{-4}
	-3	1.076^{+5}	3.0^{+6}	2.2^{-10}	8.0^{-6}	1.2^{+5}	1.4^{-2}
	-4	1.281^{+5}	3.0^{+7}	2.6^{-11}	3.0^{-7}	3.3^{+6}	4.3^{-1}
1.0	1	3.25^{+5}	7.0^{-1}	9.8^{-4}	2.0	5.0^{-1}	4.0^{-8}
	0	2.14^{+5}	1.4^{+1}	3.2^{-5}	1.0^{-1}	1.0^{+1}	5.2^{-7}
	-1	1.923^{+5}	2.0^{+2}	2.0^{-6}	7.0^{-3}	1.4^{+2}	6.7^{-6}
	-2	2.45^{+5}	6.0^{+3}	8.6^{-8}	4.0^{-4}	2.5^{+3}	1.5^{-4}
	-3	2.69^{+5}	8.0^{+4}	7.1^{-9}	3.5^{-5}	2.9^{+4}	1.9^{-3}
	-4	2.20^{+5}	1.3^{+6}	3.6^{-10}	1.4^{-6}	7.1^{+5}	3.8^{-2}
2.0	1	2.50^{+6}	2.1^{-2}	3.1^{-2}	2.2^{+2}	4.5^{-3}	1.7^{-10}
	0	2.02^{+6}	3.3^{-1}	1.6^{-3}	1.7^{+1}	5.9^{-2}	1.8^{-9}
	-1	1.335^{+6}	1.0^{+1}	3.5^{-5}	9.0^{-1}	1.1	2.3^{-8}
	-2	9.64^{+5}	5.5^{+2}	4.6^{-7}	1.0^{-2}	1.0^{+2}	1.5^{-6}
	-3	7.37^{+5}	2.5^{+4}	7.8^{-9}	2.3^{-4}	4.3^{+3}	4.9^{-5}
	-4	6.53^{+5}	8.0^{+5}	2.2^{-10}	4.5^{-6}	2.2^{+5}	2.2^{-3}
5.0	1	2.56^{+7}	2.7^{-3}	1.6^{-1}	3.5^{+2}	2.9^{-3}	2.8^{-11}
	0	1.554^{+7}	1.4^{-1}	1.9^{-3}	1.4^{+1}	7.1^{-2}	4.3^{-10}
	-1	1.045^{+7}	6.2	2.8^{-5}	4.0^{-1}	2.5	1.0^{-8}
	-2	7.37^{+6}	2.8^{+2}	4.5^{-7}	9.0^{-3}	1.1^{+2}	3.2^{-7}
	-3	5.44^{+6}	1.9^{+4}	4.8^{-9}	1.3^{-4}	7.7^{+3}	1.6^{-5}
	-4	4.31^{+6}	2.0^{+6}	3.6^{-11}	3.0^{-6}	3.3^{+5}	5.6^{-4}

Table 5 (Continued)

θ (ev)	$\log_{10}(\rho/\rho_o)$	$\lambda^{\dagger}$ (erg/cm-sec°K)	$\bar{\ell}_{L,Ro}{}^{\ddagger}$ (cm)	a_1	$k_{L,P\ell}{}^{\S}$ (cm^{-1})	$\bar{\ell}_{L,P\ell}$ (cm)	$a_2 L/\nabla T$ ($cm^2/°K$)
10.0	1	1.312^{+8}	4.0^{-3}	6.9^{-2}	2.7^{+2}	3.7^{-3}	1.2^{-11}
	0	7.32^{+7}	1.7^{-1}	9.1^{-4}	1.0^{+1}	1.0^{-1}	1.8^{-10}
	-1	4.66^{+7}	9.0	1.1^{-5}	2.0^{-1}	5.0	5.7^{-9}
	-2	3.20^{+7}	5.0^{+2}	1.4^{-7}	4.0^{-3}	2.5^{+2}	1.9^{-7}
	-3	2.36^{+7}	4.0^{+4}	1.2^{-9}	7.0^{-5}	1.4^{+4}	8.2^{-6}
	-4	1.860^{+7}	3.8^{+6}	1.0^{-11}	9.0^{-7}	1.1^{+6}	5.0^{-4}
15.0	1	3.93^{+8}	7.0^{-3}	3.5^{-2}	1.8^{+2}	5.6^{-3}	1.0^{-11}
	0	1.702^{+8}	3.0^{-1}	3.6^{-4}	5.0	2.0^{-1}	1.6^{-10}
	-1	1.056^{+8}	2.1^{+1}	3.2^{-6}	8.0^{-2}	1.2^{+1}	6.3^{-9}
	-2	7.41^{+7}	2.1^{+3}	2.2^{-8}	1.0^{-3}	1.0^{+3}	3.6^{-7}
	-3	5.67^{+7}	1.9^{+5}	1.9^{-10}	1.0^{-5}	1.0^{+5}	2.7^{-5}
	-4	4.59^{+7}	1.0^{+7}	2.9^{-12}	1.2^{-7}	8.3^{+6}	1.8^{-3}
20.0	1	5.40^{+8}	1.7^{-2}	8.4^{-3}	1.1^{+2}	9.1^{-3}	7.5^{-12}
	0	2.92^{+8}	8.0^{-1}	9.7^{-5}	2.0	5.0^{-1}	2.2^{-10}
	-1	1.878^{+8}	6.0^{+1}	8.3^{-7}	2.3^{-2}	4.3^{+1}	1.2^{-8}
	-2	1.365^{+8}	5.0^{+3}	7.2^{-9}	3.0^{-4}	3.3^{+3}	6.9^{-7}
	-3	1.071^{+8}	5.0^{+5}	5.7^{-11}	3.0^{-6}	3.3^{+6}	5.4^{-5}
	-4	8.76^{+7}	2.1^{+7}	1.1^{-12}	3.0^{-8}	3.3^{+7}	4.4^{-3}

Note: ρ = air density, $\rho_o = 1.293 \times 10^{-3}$ g/cm^3. Superscripts denote multiplication by the corresponding power of ten.

†For T = 0.7 and 1.0 eV, λ was found from the data of Ref. 23; for T > 1.0 eV, λ was calculated from eq. 125.

‡Values of $\bar{\ell}_{L,Ro}$ were obtained from Fig. 12 of Ref. 22.

§Values of $\bar{k}_{L,P\ell}$ were obtained from Fig. 11 of Ref. 22.

The dependence of a_1 on temperature and density is shown in Fig. 21. The initial rise of a_1 with temperature is caused by the rapid decrease with temperature of $\overline{\ell}_{L,Ro}$. However, as is shown in Fig. 12 of Ref. 22, $\overline{\ell}_{L,Ro}$ increases sharply at temperatures above 10eV at high densities and at somewhat lower temperatures for lower densities; hence a_1 decreases above a well-defined temperature (see Fig. 21). The increase in $\overline{\ell}_{L,Ro}$ occurs as a result of the shift in the maximum of $k_{\nu,L}$ (the spectral linear absorption coefficient) toward higher frequencies (i.e., away from the maximum of the Rosseland weighting function). This shift results from bound-free contributions of nitrogen and oxygen ions. Thus the peak of the spectral absorption coefficient of nitrogen occurs at $h\nu/kT \simeq 6.0$ and 10.0 for $kT = 5$ and 10eV, respectively, at a number density of 10^{17} cm^{-3}. The maximum of the Rosseland weighting function occurs at $h\nu/kT = 3.83$.

The variation of $a_2 L/\nabla T$ with temperature and density is shown in Fig. 22. The Planck mean absorption coefficient rises at low temperatures which, when combined with the $(1/T^4)$ factor in eq. 124, causes a downward trend in a_2. At high temperatures, $\overline{k}_{L,P\ell}$ decreases sharply and, therefore, the parameter a_2 tends to increase.

B. Representative Applications of the Heat Transfer Parameters to Problems of Engineering Interest

The numerical values of $\overline{\ell}_{L,Ro}$ and $\overline{\ell}_{L,P\ell}\left[\equiv (\overline{k}_{L,P\ell})^{-1}\right]$ in Table 5 determine the validity of the diffusion or transparent gas approximations. If L is a characteristic length of the system, the condition $\overline{\ell}_{L,Ro} \ll L$ implies that the diffusion approximation is

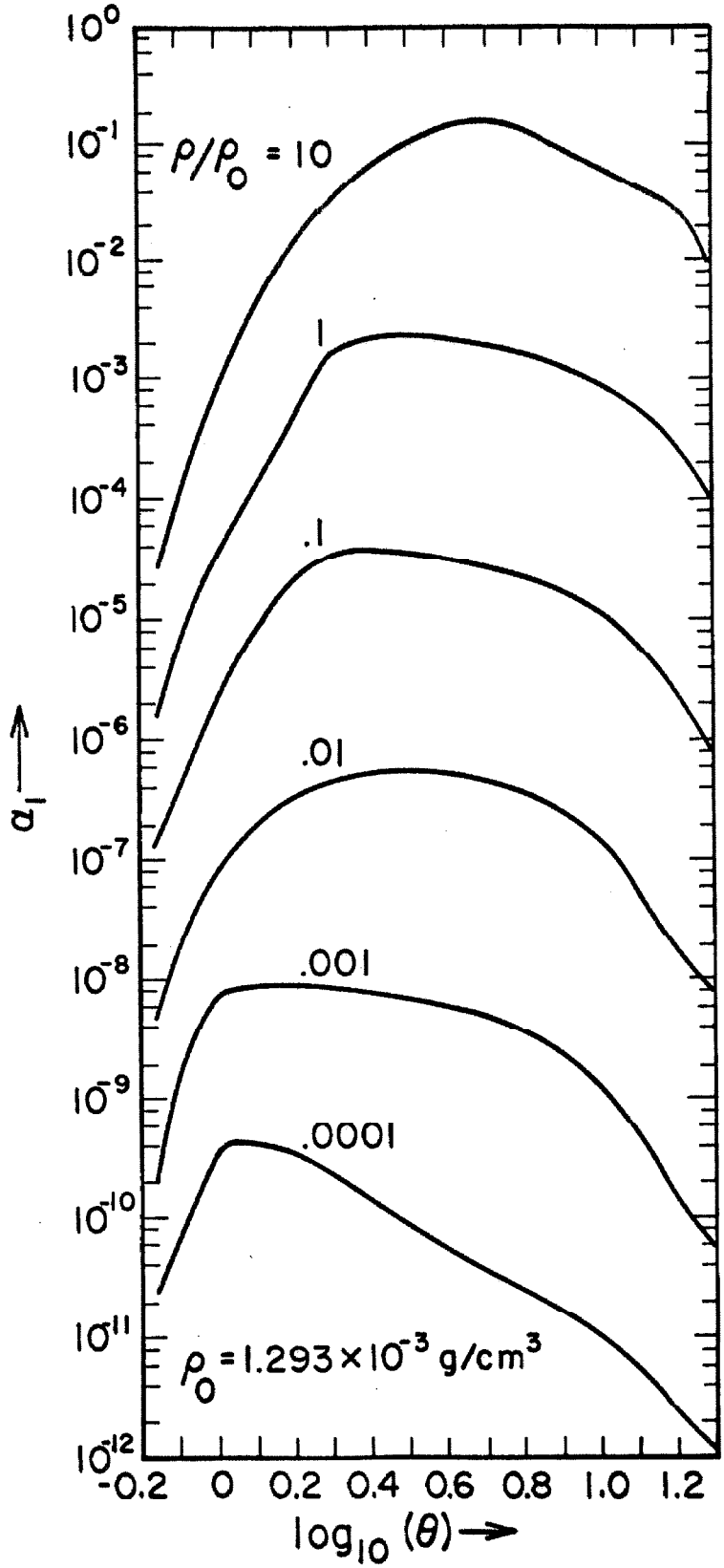

Fig. 21. The ratio of the heat transfer by thermal conduction to the heat transfer by radiation for optically thick air as a function of temperature and density; θ is expressed in eV.

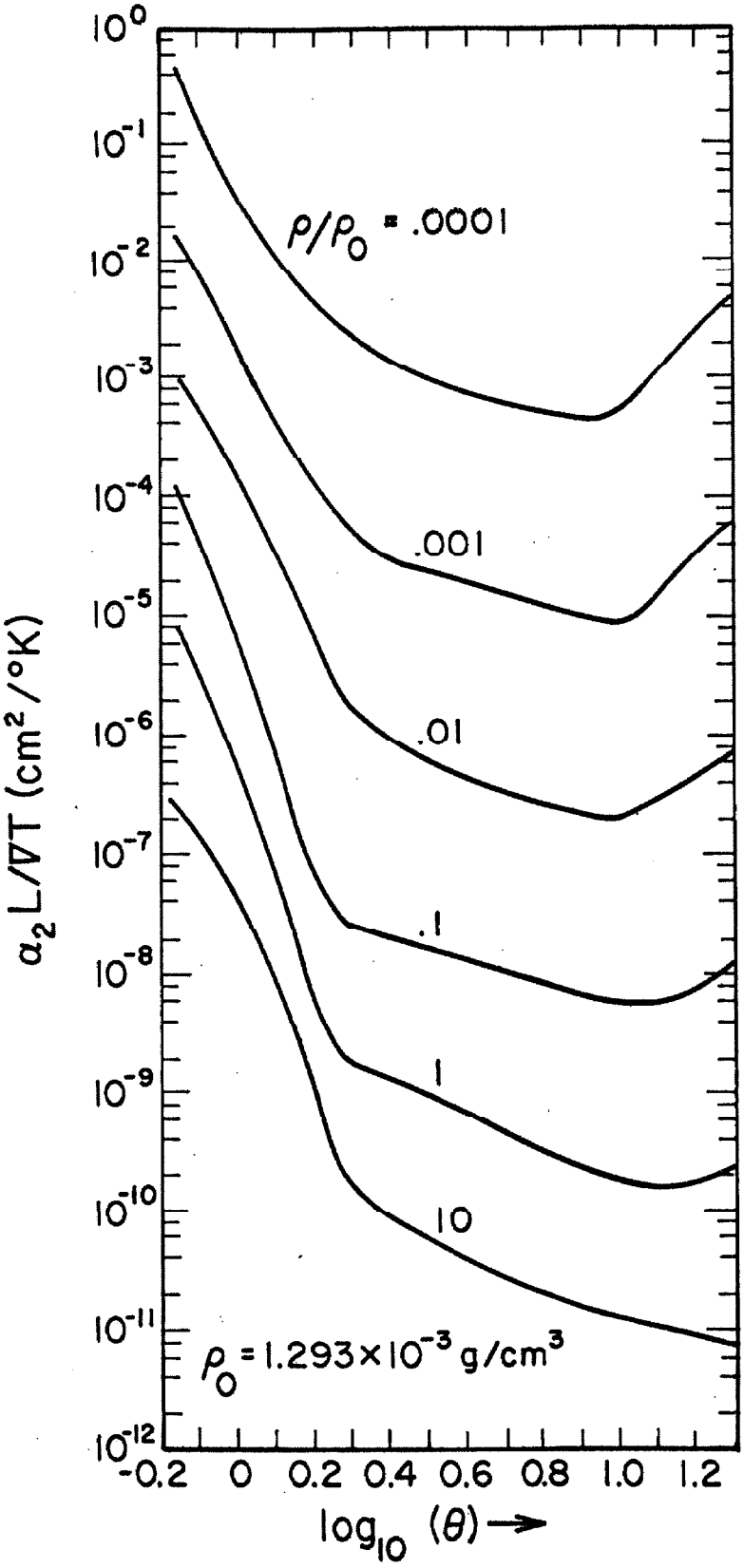

Fig. 22. The ratio of the heat transfer by thermal conduction to the heat transfer by radiation for optically thin air as a function of temperature and density; θ is expressed in eV.

applicable; similarly, the condition $\overline{\ell}_{L,P\ell} >> L$ indicates the validity of the transparent gas approximation. It is of some interest to consider the relative importance of radiant energy transfer in various regimes of gas dynamics.

$L \simeq 0.01$ cm. This value for L is of the order of magnitude of the wall boundary layer thickness in a shock tube from 1 to 100μ sec after the passage of the shock front; alternatively, L applies to the thermal layer thickness formed on a fast (velocity $\simeq$ 35,000-40,000 ft/sec, ρ/ρ_o = 1 to 10) atmospheric entry vehicle. For density ratios of 1 to 10 and temperatures below 2eV, $\overline{\ell}_{L,Ro}$ varies from 0.02 to 1.1×10^3 cm and $\overline{\ell}_{L,P\ell}$ varies from 4.5×10^{-3} to 25 cm. The diffusion approximation is therefore not valid whereas the transparent gas approximation applies only at the lower temperatures. Assuming a temperature drop of 10,000°K across the thermal layer, Fig. 22 shows that a_2 varies from 40 to 500 (corresponding to T = 1eV, ρ/ρ_o = 10 or 1), i.e., radiation energy transfer is relatively unimportant. Under more extreme conditions (ρ/ρ_o = 10, T = 2eV), $a_2 \simeq 0.02$, but the transparent gas approximation now begins to become invalid since $\overline{\ell}_{L,P\ell} \simeq 4.5 \times 10^{-3}$ cm.

$L \simeq 0.1$-1.0 cm. This estimate for L is of the order of magnitude of the thermal layer thickness on an atmospheric entry vehicle at high altitudes (altitude $\simeq$ 100,000 ft, velocity $\simeq$ 35,000 ft/sec, $\rho/\rho_o \simeq 10^{-1}$). The gas is transparent, $a_2 >> 1$, and radiation heating is relatively unimportant.

$L \simeq 1.0$-1000 cm. This range of values for L corresponds to

typical vehicle dimensions. For $T \simeq 0.7$eV, $\rho/\rho_o = 0.1$, $L = 10$ cm, $\nabla T = 10^3$ °K/cm, it is found that $\alpha_2 = 1.1 \times 10^{-2}$ and the transparent gas approximation is valid. In this case, radiation losses are more important than conduction losses.

$\underline{L \simeq 10^3\text{-}10^4 \text{ cm.}}$ These lengths correspond to characteristic diameters of initial fireballs of nuclear bombs. Taking $T \simeq 10$eV, $\rho/\rho_o = 0.1$ and $L = 10^4$ cm, we find from Table 5 that $\overline{\ell}_{L, Ro} = 9$ cm, and, therefore, the gas is optically thick. Also $\alpha_1 = 1.1 \times 10^{-5}$ and, for this reason, conductive heating is completely negligible inside the fireball.

$\underline{L > 10^4 \text{ cm.}}$ The next range of interest is mainly of astrophysical importance (we use air estimates since the continuum radiation in heated plasmas is not very sensitive to chemical composition). The values of $\overline{\ell}_{L, Ro}$ for air as found in Table 5 for low densities and $T = 20$eV will give an idea of some phenomena that may be important. We find $\overline{\ell}_{L, Ro} \simeq 100$ miles and $\alpha_1 \ll 1$ so that, as is well known, the diffusion approximation is valid for the atmospheres of stars and conductive energy transport is of lesser importance.

X. AN APPROXIMATE SEMI-ANALYTICAL EXPRESSION FOR THE SPECTRAL ABSORPTION COEFFICIENT IN AN IONIZED, POLYELECTRONIC PLASMA

Approximate expressions for the Rosseland and Planck mean free paths associated with the continuum radiation in ionized plasmas have been derived by Menzel and Pekeris (27) and by Pappert and Penner (28). The last-named authors followed a procedure described by Raizer (29, 30). The method of calculation introduced by Raizer (29, 30) and used by Pappert and Penner (28) differs from that employed in the earlier work of Menzel and Pekeris (27) by including only two representative m times ionized atoms instead of approximating the sum over the ions by an integral. The physical reasons for the use of this approximation may be made plausible by referring to the schematic diagram shown in Fig. 23 where the concentration of m-ions (i.e., of m times ionized atoms) is shown as a function of temperature. We note that there will be temperatures T at which the plasma composition is well described by the presence of two ionic constituents that are present in equal concentrations. Since all physical observables are expected to vary continuously with temperature, we expect that the use of the assumption that only two m-ions are present in equal concentrations for all values of T must lead to a good prediction of electron concentration at all temperatures. The use of this idea, together with the introduction of several supplementary simplifications due to Raizer, has been shown previously (28) to lead to results that agree, within about a factor of two, with the best available numerical computations for

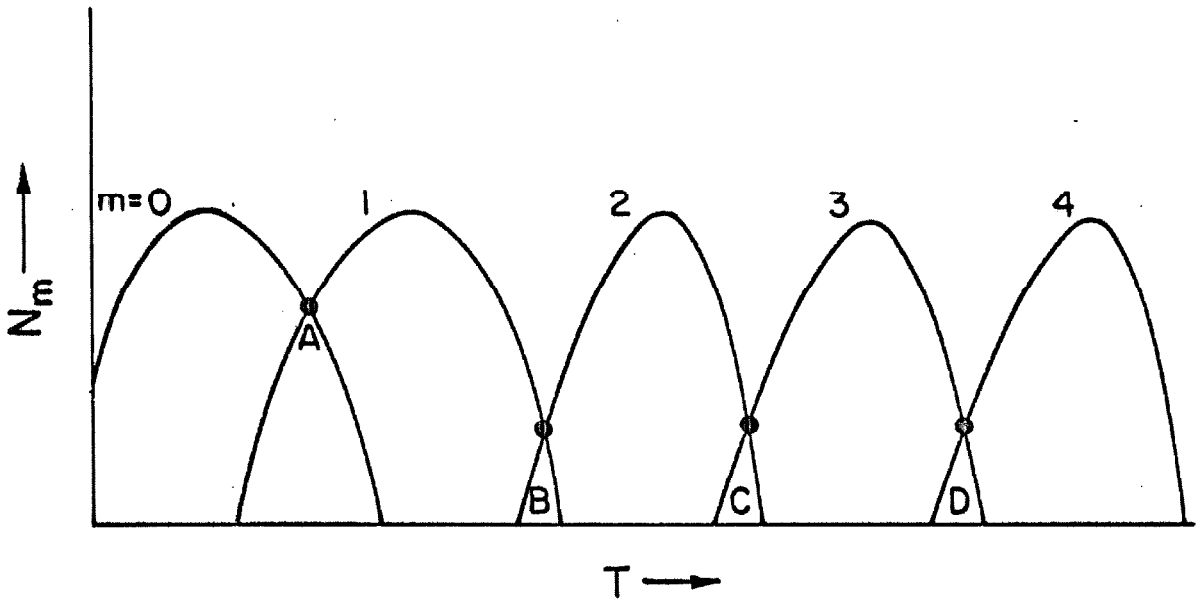

Fig. 23. Schematic diagram showing the concentration of m-ions, N_m, as a function of temperature, T. At the points A, B, C, D, etc., the plasma composition is well described by the presence of two m-ions that are present in equal concentrations.

Rosseland and Planck mean free paths (15). On the other hand, it is known[†] that the errors introduced by neglecting line radiation are of the same magnitude as or larger than, the previously noted discrepancies resulting from the use of highly simplified computational procedures, particularly at elevated temperatures and low densities. For this reason, it appears justified to avoid the labor involved in obtaining a complete solution to the Saha equation and to utilize again the approximation of two m-ions present in equal concentrations. We shall then show that the resulting estimates for the spectral absorption coefficients also agree, well within afactor of two over most of the frequency range, with the best available numerical computations.

A. Theoretical Considerations

In the following discussion we shall deviate from the analysis of Pappert and Penner (28) by considering the corrections required through proper introduction of statistical weight factors, which were not treated in an entirely consistent manner by Raizer (29, 30).

1. Degree of Ionization and Planck and Rosseland Mean Free Paths

The Saha equation for equilibrium between the concentrations N_m and N_{m+1} of m- and (m+1)-ions[‡], respectively, may be written in the form

$$\frac{N_{m+1}}{N_m} N_e = A' \left(\frac{g_e g_{m+1}}{g_m} \right) \theta^{3/2} \exp\left(- \frac{I_m}{\theta} \right) \tag{126}$$

[†] Private communication from Dr. J. C. Stewart of General Dynamics/ Astronautics, San Diego, California.

[‡] An m-ion is an m times ionized atom.

where N_e denotes the electron concentration;

$$A' = \left(\frac{2\pi m_e (1.6 \times 10^{-12})}{h^2} \right)^{3/2} \simeq 3.0 \times 10^{21} \text{ cm}^3\text{-eV}^{-3/2}$$

(m_e = electron mass, h = Planck's constant); g_e, g_{m+1}, and g_m are the statistical weights for the electron, the (m+1)-ion, and the m-ion, respectively; θ represents the energy-equivalent of the temperature in eV (in this section, all energies are expressed in electron volts); I_m denotes the ionization potential of the m-ion. Raizer (29, 30) and Pappert and Penner (28) set $g_e = 2$ and $g_{m+1}/g_m = 1$ whereas they used the Unsöld approximation $g_e g_{m+1}/g_m = 1$ in the opacity formulae. Actually the use of the assumption $g_e g_{m+1}/g_m = 1$ leads to a somewhat more satisfactory prediction of the average degree of ionization $\bar{m}$ than the statement $g_e g_{m+1}/g_m = 2$, as may be seen by reference to Fig. 24. In any case, a consistent approximation procedure requires the use of the same estimates for $g_e g_{m+1}/g_m$ everywhere.

If we employ the assumption $g_e g_{m+1}/g_m = 1$ everywhere, then the value of $A = 2A'$ appearing in the formulas of Pappert and Penner (28) for the Rosseland and Planck mean free paths should be divided by the factor 2 and, accordingly, all of the mean free path estimates should also be divided by a factor of two. Representative results plotted in Fig. 25 show that the data, obtained by introducing the specified change into the MR method of Ref. 28 for the Rosseland mean free path, still agree well with Armstrong's results, and that the approximate computations tend to be somewhat too low. However, with $A = 2A'$ replaced by A', the MR method leads to a larger deviation from

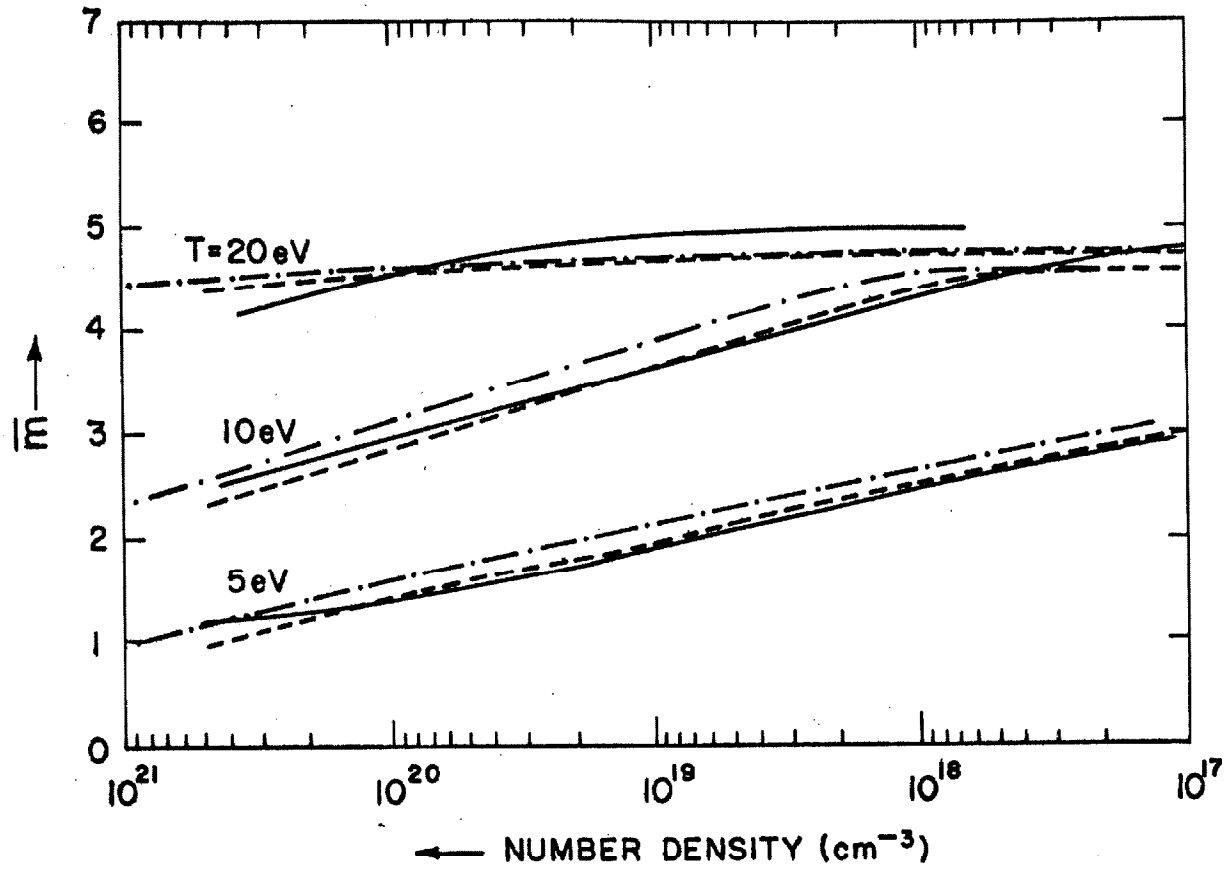

Fig. 24. The average number of electrons per atom ($\overline{m}$) as a function of the number density $N(cm^{-3})$ at various temperatures. The dashed curve refers to results derived from eq. 126 with $g_e g_{m+1}/g_m = 1$; the dot-dash curve (which has been given previously) refers to $g_e g_{m+1}/g_m = 2$; the solid curve is based on Armstrong's data (15).

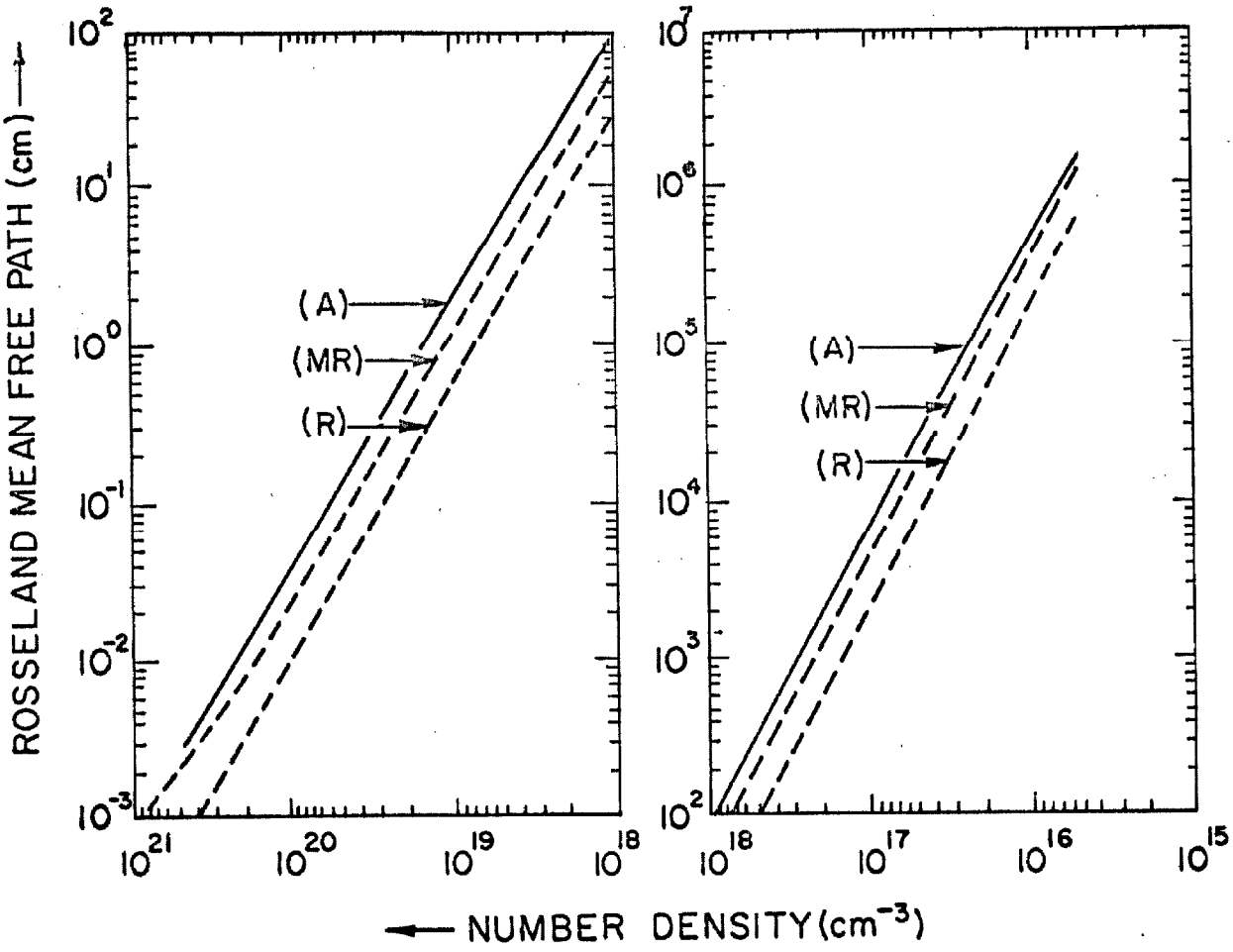

Fig. 25. The Rosseland mean free path (in cm) as a function of number density (in cm^{-3}) for nitrogen at 5 eV. The symbols (A), (R), and (MR) identify results obtained by Armstrong (A) and derived from the Raizer (R) and modified Raizer (MR) method of Pappert and Penner, respectively. In the (R) and (MR) plots, we have used consistently the approximation $g_e g_{m+1}/g_m = 1$. The theoretical formulae for the (R) and (MR) plots are given in Ref. 28.

Armstrong's results for the Planck mean free path, as may be seen in Fig. 26.

2. Theoretical Calculation of Spectral Absorption Coefficients

The following expression may be derived readily for the total linear absorption coefficient $k_m(x)$ associated with the bound-free contribution for an m-ion and the free-free contribution from an (m+1)-ion:

$$k_m(x) = a(g_e g_{m+1}/g_m)N_m(m+1)^2\theta^{-2}\exp(-x_{1m})F_m(x) \ . \qquad (127)$$

where

$$a = \frac{16\pi^2}{3\sqrt{3}} \frac{e^2}{ch} (1.6\times10^{-12})^{-2} \simeq 7.3\times10^{-16}\,\mathrm{cm}^2\text{-}(\mathrm{eV})^2, \quad x = \frac{h\nu}{\theta} \ ,$$

$$x_{1m} = \frac{I_m}{\theta} \ . \qquad (128)$$

Here N_m is the number density (cm^{-3}) of m-ions in the ground state.† For atoms and ions more complicated than those treated here, the labor involved is increased because of the necessity of estimating the ionization potentials of the contributing ions. Since the hydrogenic approximation has been made for the excited states, the frequency-dependent factor is given by

$$F_m(x) = x^{-3}\left[2x_{1m}\sum n^{-3}\exp\left(\frac{x_{1m}}{n^2}\right) + 1\right] . \qquad (129)$$

The first term in the brackets represents the bound-free contribution while the second term represents the free-free contribution to the absorption coefficient. In an ionized gas containing m-ions with

† For all practical purposes, N_m equals the total number of m-ions per unit volume.

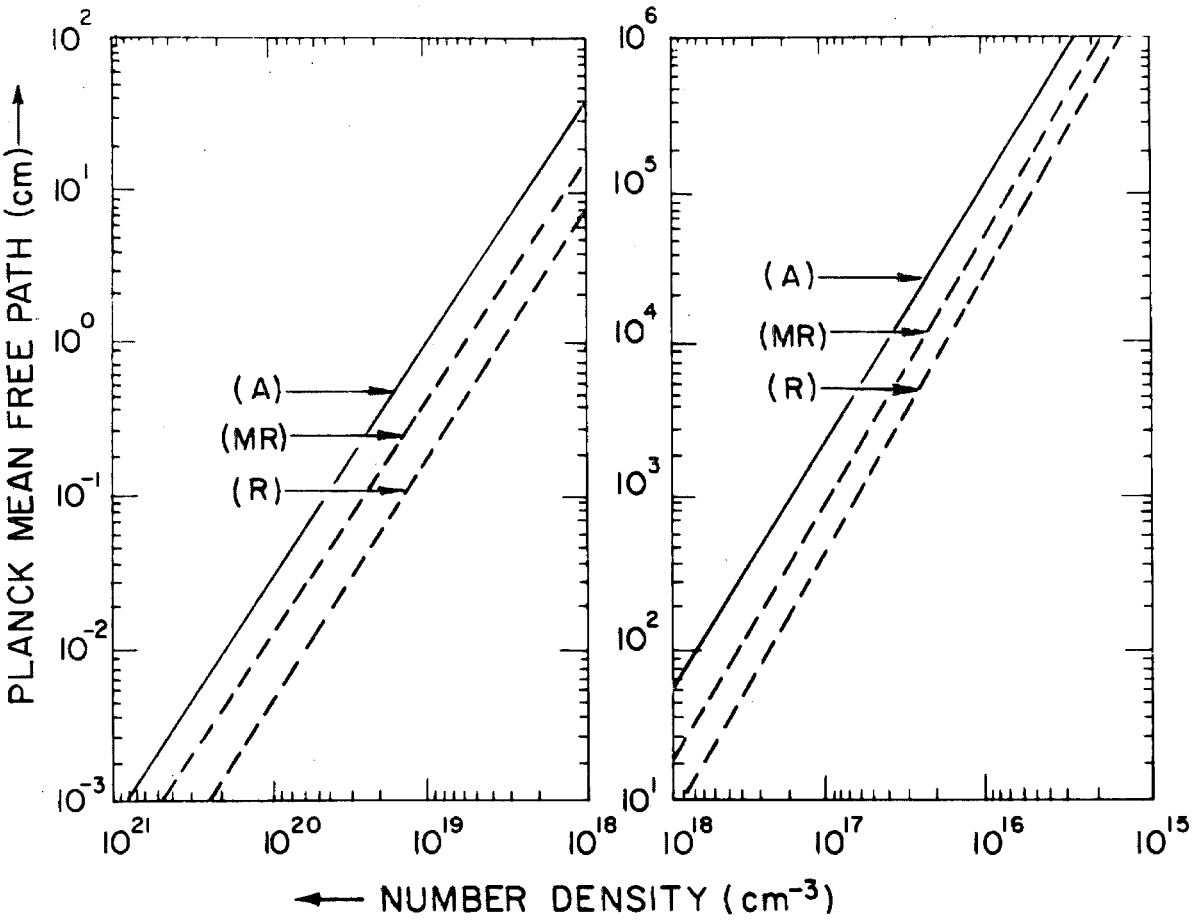

Fig. 26. The Planck mean free path (in cm) as a function of number density (in cm^{-3}) for nitrogen at 5 eV. The symbols (A), (R), and (MR) identify results obtained Armstrong (A) and derived from the Raizer (R) and modified Raizer (MR) method of Pappert and Penner, respectively. In the (R) and (MR) plots, we have used consistently the approximation $g_e g_{m+1}/g_m = 1$. A complete discussion of the theoretical formulae for the (R) and (MR) curves is given in Ref. 28.

$m = 0, 1, 2, \ldots$, the total continuum absorption coefficient is finally obtained by summing the contributions made by the separate m-ions. Thus,

$$k'(x) = \frac{k(x)}{1-\exp(-x)} = a\theta^{-2} \sum_{m} N_m (g_e g_{m+1}/g_m)(m+1)^2 \exp(-x_{1m}) F_m(x) \tag{130}$$

where $k'(x)$ denotes the spectral absorption coefficient with the induced emission term excluded.

Menzel and Pekeris (27) and Raizer (30) have performed an approximate evaluation for the radiation mean free paths by utilizing the fact that configuration splitting of the $2n^2$ degenerate hydrogenic levels makes plausible the replacement of the sum over n, which occurs in eqs. 129 and 130, by an integration, i.e.,

$$\sum \frac{2x_{1m}}{n^3} \exp\left(\frac{x_{1m}}{n^2}\right) \rightarrow \int_o^x e^y \, dy = e^x - 1, \quad x < x_{1m}, \tag{131}$$

whence

$$F_m(x) \simeq x^{-3} e^x \quad \text{for} \quad x < x_{1m}. \tag{132}$$

Thus, for the case in which the energy of the incident photon is less than the ionization potential of the m-ion, the frequency dependent factor $F_m(x)$ is a universal function of x.

For $x > x_{1m}$, it is assumed that the dominant role is played by the ground level $n = 1$. Therefore,

$$F_m(x) \simeq 2x_{1m} x^{-3} \exp(x_{1m}), \quad x > x_{1m}. \tag{133}$$

In view of eqs. 132 and 133, we may use the following approximate representation for $F_m(x)$:

$$F_m(x) \simeq \begin{cases} \dfrac{\exp(x)}{x^3} & \text{for } x < x_{1m} , \\ \dfrac{2x_{1m}}{x^3} \exp(x_{1m}) & \text{for } x \geq x_{1m} . \end{cases} \tag{134}$$

Hence

$$k'(x) = \frac{a}{\theta^2 x^3} \begin{cases} [\exp(x)] \sum_m N_m (g_e g_{m+1}/g_m)(m+1)^2 \exp(-x_{1m}) & \text{for } x < x_{1m} \\ 2 \sum_m N_m (g_e g_{m+1}/g_m)(m+1)^2 x_{1m} & \text{for } x \geq x_{1m}. \end{cases} \tag{135}$$

In order to obtain an explicit relation for $k'(x)$, it is now necessary to evaluate the sums over the m-ions. A rigorous evaluation of these sums requires the determination of N_m with proper allowance for each of the equilibria

$$N \rightleftharpoons N_{m+1} + e^- . \tag{136}$$

Instead of solving the complete set of simultaneous Saha equations, we estimate the average degree of ionization $\overline{m}$ from eq. 126 written in the form

$$I_{\overline{m}-(1/2)} = \theta \ln \left\{ \frac{A' \left[g_e g_{\overline{m}} + (1/2)/g_{\overline{m}} - (1/2) \right] \theta^{3/2}}{N \overline{m}} \right\} . \tag{137}$$

In accord with our earlier discussion and with the method of Pappert and Penner (28), we regard eq. 137 to be consistent with the Saha equation in the sense that the hypothetical ion species corresponding

to $m = \bar{m} + (1/2)$ and $m = \bar{m} - (1/2)$ are equal in number. Using eq. 126, it is now possible to rewrite one of the sums occurring in eq. 135 as

$$\sum_m N_m (g_e g_{m+1}/g_m)(m+1)^2 \exp(-x_{1m}) = \frac{N\bar{m}}{A'\theta^{3/2}} \sum_m N_{m+1}(m+1)^2 . \tag{138}$$

Furthermore, since

$$N_{\bar{m}+(1/2)} = N_{\bar{m}-(1/2)} = \frac{N}{2} , \tag{139}$$

only the two terms $m = \bar{m} - (3/2)$ and $m = \bar{m} - (1/2)$ contribute to the sums in the first of the eqs. 135 and in eq. 138. We find the following results for the sums occurring in eq. 135:

$$\begin{aligned} \sum_m N_m (g_e g_{m+1}/g_m)(m+1)^2 \exp(-x_{1m}) &= \frac{N\bar{m}}{A'\theta^{3/2}} \sum_m N_{m+1}(m+1)^2 \\ &\simeq \frac{N^2\bar{m}}{A'\theta^{3/2}} (\bar{m}^2 + \tfrac{1}{4}) \quad \text{for } x < x_{1m_1}, \\ &\simeq \frac{N^2\bar{m}}{2A'\theta^{3/2}} (\bar{m} + \tfrac{1}{2})^2 \quad \text{for } x_{1m_1} < x < x_{1m_2}; \end{aligned} \tag{140}$$

$$\begin{aligned} 2\sum_m N_m (g_e g_{m+1}/g_m)(m+1)^2 x_{1m} &\simeq N(\bar{m} + \tfrac{1}{2})^2 x_{1m_1} \quad \text{for } x_{1m_1} < x < x_{1m_2}, \\ &\simeq N\left[(\bar{m} + \tfrac{1}{2})^2 x_{1m_1} + (\bar{m} + \tfrac{3}{2})^2 x_{1m_2}\right] \\ &\quad \text{for } x > x_{1m_2}. \end{aligned} \tag{141}$$

Here N is the total number density per cm^3 and $m_1 = \bar{m} - (1\ 2)$, $m_2 = \bar{m} + (1/2)$, and we have made the assumption $g_e g_{m+1}/g_m = 1$ in eq. 141. It should be noted that $x < x_{1m_1}$ corresponds physically to $h\nu < I_{\bar{m}} - (1/2)$, $x_{1m_1} < x < x_{1m_2}$ to $I_{\bar{m}} - (1/2) < h\nu < I_{\bar{m}} + (1/2)$, and $x > x_{1m_2}$ to $h\nu > I_{\bar{m}} + (1/2)$. Thus we obtain the following expressions for the spectral absorption coefficient

$$k'(x) = \frac{a}{\theta^2 x^3} \begin{cases} \dfrac{N^2 \bar{m}}{A'\theta^{3/2}} \left(\bar{m}^2 + \dfrac{1}{4}\right) \exp(x) & \text{for } x < x_{1m_1}, \\ \left\{\dfrac{N^2 \bar{m}}{2A'\theta^{3/2}} \left(\bar{m} + \dfrac{1}{2}\right)^2 [\exp(x)] + N\left(\bar{m} + \dfrac{1}{2}\right)^2 x_{1m_1}\right\} & \text{for } x_{1m_1} < x < x_{1m_2}, \\ N\left[\left(\bar{m} + \dfrac{1}{2}\right)^2 x_{1m_1} + \left(\bar{m} + \dfrac{3}{2}\right)^2 x_{1m_2}\right] & \text{for } x > x_{1m_2}. \end{cases} \tag{142}$$

The assumption $g_e g_{m+1}/g_m = 1$ affects only the terms in eq. 142 which do not contain A'. Actual calculations of this ratio for poly-electronic atoms may be performed easily for the ground electronic state and indicate that $g_e g_{m+1}/g_m$ may be smaller or larger than unity by as much as factors of about 1/3 to about 3 and that an average value of unity is not an unreasonable choice.

In order to complete the semi-analytical representation for k'(x), it is now necessary to specify $\bar{m}$ in terms of θ and N. An implicit representation for $\bar{m}$ is given through the Raizer approximation specified in eq. 137. Equations 142 and 137 permit ready calculation of k'(x) to the hydrogenic, modified Raizer, representation for all values of θ and N. Reference to eqs. 142 and 137 shows that k', for fixed values of N and θ, increases as $\nu^{-3} \exp(h\nu/\theta)$ until $\nu = I_{\bar{m}} - (1/2)/h$;

for $I_{\bar{m}} - (1/2) < h\nu < I_{\bar{m}} + (1/2)$, k' is given by the sum of two terms, one of which increases as $\nu^{-3} \exp(h\nu/\theta)$ and the other of which decreases as ν^{-3}; finally, for $\nu > I_{\bar{m}} + (1/2)/h$, k' becomes inversely proportional to ν^3. This simplified form for $k'(x)$ is the direct result of the approximation that the number density of ionized atoms has been assumed to be vanishingly small except for the m-ions characterized by $m = \bar{m} \pm (1/2)$.

B. Comparison Between the Approximate and Numerical Results

Representative plots of $k(x = h\nu/\theta) = k'(x)[1 - \exp(-x)]$, i.e., of the spectral absorption coefficient with the induced emission term included, as a function of ν are shown in Fig. 27 for nitrogen at 5 eV, 10 eV and 20 eV for a number density of 10^{17} cm^{-3}; $k(x)$ is shown in Fig. 28 as a function of ν for $\theta = 10$ eV and for number densities of 10^{17}, 10^{19} and 10^{21} cm^{-3}. In constructing the plots shown in Figs. 27 and 28, we have used the calculated values for $\bar{m}$ based on Armstrong's data (15).

Figure 29 shows the values of $k'(x) = k(x)[1 - \exp(-x)]^{-1}$ calculated from eq. 142 with values of $\bar{m}$ taken from Ref. 15. Also shown in Fig. 29 are Armstrong's (15) more accurate calculations. Armstrong did not use the method of Seaton† but employed screened hydrogenic cross sections, made full allowance for LS term splitting, for the correct ionization potentials, and for an approximate plasma interaction effect.‡

† See footnote on p.99

‡ The author wishes to thank Dr. Armstrong for furnishing a precise categorization of the assumptions used in his calculations.

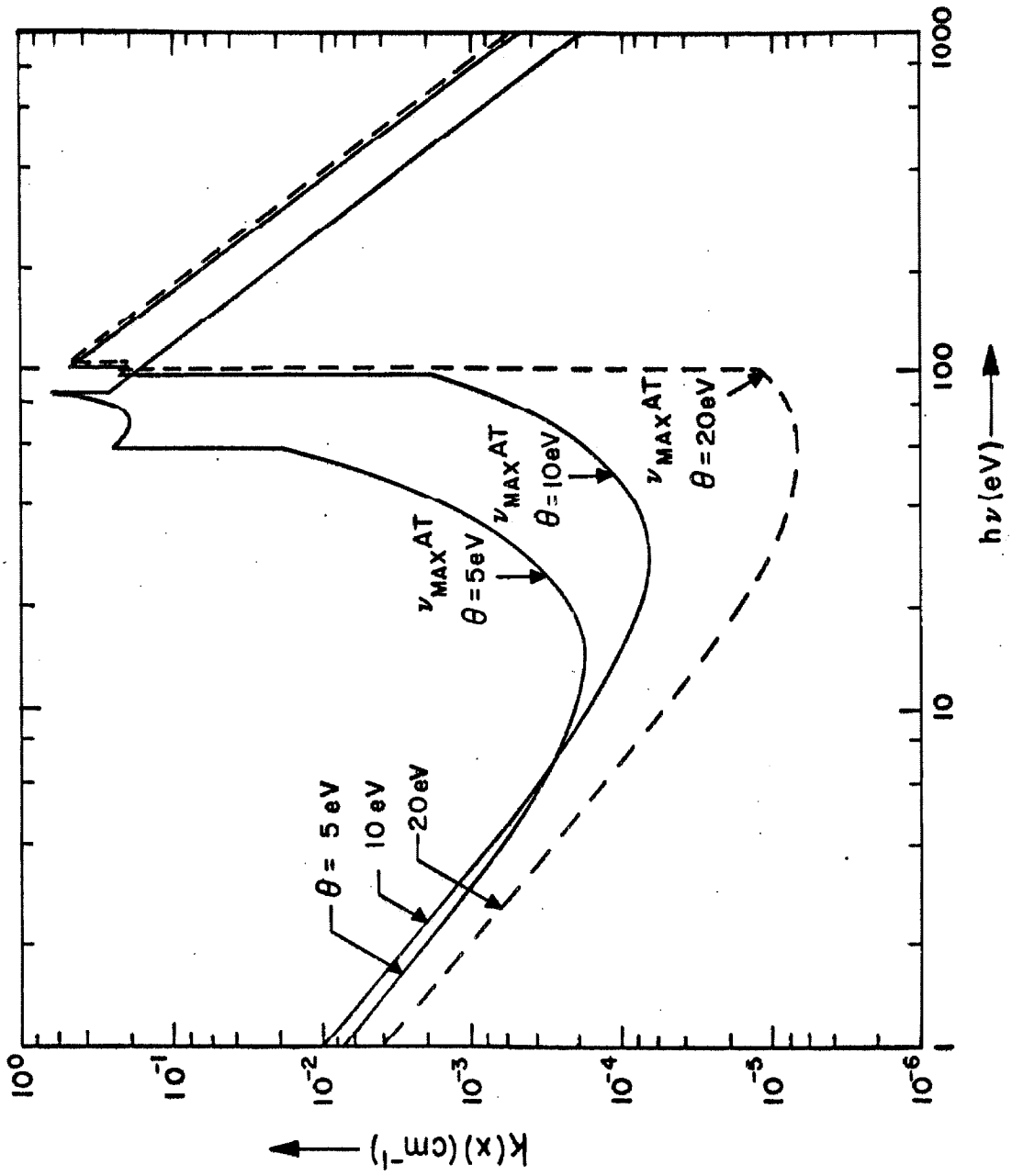

Fig. 27. A simplified representation for the spectral absorption coefficient of nitrogen as a function of frequency for θ = 5, 10, and 20 eV for 10^{17} atoms per cm^3.

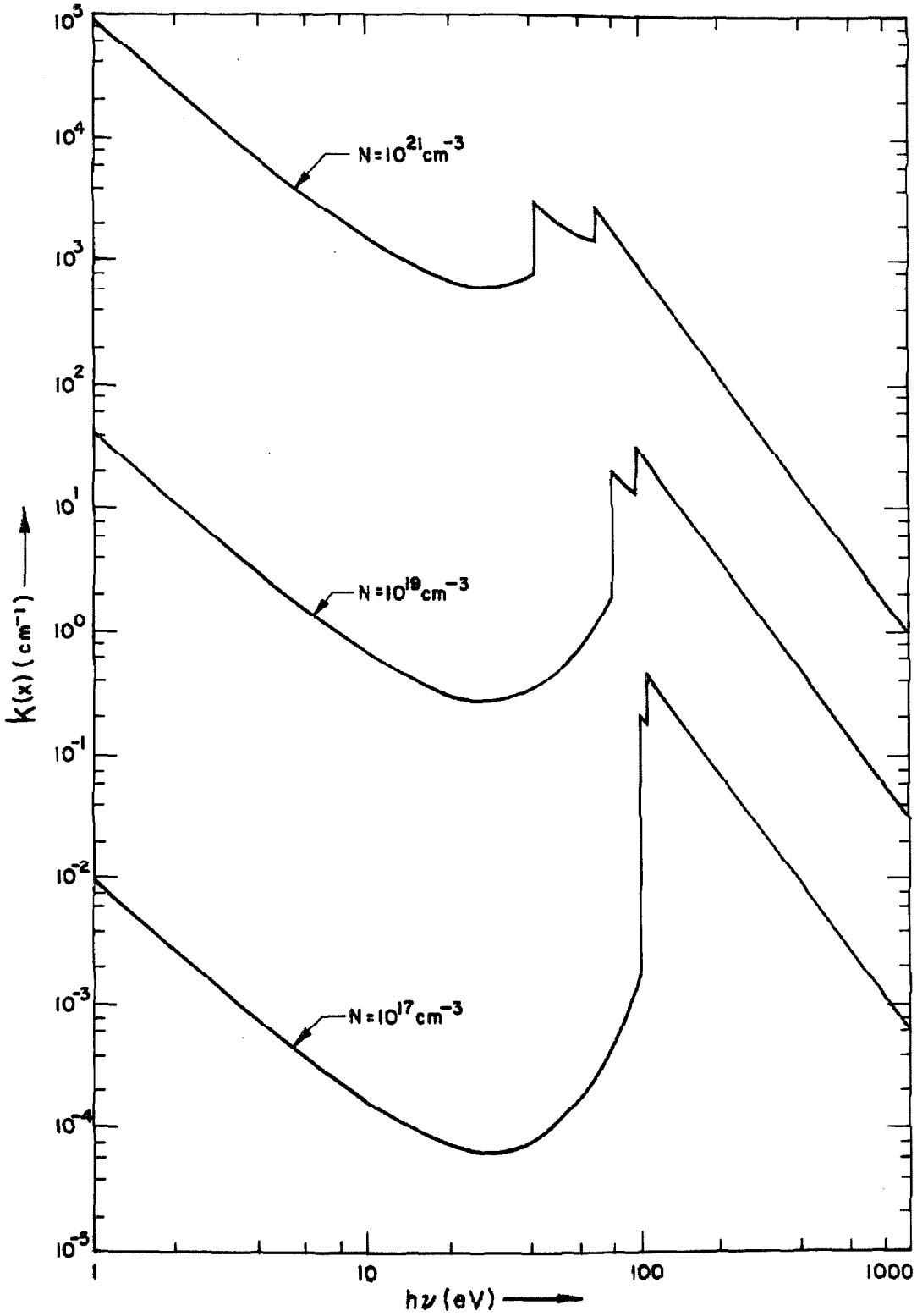

Fig. 28. A simplified representation for the spectral absorption coefficient of nitrogen at 10 eV for 10^{17}, 10^{19}, and 10^{21} atoms per cm^3.

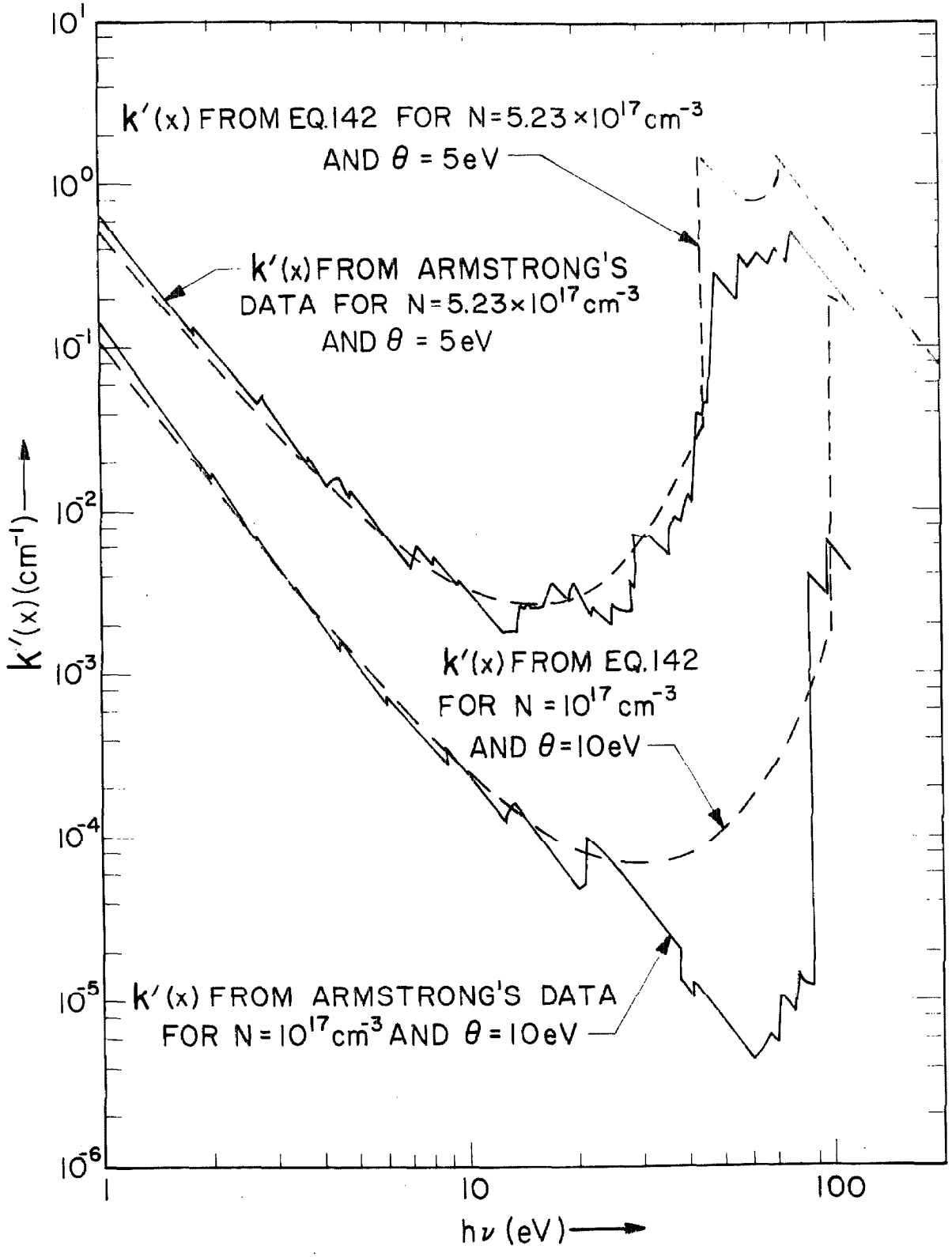

Fig. 29. The spectral absorption coefficient, without the induced emission term, for nitrogen as calculated from eq. 142 and, using the best available methods, as calculated by Armstrong (15) for $\theta = 5$ eV, $N = 5.23 \times 10^{17}$ cm^{-3} and $\theta = 10$ eV, $N = 10^{17}$ cm^{-3}.

Reference to Fig. 29 shows that significant discrepancies occur only for photon energies which are sufficiently large to ionize the nitrogen ion in its ground state because the hydrogenic model is then no longer a reasonable approximation and because statistical weight factors influence the results.[†] On the other hand, over most of the spectral range, the approximate treatment provides a good representation of the spectral absorption coefficient. Hence we conclude that the highly simplified procedure which we have employed provides an adequate representation for thermodynamic function and opacities of plasmas containing polyelectronic atoms.

[†] As was indicated previously in this discussion, we have avoided the complications associated with the statistical weight factors in terms not containing A' by setting $g_e g_{m+1}/g_m$ arbitrarily equal to unity.

Appendix A

The Diffusion Approximation

Consider a radiating layer of gas as pictured in Fig. A-1.

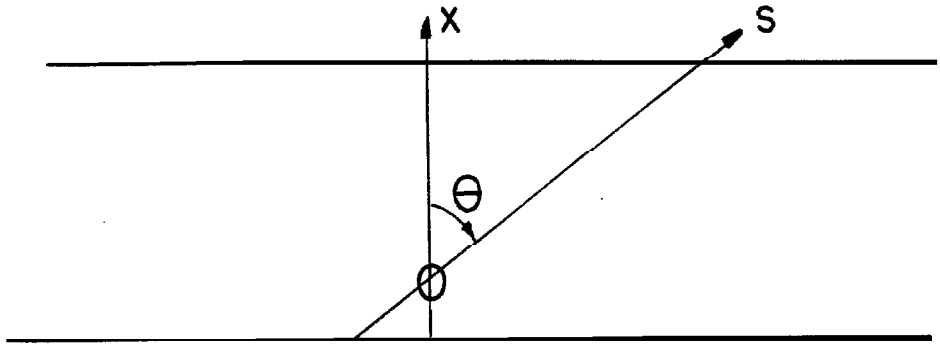

Fig. A-1. A cross section of a radiating gas layer is shown defining the distances x and s and the angle θ.

We calculate the total radiant flux in the x direction, which was chosen so that near the point of observation, O, $\nabla T = \partial T/\partial x$. For a highly absorbing gas, eq. 116 gives

$$B_\nu = B_\nu^o - \frac{1}{k_\nu}\frac{\partial B_\nu^o}{\partial s} + \frac{1}{k_\nu^2}\left[\frac{\partial^2 B_\nu^2}{\partial s^2} - \frac{\partial B_\nu^o}{\partial s}\frac{d \ln k_\nu}{ds}\right] + \cdots$$

where all quantities are evaluated at the point of observation, O. But, near this point,

$$\frac{\partial}{\partial s} = \cos\theta \frac{\partial}{\partial x} \tag{A1}$$

and hence

$$B_\nu \simeq B_\nu^o - \cos\theta \frac{1}{k_\nu}\frac{\partial B_\nu^o}{\partial x} + \frac{\cos^2\theta}{k_\nu^2}\left[\frac{\partial^2 B_\nu^o}{\partial x^2} - \frac{\partial B_\nu^o}{\partial x}\frac{\partial \ln k_\nu}{\partial x}\right]. \tag{A2}$$

The spectral flux is given by the expression

$$\vec{F}_\nu = \int_\Omega B_\nu \cos\theta \, d\Omega \, . \tag{A3}$$

Substituting eq. A2 into eq. A3 and integrating we obtain

$$\vec{F}_\nu = - \frac{4\pi}{3k_\nu} \frac{\partial B_\nu^o}{\partial x} \tag{A4}$$

since $\overline{\cos\theta} = \overline{\cos^3\theta} = 0$ and $\overline{\cos^2\theta} = 2/3$. Thus

$$\vec{F}_\nu = - \frac{4\pi}{3k_\nu} \frac{\partial B_\nu^o}{\partial T} \frac{\partial T}{\partial x} \, ,$$

or

$$\vec{F} = - \lambda_{ra} \nabla T \tag{A5}$$

if

$$\lambda_{ra} = \int \frac{4\pi}{3k_\nu} \frac{\partial B_\nu^o}{\partial T} d\nu = \frac{16\sigma T^3}{3\bar{k}_{L,R_o}}$$

as indicated in Sec. III, (B). The first correction term to the diffusion approximation formula given in eq. A5 may be found from the third order term in eq. 116. The first correction term is

$$- \frac{4\pi}{5k_\nu^3} \left[\frac{\partial^3 B_\nu^o}{\partial T^3} - 3 \frac{d^2 B_\nu^o}{dT^2} \frac{d \ln k_\nu}{dT} - \frac{dB_\nu^o}{dT} \frac{d^2 \ln k_\nu}{dT^2} + 2 \frac{dB_\nu^o}{dT} \left(\frac{d \ln k_\nu}{dT} \right)^2 \right] \nabla^3 T.$$

Hence, the Navier-Stokes form of the heat flux is only good to the second order.

Appendix B

Solution to the Radiant Energy Transfer Equation Using the Lunblad Series Expansion

We derived eq. 116, the solution to the radiant energy equation for large optical lengths, using the iterative procedure

$$B_{\nu_{i+1}} = B^{o}_{\nu} - \frac{\partial B_{\nu_i}}{\partial \tau} \quad , \quad B_{\nu_1} = B^{o}_{\nu} \tag{B1}$$

where the subscript i indicates the i^{th} order solution. Let us determine the form of the solution if

$$B^{o}_{\nu} = \sum_{i=0}^{n-1} a_i \tau^i \tag{B2}$$

i.e., we approximate B^{o}_{ν} by n terms in the Lunblad series (see Sec. VII). From eq. B1 it follows that

$$B_{\nu_2} = \sum_{i=0}^{n-1} (1 - \frac{i}{\tau}) a_i \tau^i \quad . \tag{B3}$$

After n-1 iterations we have

$$B_{\nu_n} = \sum_{i=0}^{n-1} \left[1 - \frac{i}{\tau} + \frac{i(i-1)}{\tau^2} - \ldots + \frac{i(i-1)\ldots(i-n+2)}{(-\tau)^{n-1}} \right] a_i \tau^i \quad . \tag{B4}$$

However, it is now seen that further iteration will not change B_{ν} from the value B_{ν_n} as all the coefficients of form

$$i(i-1) \ldots (i-n+2)(i-n+1) \ldots$$

will vanish. Therefore, eq. B4 is the exact solution to the heat transfer equation when B^{o}_{ν} is given by the Lunblad series. For n terms kept

in the Lunblad series, the exact solution will contain only n terms. We may conclude that in an expansion of the form of eq. 120 for a general temperature profile, the first n terms will be correct but the n+1 and successive terms will in general be incorrect.

Furthermore, if the j^{th} term in eq. 116 is set equal to zero, a j^{th} order differential equation results which may be reduced to an equation which determines (to within certain constants) the temperature profile. It is easily seen that the analysis leading to eq. 120, when additional terms in the Lunblad series are used, will also yield a j^{th} order differential equation when the j^{th} term is set equal to zero. When the Lunblad series is exact to the $(j-1)^{th}$ order, the j^{th} term must vanish in both the exact solution and the solution of the type presented in eq. 120. This results in two j^{th} order differential equations having the same solution. Hence they must be the same to within a constant factor. Therefore the j^{th} and successive terms are the same in both types of solutions to within a constant factor.

Equation B4 may also be derived combining eq. B2 with the general solution to the radiant transfer equation (eq. 51). Below we look at the special case considered in Sec. VII, viz. an infinitely thick medium. The solution to the radiant transfer equation may be written

$$B_\nu(\tau)e^{\tau} - B_\nu(0) = \int_0^{\tau} B_\nu^o(\tau')e^{\tau'}\, d\tau' \tag{B5}$$

where τ is the optical length ($\tau = \int^s k_\nu ds$). Letting $\tau \rightarrow -\infty$, we obtain, in analogy with eq. 74,

$$B_\nu(0) = \sum_{i=0}^{n-1} a_i(-1)^i\, i! \tag{B6}$$

having kept n terms in the Lunblad series. The alternating sign of each term results from having chosen τ and s in the same direction; the analysis of Sec. VI assumed τ and the direction of radiant energy transfer to be in opposite directions. It is easily seen that eq. B4 reduces to eq. B6 for $\tau = 0$.

It is now possible to demonstrate that the condition

$$B_\nu(0) \simeq B_\nu^o \ (\tau = 1), \tag{B7}$$

which was applied in Sec. VIII for a general temperature profile is valid only for large optical depths. Starting with eq. 131, we have

$$B_\nu(\tau) = B_\nu^o(\tau) - \frac{\partial B_\nu^o}{\partial \tau} + \frac{\partial^2 B_\nu^o}{\partial \tau^2} - \ldots \quad . \tag{B8}$$

We may expand B_ν^o in a Taylor series about an optical length, t, resulting in the equation

$$B_\nu^o(t) = B_\nu^o(\tau) - (\tau - t)\frac{\partial B_\nu^o}{\partial \tau} + \frac{(\tau - t)^2}{2!}\frac{\partial^2 B_\nu^o}{\partial \tau^2} - \ldots \tag{B9}$$

We see that $B_\nu(0)$ will equal $B_\nu^o(t)$, independent of the choice of temperature profile, only if

$$\begin{aligned} (-t) &= 1 \\ (-t)^2 &= 2! \\ (-t)^3 &= 3! \\ &\vdots \end{aligned}$$

these conditions are mutually exclusive. For large n

$$(-t) = (n!)^{1/n} \approx n/e \gg 1 ,$$

where e is the base of the natural logarithms. Equation B7 will be valid

only for large optical depths where the high order terms in Eq. B8 are negligible.

A symbolic derivation of eq. B8 is obtained by writing the heat transfer equation, eq. B1, as

$$(1 + \frac{\partial}{\partial \tau}) B_\nu = B_{\nu_o} . \tag{B10}$$

Therefore

$$B_\nu = (1 + \frac{\partial}{\partial \tau})^{-1} B_{\nu_o} . \tag{B11}$$

Expansion of the operator results in eq. B8.

References

1. Bridgman, P. W., Dimensional Analysis (Yale University Press, 1931).

2. Penner, S. S., Combustion Researches and Reviews (Butterworth, London, 1955), Chap. 12.

3. Hirschfelder, J. O., Curtiss, C. F., and Bird, R. B., Molecular Theory of Gases and Liquids (John Wiley & Sons, Inc., New York, 1954).

4. Damköhler, G., "Einflüsse der Strömung, Diffusion und des Wärmeüberganges auf die Leistung von Reaktionsöfen," Z. Elektrochem, 42, 846-862 (1936).

5. Penner, S. S., Chemistry Problems in Jet Propulsion (Pergamon Press, Ltd., New York, 1957).

6. Butler, J. N. and Brokaw, R. S., "Thermal conductivity of gas mixtures in chemical equilibrium," J. Chem. Phys. 26, 1636-1643 (1957).

7. Penner, S. S., Quantitative Molecular Spectroscopy and Gas Emissivities (Addison-Wesley Publishing Co., Reading, Mass., 1959).

8. Adrianov, V. N. and Shorin, S. N., "Radiant heat transfer in a flowing radiating medium," Izvestiia Akad. Nauk SSSR, Otdel. Tekh. Nauk, no. 5, 46-56 (1958); translation in AIAA J. 1, 1729-1734 (1963).

9. Goulard, R., and M., "One-dimensional energy transfer in radiant media," Int. J. Heat Mass Transfer 1, 81-91 (1961).

10. Penner, S. S. and Patch, R. W., "Radiative transfer studies and opacity calculations for heated gases," AFOSR-1901, T. R. No. 6, California Institute of Technology (January, 1962).

11. Unsöld, A., Physik der Sternatmosphären (Springer-Verlag, Berlin, 1955).

12. Thomas, M., Jr., "Transport properties of high-temperature gases," Magnetohydrodynamics-Proceedings of the Fourth Biennial Gas Dynamics Symposium (Northwestern University Press, Evanston, 1962), pp. 89-107.

13. Sobolev, N. N., "Optical methods of measuring the temperatures of flames," Trud. Fisich. Inst., VII, 161-229 (Akad. Nauk, SSSR, 1956); translated by M. Thomas, Jr., Translation Project, California Institute of Technology (1962).

14. Breene, R. G., Jr., and Nardone, M., "Radiant emission from high temperature equilibrium air," General Electric TIS Ser. R61SD020, General Electric Co., Space Sciences Lab., Philadelphia (May, 1961); also, with fewer graphical data, in J. Quant. Spectrosc. Radiat. Transfer 2, 272-292 (1962).

15. Armstrong, B. H., "Mean absorption coefficients of air, nitrogen, and oxygen from 22,000° to 220,000°," Report LMSD-4979, Lockheed Missiles and Space Division, Palo Alto, California (July, 1959); see also Armstrong, B. H. and Meyerott, R. E., "Absorption coefficients for high-temperature nitrogen, oxygen, and air," Phys. Fluids 3, 138-140 (1960).

16. Gilmore, F. R., "Equilibrium composition and thermodynamic properties of air to 24,000°K," Report RM-1543, Rand Corp. (August, 1955).

17. Rigdon, W.S. and Thomas, M., "Stagnation point heat transfer in a real gas," Report SM-45730, Missiles and Space Systems Division, Douglas Aircraft Co., Inc. (September, 1963).

18. Sobolev, V. V., A Treatise on Radiative Transfer, translated by S. I. Gaposchkin (D. Van Nostrand Company, Inc., Princeton, 1963), pp. 141-150.

19. Lundblad, R., "On the radiation and temperature of the external photospheric layers," Ap. J. 58, 113-137 (1923).

20. Pearson, K., Tables of the Incomplete Γ-Function (Cambridge University Press, Cambridge, 1957).

21. Thomson, J. A. L., "Radiative transfer in rocket exhaust gases," Eight International Combustion Symposium (William & Wilkins Co., Baltimore, 1962), pp. 69-81.

22. Armstrong, B. H., Sokoloff, J., Nicholls, R. W., Holland, D. H., and Meyerott, R. E., "Radiative properties of high temperature air," J. Quant. Spectrosc. Radiat. Transfer 1, 143-162 (1961).

23. Peng, T. and Pindroh, A. L., "An improved calculation of gas properties at high temperatures--air," Magnetohydrodynamics - Proceedings of the Fourth Biennial Gas Dynamics Symposium (Northwestern University Press, Evanston, 1962), pp. 67-88.

24. Hansen, C. F., "Approximations for the thermodynamic and transport properties of high-temperature air," NASA TR R-50 (1959).

25. Spitzer, L., Jr., and Härm, R., "Transport phenomena in a completely ionized gas," Phys. Rev. 89, 977-981(1953).

26. Shkarofsky, I. P., "Values of the transport coefficients in a plasma for any degree of ionization based on a Maxwellian distribution," Can. J. Phys. 39, 1619-1703 (1961).

27. Menzel, D. H. and Pekeris, C. L., "Absorption coefficients and hydrogen line intensities," Mon. Not. Roy. Astr. Soc. 96, 77-11 (1935).

28. Pappert, R. A. and Penner, S. S., "Approximate opacity calculations for polyelectronic atoms at high temperatures," J. Quant. Spectrosc. Radiat. Transfer 1, 258-268 (1961).

29. Raizer, Yu. P., "A simple method of calculating the degree of ionization and thermodynamic functions of a multiply ionized ideal gas," Sov. Phys. JETP 9, 1124-1125 (1959).

30. Raizer, Yu. P., "Simple method for computing the mean range of radiation in ionized gases at high temperatures," Sov. Phys. JETP 10, 769-771 (1960).